

**New group theoretical methods for
applications in virology and
quasicrystals**

Emilio Zappa

PhD

University of York

Mathematics

July 2015

To my parents

Sometimes, immersed in his books, there would come to him the awareness of all that he did not know, of all that he had not read; and the serenity for which he labored was shattered as he realized the little time he had in life to read so much, to learn what he had to know.

J. Williams, *Stoner*.

Abstract

Non-crystallographic symmetries are ubiquitous in physics, chemistry and biology. Prominent examples are quasicrystals, alloys with long-range order but no translational periodicity in their atomic organisation, and viruses, micro-organisms consisting of a protein shell, the capsid, that in most cases displays icosahedral symmetry. Group theory plays a crucial role in understanding their structures and their physical and geometrical properties. In this thesis new group theoretical methods are introduced, to characterise virus organisation and model structural transitions of icosahedral quasicrystals. It is shown that these problems can be described via the embedding of non-crystallographic groups into the point group of higher dimensional lattices. Indeed, the analysis of orbits of such embeddings, akin to the construction of quasicrystals via the cut-and-project method, provides a rigorous mathematical construction of finite nested point sets with non-crystallographic symmetry at each distinct radial level. In the case of icosahedral symmetry, it is shown that the point arrays thus obtained can be used to provide constraints on the geometry of viral capsids, encoding information on the organisation of the capsid proteins and the genomic material collectively. Moreover, structural transitions of icosahedral quasicrystals can be analysed in a group theoretical framework through continuous rotations in the higher dimensional space connecting distinct copies of the embedded icosahedral group, sharing a common maximal subgroup. These rotations induce in projection continuous transformations between aperiodic point sets that preserve the symmetry described by the common subgroup. Theoretical methods as well as applications are discussed, with emphasis on the computational and geometric aspect of group theory.

Contents

Abstract	4
List of Figures	7
List of Tables	9
Acknowledgements	10
Author's declaration	11
Preface	12
1 An introduction to Quasicrystals and Mathematical Virology	18
1.1 Lattices and non-crystallographic groups	18
1.1.1 Icosahedral symmetry	20
1.2 Quasicrystals	22
1.2.1 Cut-and-project schemes and model sets	22
1.2.2 Crystallographic embedding of non-crystallographic groups	24
1.2.3 Tilings	27
1.3 Mathematical Virology	29
1.3.1 Caspar-Klug theory	30
1.3.2 Viral tiling theory	32
1.3.3 Beyond Caspar-Klug: affine extensions of the icosahedral group	34
2 On the subgroup structure of the hyperoctahedral group in six dimensions	37
2.1 Crystallographic embedding of the icosahedral group	38
2.1.1 Representations of the hyperoctahedral group B_6	40
2.1.2 Classification of the crystallographic representations of \mathcal{I}	41
2.1.3 Projection into the 3D space	43
2.2 Subgroup structure	46

2.2.1	Subgroups of the crystallographic representations of \mathcal{I}	48
2.2.2	Some basic results of graph theory and their spectra	49
2.2.3	Applications to the subgroup structure	50
3	A group theoretical approach to structural transitions of icosahedral quasicrystals	54
3.1	Schur rotations between icosahedral quasicrystals	54
3.2	Computations and applications	59
3.2.1	Tetrahedral group \mathcal{T}	60
3.2.2	Dihedral group \mathcal{D}_{10}	63
3.2.3	Dihedral group \mathcal{D}_6	65
4	Construction of finite nested point sets with non-crystallographic symmetry	69
4.1	Nested point sets obtained from projection	70
4.2	Applications to finite Coxeter groups and polytopes	74
4.2.1	Finite Coxeter groups	74
4.2.2	Minkowski embedding of $I_2(n)$ and planar nested structures	77
4.2.3	Nested polyhedra with icosahedral symmetry H_3	85
4.2.4	Nested polychora with generalised icosahedral symmetry H_4	88
5	Applications to viral capsid architecture	93
5.1	Nested point sets with icosahedral symmetry	93
5.2	Projected orbits as blueprints for viral capsids	97
	Conclusions	104
	Appendix	107
	Bibliography	115

List of Figures

1.1	Fundamental domains for chiral and achiral icosahedral symmetry.	21
1.2	Illustration of the cut-and-project method for a one-dimensional model set.	24
1.3	Example of Penrose tilings of the plane.	29
1.4	Example of a capsid with icosahedral symmetry.	30
1.5	Construction of the Caspar-Klug icosideltahedra.	31
1.6	Possible T -numbers in the Caspar-Klug classification.	32
1.7	Viral tiling theory	33
1.8	Prototiles for the tiling of Simian Virus 40	33
1.9	Planar example of affine extensions of five-fold symmetry	36
1.10	Structural constraints on virus architecture via affine extensions.	36
2.1	Five-fold axes of an icosahedron.	39
2.2	Icosahedral tiling in the space.	46
3.1	Illustration of the Schur rotation for a one-dimensional quasicrystal.	57
3.2	Example of a transition with tetrahedral symmetry.	63
3.3	Patch of a quasilattice with \mathcal{D}_{10} -symmetry.	65
3.4	Example of a structural transition with \mathcal{D}_6 -symmetry.	68
3.5	A three-dimensional lattice obtained from a transition with \mathcal{D}_6 -symmetry.	68
4.1	Illustration of the construction of finite nested point sets.	73
4.2	The root system, simple roots and fundamental weights for H_2	84
4.3	Planar nested structures with five-fold symmetry.	85
4.4	Nested polyhedra with icosahedral symmetry.	88
4.5	Sections of nested polychora with H_4 -symmetry.	92

5.1	Graph of inclusions of the subgroups of the hyperoctahedral group containing the crystallographic representation $\tilde{\mathcal{I}}$ of the icosahedral group. . .	96
5.2	Nested point set with icosahedral symmetry induced by projection.	97
5.3	Blueprints for the capsid of Pariacoto Virus.	101
5.4	Blueprints for the capsid of Bacteriophage MS2.	103

List of Tables

2.1	Explicit forms of the irreps ρ_3 and ρ'_3 with $\tilde{\mathcal{I}} \simeq \rho_3 \oplus \rho'_3$	45
2.2	Non-trivial subgroups of the icosahedral group.	47
2.3	Order of the classes of subgroups of the icosahedral group in \mathcal{I} and B_6 . . .	48
2.4	Spectra of the \mathcal{G} -graphs, for \mathcal{G} subgroup of the icosahedral group.	51
4.1	Coxeter graphs corresponding to the irreducible finite Coxeter groups. . .	75
4.2	Isogonal polyhedra with H_3 -symmetry.	86
4.3	Isogonal polychora with H_4 -symmetry.	91
5.1	Classification of the subgroups of B_6 containing the crystallographic representation $\tilde{\mathcal{I}}$ of the icosahedral group \mathcal{I} as a subgroup.	95

Acknowledgements

There are many people that I would like to thank for making the last three years in York such a unique experience.

First of all, I would like to thank my supervisor, Professor Reidun Twarock, whose constance, passion, strength, integrity will be always be a source of inspiration for me, and for teaching me to look at group theory from a different perspective. A great thanks to Professor Paolo Cermelli, Dr Giuliana Indelicato and Dr Eric Dykeman, for their invaluable advise and help through my PhD studies, and to Dr Briony Thomas, for showing me the artistic side of mathematics. Special thanks must go to Motiejus Valiunas, for the useful, long and stimulating maths discussions.

I was very fortunate to find myself in such a wonderful and exciting work environment. Thanks to the YCCSA people, and to the Math Virology group, James, Rich, Pierre, Eva, Simon Hickinbotham and Simon Milewski (the honorary member!), especially for bearing with my continuous questions on coding and computer science (and allowing me to use all their PCs!). A great thanks to my PhD fellows in Maths, for the weekly meetings and socials, and to the maths students, to whom I had the privilege to teach their seminars.

The first year in York would not have been the same without my Walmgate housemates, in particular Martin, Laura, Simon, Jess and Megan. Thanks to Anna, for the good time spent together, and to Riccardo and Silvia, for the many trips to London. A great thanks to Marta, for the long chats and her great understanding, and to Alejandro, for dragging me out of my room and reminding me to have fun in life. Thanks to Doon, for encouraging me to enjoy freedom, and not to be scared.

Last, but not least, thanks to my parents. I would not be here without their endless love and support.

Author's declaration

I declare that the work presented in this thesis is original and that it has not been previously submitted for a degree in any university.

Most of the work presented in this thesis has been published or accepted for publication. Chapter 2 contains the work published in [30], whereas part of the contents of Chapter 4 have been published in [31]. The first part of Chapter 4 and the whole of Chapter 5 contain material accepted for publication in [32]. The results of Chapter 3 have never been published.

I am the main author of [30], while my contribution to [31] and [32] is equal to the other co-authors. The results of Chapter 3 are entirely my own.

Preface

Group theory is the mathematical language that describes symmetries in nature. Prominent examples of solids with high symmetry are crystals, whose atomic arrangements form periodic lattices in space. The symmetry groups of lattices, known as crystallographic groups, correspond, in two and three dimensions, to the 17 wallpaper groups in the plane and the 230 space groups, respectively, and were classified by Fedorov, Schoenflies and Bravais in the nineteenth century [1]. These groups are characterised by the crystallographic restriction, which dictates that the order of their elements must be one, two, three, four or six [2]. As a consequence, lattices with five- and n -fold symmetry, for n greater than six, cannot exist in the plane or in 3D space. Therefore, discrete groups of isometries containing elements of such orders are called non-crystallographic.

Quasicrystals and viruses are prominent examples of non-crystallographic symmetries in nature. The former are solids whose atomic arrangements display long-range order but no translational periodicity. They were first discovered experimentally in 1984 by Shechtman [3], who found that the diffraction pattern of an aluminium-manganese alloy possessed icosahedral point symmetry. Scientists realised, after an initial scepticism, that this discovery had shaken the foundations of crystallography, since long-range order had always been regarded as a synonymous to periodicity. Since then, physicists and mathematicians have developed new mathematical tools to analyse aperiodic structures, and the theory of quasicrystals has become an active field of research, which encompasses concepts from metric geometry, algebra, number theory and condensed matter physics. Steinhardt *et al.* [4, 5] were among the first to realise that quasiperiodic point arrangements could be described mathematically via the projection into a suitable subspace of points of a higher dimensional lattice. Later, Moody [6] provided a formal construction of quasilattices via cut-and-project schemes and model sets.

Viruses, micro-organisms that infect all types of life form, are striking examples of ordered structures in biology. Indeed, a virus consists of a protein shell, called capsid, that encapsulates the genomic material (RNA or DNA) inside, and in most cases displays icosahedral symmetry [7]. This symmetrical property allows the use of mathematical tools to describe and predict the structure of viral capsids. In this sense, the first mathematical model for virus architecture was provided in 1962 by Caspar and Klug [8]. In their seminal paper, inspired by Buckminster Fuller's geodesic dome, they describe the construction of a family of polyhedra with icosahedral symmetry, known as icosideltahedra, that provide constraints on the positions and relative orientations of the capsid proteins. Although this theory remains a fundamental framework in virology, there is a significant number of viruses whose structures fall outside of this construction. In 2004, Twarock [9] showed how the mathematical principles of quasicrystals can be used to understand the geometry of viral capsids, by solving a long-standing open structural puzzle in virology. The new paradigm is the introduction of more general tessellations of the icosahedral net representing a planar embedding of the capsid surface. By construction, these tessellations are similar to the Penrose tilings [10]. In this framework, Caspar-Klug theory corresponds to tessellations with regular triangles. This novel approach in virology, known as Viral Tiling Theory, has provided new insights into viral capsid assembly and dynamics; moreover, it has strengthened the connection between viruses and quasicrystals, and opened up new directions for mathematical applications of techniques from the area of quasicrystals in virology. Indeed, Salthouse *et al.* [11] have recently developed a procedure to approximate viral capsids via icosahedral tilings obtained with the cut-and-project method.

Besides providing insights into virus structure, group theory plays an important role in modelling the thermodynamical properties of quasicrystals and viruses. Specifically, the former undergo structural transitions as a consequence of changes of thermodynamical parameters, such as temperature and pressure. Typically, quasicrystals transform continuously into either higher ordered crystalline states, or other aperiodic structures [12], and a symmetry breaking occurs. Such transformations can be characterised in the framework of the phenomenological Landau theory for second-order phase transitions [13], by identifying the order parameters that account for the symmetry breaking. Usually, some symmetry is preserved, and this is described mathematically by a common subgroup of the symmetry groups of the initial and final states. Similar transformations occur in virology: viral

capsids undergo conformational changes as part of their maturation process, resulting in an expansion of the capsid that creates openings on the protein coat through which the genomic material is released. An example is given by the capsid of Equine Rhinitis A Virus (ERAV), whose shape can be approximated by a dodecahedron, which undergoes an expansion process resulting in an icosidodecahedral shape [14].

The aim of this thesis is to provide new group theoretical methods for the analysis of structural transitions of icosahedral quasicrystals and the three-dimensional geometry of viral capsids. Indeed, it is demonstrated that these problems can be addressed via a common mathematical framework, specifically the embedding of non-crystallographic groups into the point group of higher dimensional lattices. Theoretical methods as well as applications are discussed, with emphasis on the computational aspect of group theory.

Caspar-Klug theory and viral tiling theory describe the capsid of a virus as a two-dimensional object rather than in the three-dimensional space, predicting only the locations of the protein subunits on the surface of the capsid, and not providing information about the organisation of the genomic material encapsulated inside. Indeed, experiments have showed that a significant number of capsids display icosahedral symmetry at different radial levels; prominent examples are the dodecahedral cage of RNA observed in Paria-coto Virus [15], and the double-shell structure of the genomic material of Bacteriophage MS2 [16]. These results suggest that mathematical approaches should be extended to include information on the three-dimensional organisation of the capsid, providing additional information regarding material organisation at different radial levels. A first step towards this goal was the principle of affine extensions, described in a series of papers [17–19]. In this work, the generators of the icosahedral group have been extended by a non-compact generator acting as a translation, with the additional requirement that the resulting words of the group satisfy non-trivial relations. Such affine extensions can also be obtained via a construction similar to the one of Kac-Moody algebras [20]. In this case, icosahedral symmetry is extended via an extension of the Cartan matrix, resulting in the addition of a non-compact operator to the generators of the icosahedral group [21–23]. The orbits of the affine extensions thus constructed consist of infinite point sets that densely fill the space, since the icosahedral group is non-crystallographic in 3D. Since viral capsids are finite objects, a cut-off parameter must be introduced, that limits the number of monomials of the affine group. In this way, finite subsets of the orbits are selected, which exhibit

multi-shell structures, in which each radial level displays icosahedral symmetry. However, such a cut-off implies that the point sets are not invariant under the extended group structure, which limits the use of these concepts in the formulation of energy functions with symmetry invariance.

In this work a new method for the construction of finite nested point sets with non-crystallographic symmetry is introduced, based on the crystallographic embedding of non-crystallographic groups. Janner pioneered the idea of using points of higher dimensional lattices to describe polyhedra with icosahedral symmetry in the context of virology [24–26], and moreover he analysed double-shell structures with five-fold symmetry as projected orbits of specific point groups in higher dimensions [27]. Here we present a systematic study for general non-crystallographic symmetries. Akin to the construction of quasicrystals, a non-crystallographic group G is embedded into the point group \mathcal{P} of a lattice in the minimal dimension where the cut-and-project construction is possible. Such an embedding is, in general, not maximal; hence there exist G -containing subgroups of \mathcal{P} which extend the symmetry described by G into the higher dimensional space. The orbits of lattice points under such subgroups, projected into a lower dimensional G -invariant subspace, result in nested point sets, in which each distinct radial level displays G -symmetry. By construction, such point sets have an underlying finite group structure, induced by the higher dimensional embedding. As a first illustration of this approach, an analytical construction is presented, in the case of non-crystallographic symmetries described by finite Coxeter groups. Due to their geometrical interpretation as reflection groups, the orbit of the latter can be characterised using the concepts of root systems and fundamental weights. The convex hull of the projected orbits, constructed with the new method, define ensembles of nested polytopes with non-crystallographic symmetry. These are further characterised in the case of five-fold symmetry in two, three and four dimensions, described, in this context, by the Coxeter groups $H_2 \subseteq H_3 \subseteq H_4$, respectively.

In the case of icosahedral symmetry, the minimal dimension where the cut-and-project construction is possible is six. In particular, the icosahedral group \mathcal{I} leaves three six-dimensional Bravais lattices invariant: the simple cubic, body-centered cubic and face-centered cubic lattices [28]. Therefore, the icosahedral group can be embedded into the point group of these three hypercubic lattices, which is the hyperoctahedral group in six dimensions. The analysis of the subgroup structure of the latter is crucial for the appli-

cations highlighted. Specifically, structural transitions of icosahedral quasicrystals can be characterised by distinct copies H and K of the embedded icosahedral group sharing a common subgroup G . In fact, these can be “connected” via continuous rotations in $SO(6)$, called Schur rotations since Schur’s Lemma is fundamental for their computations, that preserve the symmetry described by G . Schur rotations were first introduced in this context by Kramer [29] for transitions from cubic to aperiodic order. The Schur rotations induce, via the cut-and-project method, continuous transformations between aperiodic structures with icosahedral symmetry, and allow for the identification of the order parameters of the transition. Therefore, the intersections and shared subgroups of the embedded copies of the icosahedral group are analysed in detail here; for this, a new computational method in group theory is introduced, which is based on results of graph theory and their spectra.

It is shown that the crystallographic embedding of the icosahedral group \mathcal{I} can provide blueprints for viral capsid organisation. In particular, the chains of \mathcal{I} -containing subgroups of the hyperoctahedral group are classified, and the results used for the construction of three-dimensional point sets with icosahedral symmetry at different radial levels via the projection of orbits of lattice points under such subgroups. Since the six-dimensional lattice is infinite, a cut-off parameter must be introduced in order to select a finite number of lattice points to which the orbits are computed. This results in a finite library of point sets, that encode different ways in which material can be organised at different radial levels consistent with this group theoretical construction, and that are then compared with the data available on simple viral capsids. Specifically, two case studies are presented, the aforementioned capsids of Pariacoto Virus and Bacteriophage MS2. Via a best-fit procedure, the point sets are selected, which provide constraints on the organisation of these viral capsids, encoding information on the structural organisation of the capsid proteins and the genomic material collectively. These methods can be applied to a wider class of capsids, and these results open up a new link between quasicrystals and viruses. Moreover, they provide for the first time a finite group structure, albeit in a higher dimensional space, underlying the geometry of the multiple layers of material in a virus, which lends itself better for the modeling of its dynamical and physical properties than its infinite dimensional counterpart in the framework of affine extensions.

The thesis is organised as follows. In Chapter 1 a review of the mathematical principles underpinning the structure of quasicrystals and viruses is presented, with particular empha-

sis on non-crystallographic symmetry as a common thread. Chapter 2 contains the analysis of the subgroup structure of the hyperoctahedral group in six dimensions, as a prerequisite to the applications in physics and virology. In Chapter 3, based on these results, structural transitions in quasicrystals, preserving the symmetry described by a maximal subgroup of the icosahedral group, are analysed, by defining and computing the possible icosahedral Schur rotations. In Chapter 4 the new construction of finite nested point sets with non-crystallographic symmetry is presented, and applications in virology are discussed and analysed in Chapter 5.

Chapter 1

An introduction to Quasicrystals and Mathematical Virology

Deep inside us is geometry ... In the external world a perfectly formed snow crystal would never exist. But in our consciousness lies the glittering and flawless knowledge of perfect ice.

P. Høeg, *Miss Smilla's Feeling for Snow*.

In this Chapter we revise the principles underpinning the geometry of viruses and the structure of quasicrystals, emphasising non-crystallographic symmetry (in particular icosahedral symmetry) as the common thread between these topics. We start by reviewing common definitions and notations from Mathematical Crystallography.

1.1 Lattices and non-crystallographic groups

Let $\mathcal{B} = \{\mathbf{b}_i\}_{i=1}^n$ be a basis of \mathbb{R}^n . A *lattice* in \mathbb{R}^n is a \mathbb{Z} -free module of rank n with basis \mathcal{B} :

$$\mathcal{L}(\mathcal{B}) = \left\{ \mathbf{x} = \sum_{i=1}^n m_i \mathbf{b}_i : m_i \in \mathbb{Z} \right\}. \quad (1.1)$$

The matrix $B \in GL(n, \mathbb{R})$, whose columns are given by the components of \mathbf{b}_i with respect to the standard basis of \mathbb{R}^n , is called the *generator matrix* of \mathcal{L} . Any other generator matrix of \mathcal{L} is given by BM , where $M \in GL(n, \mathbb{Z})$, the set of invertible matrices with integral entries [1]. The *Gram matrix* (or metric) of \mathcal{L} is the symmetric matrix $N := B^T B$; \mathcal{L} is *integral* if $N_{ij} \in \mathbb{Z}$, for all i, j , and is characterised (modulo rotations) by N [33].

Let $E(n)$ denote the group of isometries of the Euclidean space \mathbb{R}^n . The symmetry group $\Gamma \subseteq E(n)$ of a lattice \mathcal{L} in \mathbb{R}^n with generator matrix B is the set of all isometries that leave \mathcal{L} invariant. It is a well-known result that Γ contains an infinite group of translations \mathcal{T} , which is normal, abelian and of finite index [34]. Therefore, the quotient group

$$\Gamma/\mathcal{T} \simeq \mathcal{P} := \{Q \in O(n) : \exists M \in GL(n, \mathbb{Z}) : QB = BM\} \quad (1.2)$$

is finite, and it is referred to as the *point group* of \mathcal{L} . The *lattice group* of \mathcal{L} is defined by

$$\Lambda(B) := \{M \in GL(n, \mathbb{Z}) : \exists Q \in \mathcal{P} : M = B^{-1}QB\}, \quad (1.3)$$

which constitutes an *integral representation* of the point group \mathcal{P} in the lattice basis \mathcal{B} . The point group and lattice group of \mathcal{L} are related via the equation

$$\Lambda(B) = B^{-1}\mathcal{P}(B)B. \quad (1.4)$$

Moreover, the following identities hold [33]:

$$\begin{aligned} \mathcal{P}(RB) &= R\mathcal{P}(B)R^{-1}, & \mathcal{P}(BM) &= \mathcal{P}(B), \\ \Lambda(RB) &= \Lambda(B), & \Lambda(BM) &= M^{-1}\Lambda(B)M, \end{aligned} \quad (1.5)$$

where $M \in GL(n, \mathbb{Z})$ and $R \in O(n)$. Following [35], we say that two lattices \mathcal{L} and \mathcal{L}' in \mathbb{R}^n are *equivalent* if and only if the corresponding generator matrices B and B' are related via the identity

$$B' = cRBM, \quad c \in \mathbb{R} \setminus \{0\}, R \in O(n), M \in GL(n, \mathbb{Z}). \quad (1.6)$$

If $c = 1$, then \mathcal{L} and \mathcal{L}' are *congruent*. We point out that, using the relations (1.5), the condition (1.6) is equivalent to the property of conjugation in $GL(n, \mathbb{Z})$ of the lattice groups Λ and Λ' of \mathcal{L} and \mathcal{L}' , respectively [33]. A representative of a class of equivalent lattices is often referred to as a *Bravais lattice* or *Bravais type*.

The notion of lattice symmetry leads to the following:

Definition 1.1.1. *Let G be a (finite) group of isometries acting (irreducibly) on \mathbb{R}^k . G is said to be non-crystallographic in dimension k if it does not leave any lattice invariant in \mathbb{R}^k . Otherwise, it is called crystallographic.*

In other words, G is crystallographic in dimension k if and only if it is the subgroup of the point group of a lattice \mathcal{L} in \mathbb{R}^k . We point out that the property of being crystallographic

is relative to the action of G , i.e. G can be non-crystallographic in \mathbb{R}^k , but leave a lattice invariant in \mathbb{R}^d , with $d \neq k$. This fact is crucial for the study of quasicrystals, as we are going to explain in detail later in this chapter.

The following theorem is a milestone for mathematical crystallography (for the proof see, for example, [2]):

Theorem 1.1.1 (Crystallographic restriction). *Let G be a crystallographic group in two or three dimensions. Then the order of the elements of G must be 1, 2, 3, 4 or 6.*

In particular, five-fold symmetry is forbidden in the plane or space, and therefore any group G containing elements of order 5 cannot be the point group of a two- or three-dimensional lattice. We point out that there exists a generalisation of the crystallographic restriction in higher dimensions [36], which states that the least value n such that a natural number m occur as an element of the point group of a n -dimensional lattice is $n = \Phi(m)$, where Φ is the additive version of the Euler function¹.

1.1.1 Icosahedral symmetry

One of the most important examples of non-crystallographic symmetry is icosahedral symmetry, since it occurs in a very wide range of physical and biological structures. Besides the prominent examples of quasicrystals and viruses discussed in detail later in this chapter, icosahedral symmetry appears in carbon chemistry in the atomic organisation of *fullerenes*, molecules of carbon atoms arranged to form icosahedral cages [38]. The name itself comes from Buckminster Fuller, the creator of the famous geodesic dome, which was designed with an almost-spherical shape with icosahedral symmetry.

For applications in the natural sciences, it is important to distinguish between *chiral* and *achiral* symmetry. In general terms, an object possesses chirality (or handedness) if it does not correspond to its mirror image; otherwise, it is said to be achiral. Chiral icosahedral symmetry is described by the icosahedral group \mathcal{I} , which corresponds to the

¹The Euler function $\varphi(n)$ is the number of integers less than n and relatively prime with respect to n , i.e. with no common divisors. Its additive version Φ is defined as [36, 37]:

$$\Phi(n) = \begin{cases} \varphi(n) & \text{if } n = p^\alpha, \text{ with } p \text{ prime and } \alpha \in \mathbb{N}, \\ \Phi(n_1) + \Phi(n_2) & \text{if } n = n_1 n_2 \text{ and } \text{g.c.d.}(n_1, n_2) = 1. \end{cases}$$

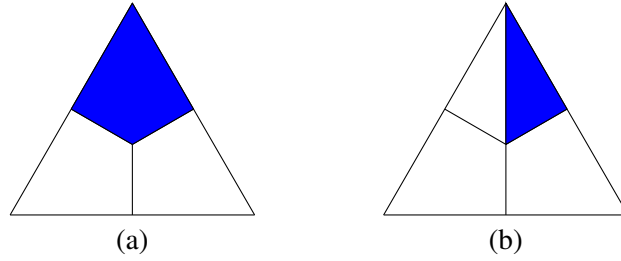


Figure 1.1: Fundamental domains for (a) the icosahedral group \mathcal{I} and (b) the Coxeter group H_3 , corresponding to chiral and achiral icosahedral symmetry, respectively.

set of all the rotations that leave an icosahedron invariant. It has order 60 and it is the largest finite subgroup of the special orthogonal group $\text{SO}(3)$ [1]. It is isomorphic to the alternating group \mathfrak{A}_5 , and has presentation

$$\mathcal{I} = \langle g_2, g_3 : g_2^2 = g_3^3 = (g_2 g_3)^5 = e \rangle,$$

where g_2 and g_3 represent, geometrically, a two- and a three-fold rotation, respectively. The element $g_5 := g_2 g_3$ is a five-fold rotation, hence \mathcal{I} is non-crystallographic in \mathbb{R}^3 .

Achiral icosahedral symmetry is described by the direct product $\mathcal{I} \times \mathbb{Z}_2$, and consists of 120 elements, given by 60 rotations and 60 reflections. It corresponds to the full symmetry group of an icosahedron, and it is isomorphic to the Coxeter group H_3 [39] (cf. Section 4.2 for a review of finite Coxeter groups). The direct product structure implies that the representation theory for H_3 easily follows from that of the icosahedral group \mathcal{I} .

The symmetry properties of an object allow the construction of the whole object starting from a smaller “building unit”. Mathematically, these are formally described by the *fundamental domains* of the group action. Specifically, we have the following [34]:

Definition 1.1.2. *Let G be a group of isometries acting on a metric space X . A fundamental domain for the action of G on X is an open, connected subset $D \subseteq X$ such that $X = \cup_{g \in G} g\overline{D}$, and $gD \cap g'D = \emptyset$, for $g \neq g' \in G$.*

The knowledge of a fundamental domain for the action of a group G is essential for the study of orbits and related polytopes with G -symmetry, as we are going to study in Chapter 4. In Figure 1.1 we show examples of two fundamental domains for icosahedral symmetry (projected into a plane), which are extensively used in virology, as explained in Section 1.3. We point out that these are referred to as *asymmetric units* in the biological literature.

1.2 Quasicrystals

In 1984, Shechtman [3] announced the discovery of an aluminium-manganese alloy whose atomic positions display long-range order and icosahedral symmetry, which is incompatible with translational periodicity. This discovery revolutioned the fields of material science and condensed matter physics: before that, non-crystallographic symmetry was regarded as a “forbidden” symmetry. After an initial scepticism, scientists realised the importance of Shechtman’s work, and new such solids, later called *quasicrystals*, were discovered [40].

Since the discovery of quasicrystals, the mathematical and physical communities have developed new theoretical tools to analyse the properties of these structures. This theory covers broad areas of mathematics and physics and combines elements of solid state physics, discrete geometry, group theory and number theory. In this section we review the basic results that we are going to use throughout this work; for a detailed treatment, we refer to Baake & Grimm [2] and Senechal [37].

1.2.1 Cut-and-project schemes and model sets

In mathematical terms, the arrangement of atoms in a solid is modeled via *infinite point sets* in a Euclidean space. The long-range order is encoded by point sets which are referred to as *Delone sets*, and are defined as follows:

Definition 1.2.1. A point set Λ in \mathbb{R}^n is a Delone set if it satisfies the following properties:

1. It is uniformly discrete, i.e. there exists $r > 0$ such that $|x - y| \geq r$, for all $x, y \in \Lambda$;
2. It is relatively dense, i.e. there exists $R_0 > 0$ such that every ball $B_R(\mathbf{x})$ in \mathbb{R}^n with radius $R \geq R_0$ and centre $\mathbf{x} \in \mathbb{R}^n$ contains at least one point of Λ .

Points of a lattice \mathcal{L} in \mathbb{R}^n form a Delone set, with the additional property that they possess translational periodicity. The atoms of a quasicrystal, on the contrary, are arranged to form Delone sets which are *aperiodic*, and these are referred to as *quasilattices*. The standard way to construct quasilattices is via the so-called *cut-and-project* method. The first approach to such objects was given by Steinhardt *et al.* [4,5]. Later, Moody provided a formal construction of quasilattices using *model sets* [6]; here we review this construction.

Let G be a locally compact Abelian group. A *cut-and-project scheme* is a collection of maps and sets:

$$\begin{array}{ccc} \mathbb{R}^d & \xleftarrow{\pi_1} & \mathbb{R}^d \times G \xrightarrow{\pi_2} G \\ & & \cup \\ & & \mathcal{L} \end{array} \quad (1.7)$$

where \mathcal{L} is a lattice² in $\mathbb{R}^d \times G$, and π_1 and π_2 are surjective projection maps, with the additional assumption that $\pi_1|_{\mathcal{L}}$ is injective and $\pi_2(\mathcal{L})$ is dense in G . \mathbb{R}^d (resp. G) is referred to as the *physical* (resp. *orthogonal*) space.

Let $W \subset G$ be a subset of G satisfying the following conditions:

1. W is non empty and relatively compact, i.e. its closure \overline{W} is a compact set.
2. The boundary ∂W has measure 0 and is such that $\partial W \cap \pi_2(\mathcal{L}) = \emptyset$.

Given a cut-and-project scheme as in (1.7), we define the *model set* $\Sigma(W)$ as

$$\Sigma(W) := \{\pi_1(\mathbf{x}) : \mathbf{x} \in \mathcal{L}, \pi_2(\mathbf{x}) \in W\}. \quad (1.8)$$

Then W is called the (acceptance) *window*. It can be proved that $\Sigma(W)$ thus constructed defines a Delone set in \mathbb{R}^d [6]. We point out that the introduction of the window is crucial, since otherwise the projection of the lattice points into \mathbb{R}^d would not produce a Delone set [2,37]. In Figure 1.2 we give the most common (and one of the very few easily visualisable) example of a one-dimensional model set (the so-called *Fibonacci chain*). Specifically, we consider the simple cubic lattice $\mathcal{L} \simeq \mathbb{Z}^2$ in \mathbb{R}^2 , and we take for \mathbb{R}^d the straight line L with irrational slope parallel to the vector $\mathbf{v} = (1, \frac{1}{\tau})$, where $\tau := \frac{1}{2}(1 + \sqrt{5})$ denotes the golden ratio. The orthogonal space G is then the straight line perpendicular to L , parallel to the vector $\mathbf{v}' = (1, -\tau)$. Due to the irrationality of τ [41], the projections $\pi_1 : \mathcal{L} \rightarrow L$ and $\pi_2 : \mathcal{L} \rightarrow G$ are injective (as can be proved directly by straightforward analytic computations). The window W can be taken as any relatively compact subset of the form $[a, b) \subset G$.

We point out that the model sets defined in (1.8) do not possess any symmetrical properties *a priori*. In this sense, this is the most general definition of quasicrystals, which is purely topological. In most physical applications, however, it is necessary to construct model sets with symmetry described by a non-crystallographic group G . In the next section we review a standard method to achieve this.

²A (generalised) lattice \mathcal{L} in $\mathbb{R}^d \times G$ is a discrete subgroup of $\mathbb{R}^d \times G$ such that $\mathbb{R}^d \times G / \mathcal{L}$ is compact.

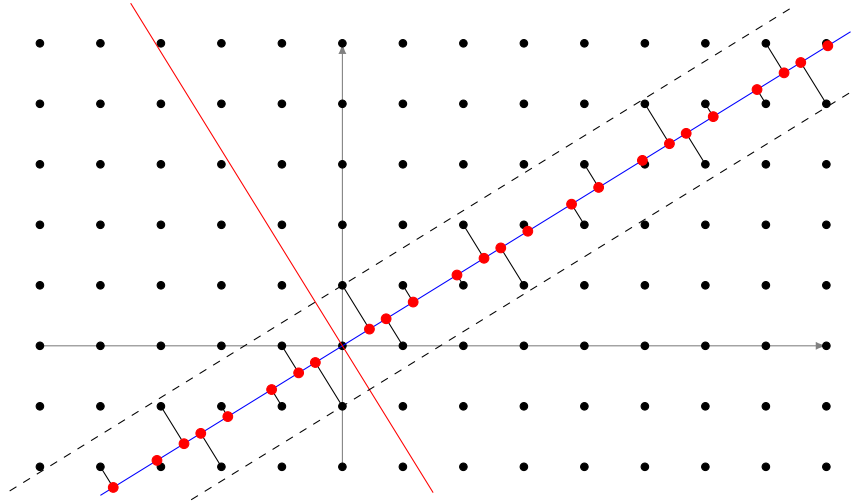


Figure 1.2: Illustration of the cut-and-project method for a one-dimensional model set: the lattice points within the stripe defined by the dashed lines are projected orthogonally onto the blue line (the physical space). The result is an infinite Delone set which is aperiodic.

1.2.2 Crystallographic embedding of non-crystallographic groups

The cut-and-project method relies on the existence of a higher dimensional lattice whose points can be suitably projected to form aperiodic Delone sets. Although it has been proven that the projection formalism is not necessary for the construction of quasicrystals [2, 37], it still remains a fundamental framework, especially for the study of their physical properties. In order to construct quasicrystals with defined symmetry properties via projection, a few concepts from the representation theory of finite groups are needed (cf. [42] for a detailed overview). Specifically, a representation of a finite group G is a homomorphism $\rho : G \rightarrow GL(V)$, where V is a (finite) dimensional vector space over a field \mathbb{K} ; the dimension of V is called the degree of ρ . In the following, we will mainly consider $\mathbb{K} = \mathbb{R}$ or \mathbb{C} and representations that are *faithful*, i.e. injective. In other words, we consider representations of G that are matrix subgroups of $GL(n, \mathbb{K})$.

A representation ρ is *irreducible* if there are no proper G -invariant subspaces of V , otherwise it is *reducible*. A theorem due to Maschke states that any representation $\rho : G \rightarrow GL(V)$ of a finite group G is completely reducible (over \mathbb{C}), i.e. there exists the decomposition

$$V = \bigoplus_k V_k^{\oplus a_k}, \quad V^{\oplus a_k} \equiv \underbrace{V_k \oplus \dots \oplus V_k}_{a_k \text{ times}}, \quad (1.9)$$

in which V_k are irreducible G -invariant subspaces of V , and a_k are non-negative integers. This induces the decomposition of representations:

$$\rho \simeq \bigoplus_k a_k \rho_k, \quad (1.10)$$

where $\rho_k : G \rightarrow GL(V_k)$ are irreducible representations (irreps) of G . The *character* of ρ is the function $\chi_\rho : G \rightarrow \mathbb{K}$ defined by $\chi_\rho(g) := \text{Tr}(\rho(g))$, for $g \in G$, where Tr denotes the trace of $\rho(g)$. Since similar matrices have the same trace, the character does not depend on the basis of V and is constant on the conjugacy classes of G . From (1.10), it follows that

$$\chi_\rho(g) = \text{Tr} \left(\bigoplus_k a_k \rho_k(g) \right) = \sum_k a_k \chi_{\rho_k}(g). \quad (1.11)$$

Hence the decomposition (1.10) of ρ can be determined by means of the character table of G . Moreover, the G -invariant subspaces V_k in (1.9) can be determined using the projection operators $P_k : V \rightarrow V_k^{\oplus a_k}$ given by

$$P_k := \frac{\dim V_k}{|G|} \sum_{g \in G} \overline{\chi_{\rho_k}(g)} \rho(g), \quad (1.12)$$

where $\overline{(\cdot)}$ denotes complex conjugation.

The construction of quasicrystals with non-crystallographic symmetry G via the cut-and-project method relies on an underlying higher dimensional G -invariant lattice. For this, based on [28], we introduce the following:

Definition 1.2.2. *Let $G \subseteq O(k)$ be a finite non-crystallographic group of isometries. A crystallographic representation of G is a matrix group \widetilde{G} satisfying the following conditions:*

- (C1) \widetilde{G} stabilises a lattice \mathcal{L} in \mathbb{R}^d , with $d > k$, i.e. \widetilde{G} is a subgroup of the point group \mathcal{P} of \mathcal{L} ;
- (C2) \widetilde{G} is reducible in $GL(d, \mathbb{R})$ and contains an irreducible representation ρ_k of G of degree k , i.e.

$$\widetilde{G} \simeq \rho_k \oplus \rho', \quad \deg(\rho') = d - k. \quad (1.13)$$

The condition (C1) implies that the matrices representing the elements of \widetilde{G} with respect to a generator matrix B of the lattice are integral or, equivalently, $B^{-1} \widetilde{G} B$ is a subgroup of the lattice group $\Lambda \subseteq GL(d, \mathbb{Z})$ of \mathcal{L} (cf. (1.3)). As a consequence, the character

$\chi_{\widetilde{G}}$ is an integer-valued function. The condition **(C2)** is necessary for the construction of quasicrystals in \mathbb{R}^k via the cut-and-project method.

The minimal dimension $d > k$ for which a crystallographic representation Γ of G is possible is called the *minimal crystallographic dimension* of G . The conditions $\chi_{\Gamma} \in \mathbb{Z}$ and (1.13) can be easily verified with the aid of the character table of G and formula (1.11). The existence, and possibly an explicit construction, of lattices in \mathbb{R}^d whose point group contains a crystallographic representation of G is a more difficult task. In the case of icosahedral symmetry, the minimal crystallographic dimension is six and the lattices in \mathbb{R}^6 have been classified in [28] (this is explained in more detail in Section 2.1). For planar non-crystallographic symmetries described by the dihedral groups \mathcal{D}_{2n} , the minimal crystallographic dimension is $\varphi(n)$, the Euler function of n . We will go back to this example in Section 4.2.2.

Let \widetilde{G} be a crystallographic representation of G of degree d . Let us denote by $V^{(k)}$ the invariant subspace of \mathbb{R}^d which carries the irrep ρ_k . Let $P_k : \mathbb{R}^d \rightarrow V^{(k)}$ be the projection into $V^{(k)}$ given by (1.12). Having fixed a basis of V_k , P_k can be represented as a $k \times d$ matrix, which we denote by $\pi^{(k)}$, that makes the diagramme

$$\begin{array}{ccc} \mathbb{R}^d & \xrightarrow{\widetilde{G}(g)} & \mathbb{R}^d \\ \downarrow \pi^{(k)} & & \downarrow \pi^{(k)} \\ V^{(k)} & \xrightarrow{\rho_k(g)} & V^{(k)} \end{array} \quad (1.14)$$

commute for all $g \in G$, i.e.

$$\pi^{(k)}(\widetilde{G}(g)\mathbf{v}) = \rho_k(g)(\pi^{(k)}(\mathbf{v})), \quad \forall g \in G, \forall \mathbf{v} \in \mathbb{R}^d. \quad (1.15)$$

Let $V^{(d-k)}$ denote the orthogonal complement of $V^{(k)}$ in \mathbb{R}^d , and $\pi^{(d-k)} : \mathbb{R}^d \rightarrow V^{(d-k)}$ the corresponding projection. We recall the following Proposition (for the proof, see [37], page 55):

Proposition 1.2.1. *If \mathcal{L} is an integral lattice, then the following are equivalent:*

1. $\pi^{(d-k)}(\mathcal{L})$ is dense in $V^{(d-k)}$;
2. $V^{(d-k)}$ is totally irrational, i.e. $V^{(d-k)} \cap \mathcal{L} = \{0\}$;
3. $\pi^{(k)}|_{\mathcal{L}}$ is injective.

If \mathcal{L} is not integral, then condition 1 in Proposition 1.2.1 is replaced by $V^{(d-k)} \cap \mathcal{L}^* = \{0\}$, where \mathcal{L}^* denotes the *dual* of \mathcal{L} , defined as

$$\mathcal{L}^* := \{\mathbf{y} \in \mathbb{R}^d : \langle \mathbf{y}, \mathbf{x} \rangle \in \mathbb{Z}, \forall \mathbf{x} \in \mathcal{L}\}.$$

With these tools, we can define the cut-and-project scheme (cf. (1.7)):

$$\begin{array}{c} \mathbb{R}^k \xleftarrow{\pi^{(k)}} V^{(k)} \oplus V^{(d-k)} \xrightarrow{\pi^{(d-k)}} V^{(d-k)} \\ \cup \\ \mathcal{L} \end{array} \tag{1.16}$$

In order to construct the associated model set, the standard choice for the window is the projection into the orthogonal space of the *Voronoi cell* of the origin, defined by

$$\mathcal{V}(\mathbf{0}) := \{\mathbf{x} \in \mathbb{R}^d : |\mathbf{x} - \mathbf{y}| \geq |\mathbf{x}|, \forall \mathbf{y} \in \mathcal{L}\}. \tag{1.17}$$

In other words, $\mathcal{V}(\mathbf{0})$ consists of all points which are closest to the origin with respect to any other lattice points. Letting $W := \pi^{(d-k)}(\mathcal{V}(\mathbf{0}))$, we define the model set

$$\Sigma(W) = \{\pi^{(k)}(\mathbf{x}) : \pi^{(d-k)}(\mathbf{x}) \in W, \mathbf{x} \in \mathcal{L}\}. \tag{1.18}$$

It follows from (1.15) that the model set $\Sigma(W)$ thus defined is invariant under the group G , and hence displays non-crystallographic symmetry.

1.2.3 Tilings

Tiling theory is the art of creating partitions of a space using a countable number of shapes, called *tiles*. Besides its artistic value, it has attracted considerable interest by scientists for its applications in the natural sciences. The mathematical theory of tilings roots back to the work of Kepler in his book *Harmonices Mundi*, where tilings by regular polygons are introduced [43]. In 1974, Penrose [10] described aperiodic tilings of the plane with five-fold symmetry, which are since then known as *Penrose tilings*. It is remarkable that these mathematical constructions were analysed years before the discovery of quasicrystals by Shechtman. In the last years, tiling theory has become an important branch of pure and applied mathematics; here we are interested in the construction of tilings based on model sets created via the cut-and-project method. In Section 1.3.2 we show how tilings play a crucial role in virology.

A formal definition of a tiling of a Euclidean space is the following:

Definition 1.2.3. A tiling \mathcal{T} of \mathbb{R}^n is a countably family of closed sets $\mathcal{T} = \{T_n\}_{n=0}^\infty$ with the properties that:

1. $\text{int}(T_i) \cap \text{int} T_j = \emptyset$, for $i \neq j$, where int denotes the interior of a set;
2. $\bigcup_{n=1}^\infty T_n = \mathbb{R}^n$.

A tiling \mathcal{T} is said to be *normal* if for every tile $T_i \in \mathcal{T}$ there exist positive numbers r_0 and R_0 such that (i) T_i contains a ball of radius r_0 and (ii) is contained in a ball of radius R_0 . In problems arising from crystallography, tilings usually consist of copies of a finite set of tiles, called *prototiles*, together with a set of rules that encode the construction of the whole tiling, denoted as *matching rules*. In the following, we will only consider tilings whose prototiles are homeomorphic to a n -dimensional ball.

Let $\Sigma(W)$ be a model set in \mathbb{R}^n (cf. (1.8)). There are two natural tilings associated with $\Sigma(W)$: the Voronoi tiling and the Delone tiling. The former consists of the union of all the Voronoi cells $\mathcal{V}(\mathbf{x})$ of each point $\mathbf{x} \in \Sigma(W)$ (compare with (1.17)):

$$\mathcal{V}(\Sigma(W)) := \bigcup_{\mathbf{x} \in \Sigma(W)} \mathcal{V}(\mathbf{x}), \quad \mathcal{V}(\mathbf{x}) = \{\mathbf{y} \in \mathbb{R}^n : |\mathbf{y} - \mathbf{x}| \leq |\mathbf{x}_0 - \mathbf{x}|, \forall \mathbf{x}_0 \in \Sigma(W)\}.$$

The tiling thus obtained will in general be made up of an infinite set of prototiles (since any two Voronoi cells are in general not alike), but it is normal, since $\Sigma(W)$ is a Delone set (cf. Definition 1.2.1) [37].

The Delone tiling induced by $\Sigma(W)$ is the “dual” of the Voronoi tiling, in the sense that its tiles are centered at the vertices of the Voronoi tiles. Specifically, let \mathbf{v} be a vertex of the Voronoi tiling $\mathcal{V}(\Sigma(W))$. Let $S(\mathbf{v})$ denote the *vertex star* of \mathbf{v} , i.e. the set of all tiles in $\mathcal{V}(\Sigma(W))$ that have \mathbf{v} as a vertex:

$$S(\mathbf{v}) := \{T \in \mathcal{V}(\Sigma(W)) : T \cap \mathbf{v} \neq \emptyset\}.$$

By construction, the set $S(\mathbf{v}) \cap \Sigma(W)$ is not empty. The Delone tiling is then given by

$$\bigcup_{\mathbf{v} \in \mathcal{V}(\Sigma(W))} \text{Conv}(S(\mathbf{v}) \cap \Sigma(W)),$$

where $\text{Conv}(S(\mathbf{v}) \cap \Sigma(W))$ denotes the convex hull of $S(\mathbf{v}) \cap \Sigma(W)$, i.e. the smallest convex set that contains $S(\mathbf{v}) \cap \Sigma(W)$.

If $\Sigma(W)$ is constructed via the cut-and-project method into a space invariant under a non-crystallographic group G (cf. (1.18)), the corresponding Voronoi and Delone tilings

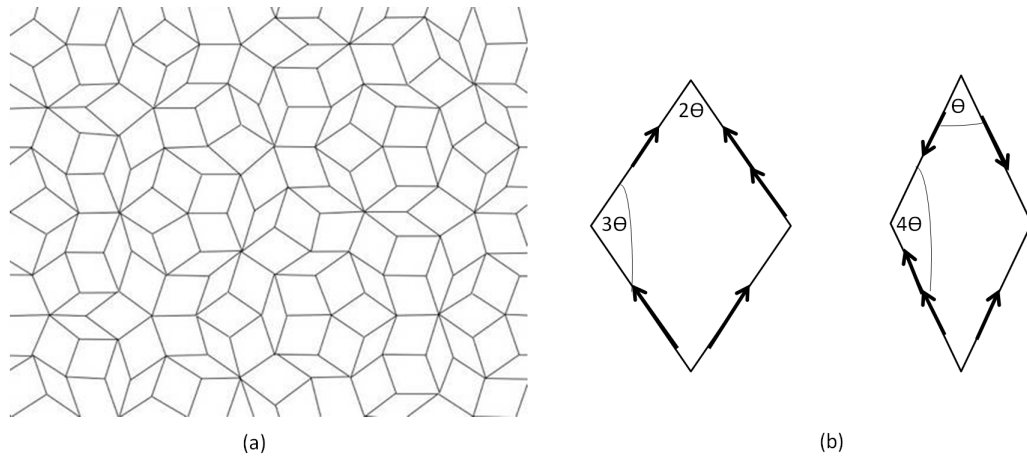


Figure 1.3: Aperiodic tilings. (a) A patch of a Penrose tiling of the plane, and (b) the corresponding rhombic prototiles with matching rules indicated by arrows ($\theta = \frac{\pi}{5}$).

possess G symmetry [37]. In particular, it can be proved that Penrose tilings of the plane can be obtained from projection of points of the simple cubic lattice in five dimensions [2, 37].

1.3 Mathematical Virology

Viruses are micro-organisms that infect every type of life form. Most viruses are made up of a protein shell, called *capsid*, that protects the viral genomic material (RNA or DNA) inside. Experimental observations have shown that viral capsids are, in most cases, almost spherical objects and possess icosahedral symmetry [7]; in particular, they exhibit 15 two-fold, 10 three-fold and 6 five-fold discrete rotational symmetry axes [44]. Their surface consists of clusters of protein subunits, called *capsomers*, appearing in groups of three, five or six centered at the symmetry axes of the virus (see Figure 1.4). The symmetry properties of capsids imply that their structures are highly ordered, and therefore mathematical arguments can be applied to predict information regarding the locations of capsid proteins.

Viruses and quasicrystals share symmetry properties, in particular non-crystallographic symmetry. Therefore, from a mathematical point of view, principles from the theory of quasicrystals can provide information on the structure of viral capsids. In this sense, group theory and tiling theory play a crucial role, as we are going to discuss in this section.

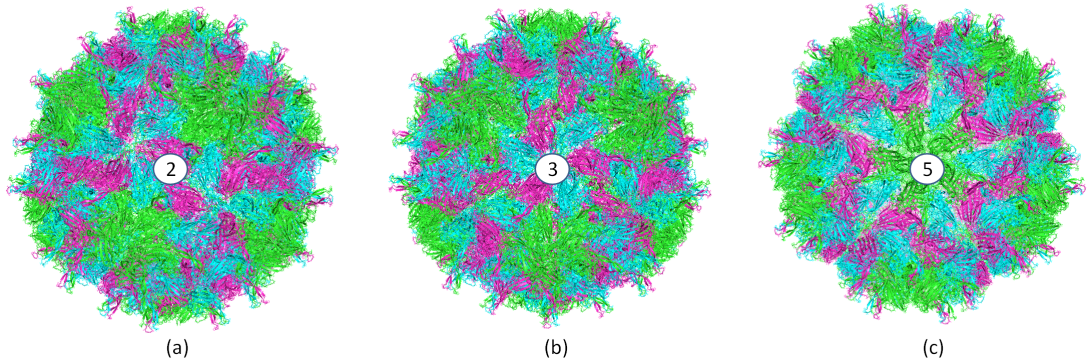


Figure 1.4: Viral symmetry. Outside view of the capsid of Pariacoto Virus (PaV), seen along (a) two-fold, (b) three-fold and (c) five-fold symmetry axis.

1.3.1 Caspar-Klug theory

The first mathematical model for viral capsid architecture was introduced by Caspar and Klug in 1962. In their seminal paper [8], they present a theory to describe and predict the locations and general orientations of the capsid proteins. Inspired by the structure of Buckminster Fuller’s geodesic dome, they derive a series of polyhedra with icosahedral symmetry by embedding an icosahedral net into a hexagonal lattice. Here we review this construction.

Let $\mathbf{b}_1, \mathbf{b}_2$ be a basis of the two-dimensional hexagonal lattice. A point of the lattice can then be written as $\mathbf{x} = h\mathbf{b}_1 + k\mathbf{b}_2 \equiv (h, k)$, with $h, k \in \mathbb{Z}$ (cf. (1.1)). Having chosen the point \mathbf{x} , the embedding of the icosahedral net is achieved by requiring that vertices of the triangles of the net meet the centres of the hexagons of the lattice. Therefore, we construct an equilateral triangle having $\mathbf{0}$ and \mathbf{x} as vertices (see Figure 1.5). By subdividing the hexagons into triangles, one obtains a triangulation of the icosahedral net compatible with icosahedral symmetry. The *triangulation number* T is defined as the number of triangles each face of the net is divided into, and it is given by

$$T := \frac{\text{area of the face}}{\text{area of the small triangle}} = \frac{\frac{\sqrt{3}}{4}|\mathbf{x}|^2}{\frac{\sqrt{3}}{4}} = |\mathbf{x}|^2 = h^2 + hk + k^2.$$

The polyhedra obtained from this construction, known as *icosideltahedra*, are made up of $20T$ faces, $30T$ edges and, by Euler’s formula, $10T + 2$ vertices. The blueprints for the capsid are obtained by placing a protein in each corner of each triangular face (this is called, in this context, the *decoration* of the tiles): thus the total number of proteins is $60T$.

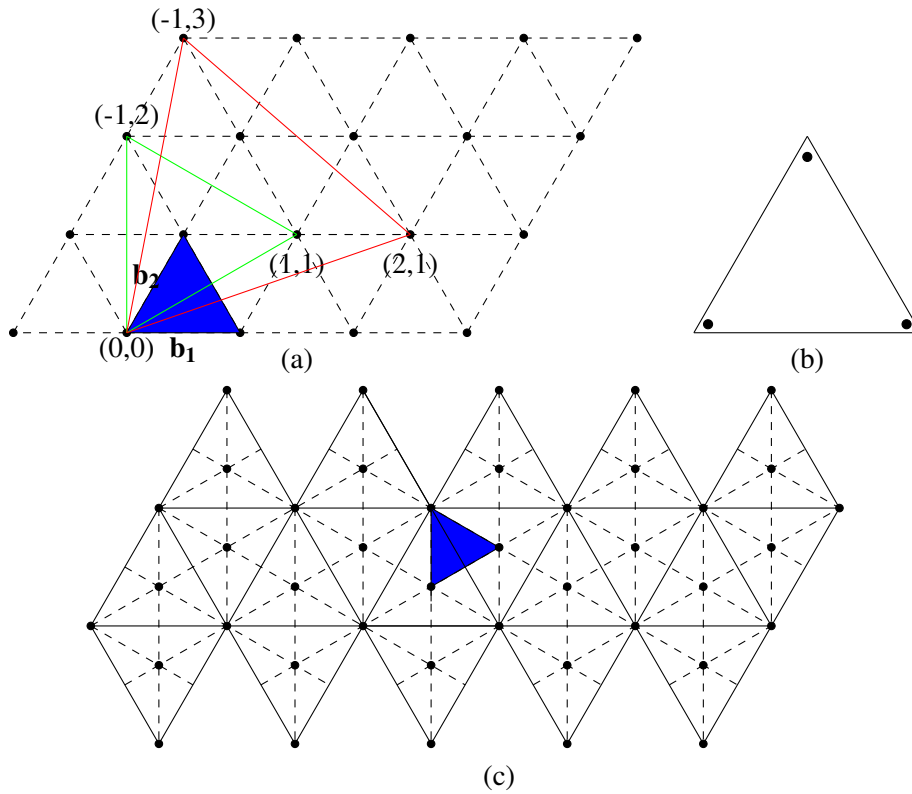


Figure 1.5: Construction of the Caspar-Klug icosideltahedra. (a) Examples of two triangulations obtained by embedding an icosahedral net into a hexagonal lattice: $T = 3$ (green, an achiral case) and $T = 7$ (red, a chiral example of laevo type); the tessellation is induced by the subdivision into smaller triangles (highlighted in blue). (b) Decoration of the triangles: the dots represent the positions of three protein subunits. (c) The resulting tiling of the icosahedral surface for a $T = 3$ triangulation.

Due to the requirement that vertices of the icosahedral grid meet vertices of the hexagonal lattice, Caspar-Klug theory predicts the locations of 12 pentamers (clusters of five protein subunits), situated on the five-fold axes of the grid, and $10(T - 1)$ hexamers (clusters of six protein subunits) elsewhere.

We notice that when the point $\mathbf{x} \equiv (h, k)$ lies either on the line bisecting the triangular face identified by the lattice vectors \mathbf{b}_1 and \mathbf{b}_2 , or is a multiple of \mathbf{b}_1 or \mathbf{b}_2 , then the corresponding tessellations are achiral, i.e. they are invariant under reflections and possess full icosahedral symmetry. Instead, all the other tilings of the icosahedral surface induced by the point \mathbf{x} are chiral, i.e. they possess a mirror image. Hence, there exists two dis-

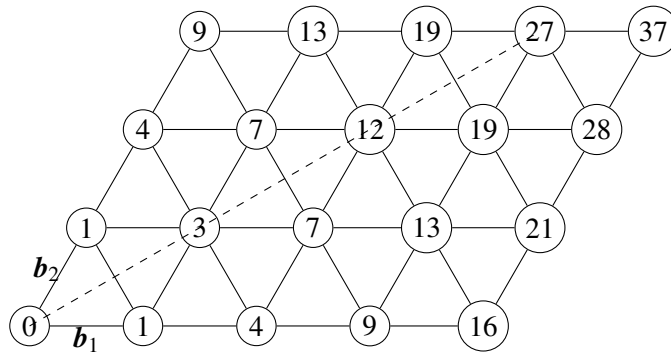


Figure 1.6: Possible T -numbers in the Caspar-Klug classification: tessellations corresponding to T -numbers not lying on the axes identified by the lattice basis or the bisecting line (dashed) have a mirror image.

tinct tessellations with the same T -number, which correspond to the two case $h > k > 0$ and $k > h > 0$, denoted by *laevo* and *dextro*, and indicated by an “l” and a “d” after the T -number, respectively (see Figure 1.6).

1.3.2 Viral tiling theory

Although Caspar-Klug theory predicts the locations of capsid proteins for a large class of viruses correctly, there is a significant number of cases that fall out of this framework. An example is the capsid of Simian Virus 40, which consists of 72 pentamers arranged into a $T = 7l$ icosahedral surface (see Figure 1.7 (a)). According to Caspar-Klug theory, the capsid would be made up of 420 proteins, instead of the 360 actually observed. The problem is that the $T = 7$ triangulation of the icosahedral surface predicts the correct location of the proteins, but not the right type, i.e. predicting hexamers instead of pentamers. The conundrum of the structure of Simian Virus 40 was posed by Liddington [45]: “The puzzle is how do the coloured pentamers (clusters of five) fit into the hexavalent holes?”.

In order to solve this structural puzzle, Twarock [9] proposed a generalisation of Caspar-Klug theory based on tiling theory. Specifically, the requirement that the surface of the capsid is subdivided into triangles is relaxed, allowing for more general tessellations of the icosahedral net, which still retain overall icosahedral symmetry, similar to the Penrose tilings of the plane (cf. Figure 1.3). The locations of the proteins in the capsid are then identified by placing a protein subunit in any tile only at corners around five-connected

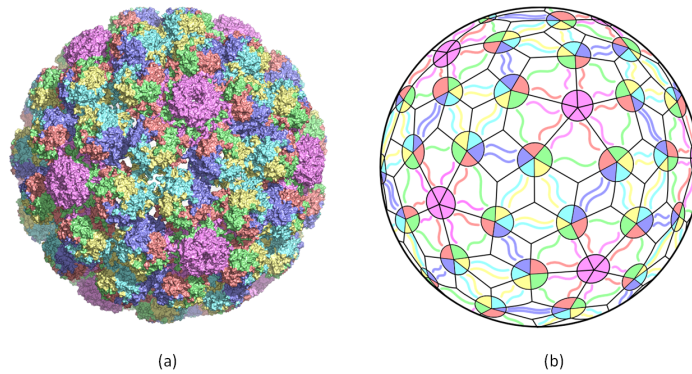


Figure 1.7: Viral Tiling Theory. (a) The capsid of Simian Virus 40, and (b) the associated tessellation. Different colours correspond to different protein positions according to icosahedral symmetry (adapted from [9]).

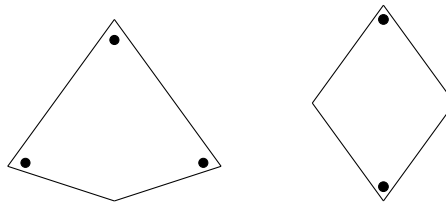


Figure 1.8: Prototiles for the tiling of Simian Virus 40 with decorations: black dots represent the location of the protein subunits.

vertices. In Figure 1.7 (b) the tessellation for Simian Virus 40 is shown, and the tiles and locations of the proteins are given in Figure 1.8. Caspar and Klug's icosideltahedra correspond, in this framework, to tessellations of the icosahedral surface consisting of regular triangles.

These first examples opened up a new chapter in virology, known as *Viral Tiling theory*, which has since its introduction provided blueprints for a wide class of viral capsids, in particular for the families of *Polyoma*- and *Papillomaviridae* [46], and new insights for viral assembly [47] and normal mode analysis of viral capsids [48]. Moreover, it has paved the way for the use of the mathematical principles underpinning quasicrystals in virology. Indeed, Keef *et al.* [18] showed that the tilings for this family of viruses can be obtained via the construction of quasilattices with icosahedral symmetry, based on the affine extensions of H_3 introduced in [49]. Specifically, icosahedral symmetry is extended via the addition

of an affine reflection to the generators of H_3 , as a result of the extension of the Cartan matrix of the root system of H_3 (cf. Section 4.2 for a review of these concepts), similar to the theory of Kac-Moody algebras [20]. More recently, Salthouse [11] constructed three-dimensional icosahedral tilings via the cut-and-project method, that provide information on the three-dimensional geometry of viral capsids.

1.3.3 Beyond Caspar-Klug: affine extensions of the icosahedral group

Caspar-Klug theory and generalisations thereof describe the capsid of a virus as a two-dimensional object rather than in the three-dimensional space. Therefore, they do not provide information about other important features of the capsid, such as its thickness and the organization of the genomic material encapsulated inside. Experiments showed that many viruses exhibit order at different radial levels: examples are the dodecahedral cage of RNA observed in Pariacoto Virus [15] and the double-shell structure of MS2 [16]. These results suggest that symmetry techniques should be developed to include information on the capsid proteins and the packaged genome collectively.

A first step towards this purpose was the introduction of *affine extensions* of non-crystallographic groups. In general terms, such extensions are obtained via the addition of a non-compact operator (a translation) to the group generators. We already mentioned in Section 1.3.2 that affine extensions of non-crystallographic groups can be constructed via the Kac-Moody algebras formalism. However, this approach is too restrictive for applications in virology; for this reason, new affine extensions were introduced in a series of papers by Keef, Wardman *et al.* [17–19,50]. In this section we summarise this construction.

Let G be a non-crystallographic group in \mathbb{R}^k , and let $O_G(\mathbf{v})$ be the orbit of $\mathbf{v} \in \mathbb{R}^k$ under G . Let $\mathbf{w} \in \mathbb{R}^k$ and let $T_{\mathbf{w}} : \mathbb{R}^k \rightarrow \mathbb{R}^k$ be the translation operator given by $T_{\mathbf{w}}(\mathbf{u}) = \mathbf{u} + \mathbf{w}$, for all $\mathbf{u} \in \mathbb{R}^k$. The operator $T_{\mathbf{w}}$ is said to be an *admissible translation* if there exist (at least) two points $\mathbf{u}_1, \mathbf{u}_2 \in O_G(\mathbf{v})$ such that $T_{\mathbf{w}}(\mathbf{u}_1)$ and $T_{\mathbf{w}}(\mathbf{u}_2)$ are located along some symmetry axes identified by G . The resulting affine group $G^{(\text{aff})}$ is defined by

$$G^{(\text{aff})} := \{(g, T_{\mathbf{w}}) : g \in G\},$$

with multiplication given by

$$(g_1, T_{\mathbf{w}}) \circ (g_2, T_{\mathbf{w}}) = (g_1 g_2, T_{g_1 \mathbf{w} + \mathbf{w}}). \quad (1.19)$$

The orbit $O_{G^{(\text{aff})}}(\mathbf{v})$ is an infinite point set which is dense in \mathbb{R}^k , since the group G is non-crystallographic in \mathbb{R}^k . For applications in virology or carbon chemistry, finite subsets of these point sets must be selected, since viral capsids and carbon molecules are finite objects. Indeed, let us define the set $\mathcal{M}^{(m)}(G, T_{\mathbf{w}})$ of all the monomials (i.e. words in the group) obtained by applying exactly $m > 0$ translations:

$$\mathcal{M}^{(m)}(G, T_{\mathbf{w}}) = \{\tilde{g} \in G^{(\text{aff})} : \tilde{g} = (g^{(1)}, T_{\mathbf{w}}) \circ \dots \circ (g^{(m)}, T_{\mathbf{w}}), g^{(i)} \in G, i = 1, \dots, m\}. \quad (1.20)$$

Let $n > 0$, and let $\mathbf{v} \in \mathbb{R}^k$. We define the set of all the points obtained from the action on \mathbf{v} of all the monomials of $G^{(\text{aff})}$ of order $m \leq n$:

$$Q(n) := \{\mathcal{M}^{(m)}(G, T_{\mathbf{w}})(\mathbf{v}) : m \leq n\}. \quad (1.21)$$

The parameter n is called the *cut-off parameter* for the orbit of the affine extension $G^{(\text{aff})}$, and limits the number of monomials in the affine group. The set $Q(n)$ in (1.21) is a finite nested point set, each radial level displaying non-crystallographic symmetry described by G . In Figure 1.9 we provide an example of this principle in the case of five-fold symmetry in the plane.

In the case of icosahedral symmetry, the affine extensions of the icosahedral group \mathcal{I} have been classified in [17]. In Figure 1.10 (a) we provide an example of a point set thus obtained. Each radial level displays icosahedral symmetry, and hence these point sets are suitable to rationalise viral capsid architecture by providing information on the capsid proteins and the material inside collectively. For a demonstration of this based on a number of case studies covering viruses of different T -numbers, we refer the reader to [19]. In Figure 1.10 (b) we show the example of the capsid of Pariacoto Virus; we will study the structure of this virus in detail in Chapter 5.

The introduction of a cut-off parameter, necessary to obtain a finite point set $Q(n)$ as in (1.21), implies the loss of an underlying algebraic structure to $Q(n)$. Specifically, the set of all monomials of order m in (1.20) is not, in general, a group, since it is not closed under the operation \circ of $G^{(\text{aff})}$ defined in (1.19). In Chapter 4 we will describe a new method for the construction of nested point sets with non-crystallographic symmetry, that is derived from the projection of orbits of crystallographic embedding of non-crystallographic groups, and demonstrate in Chapter 5 how this new group theoretical setup can be applied to viral capsid architecture.

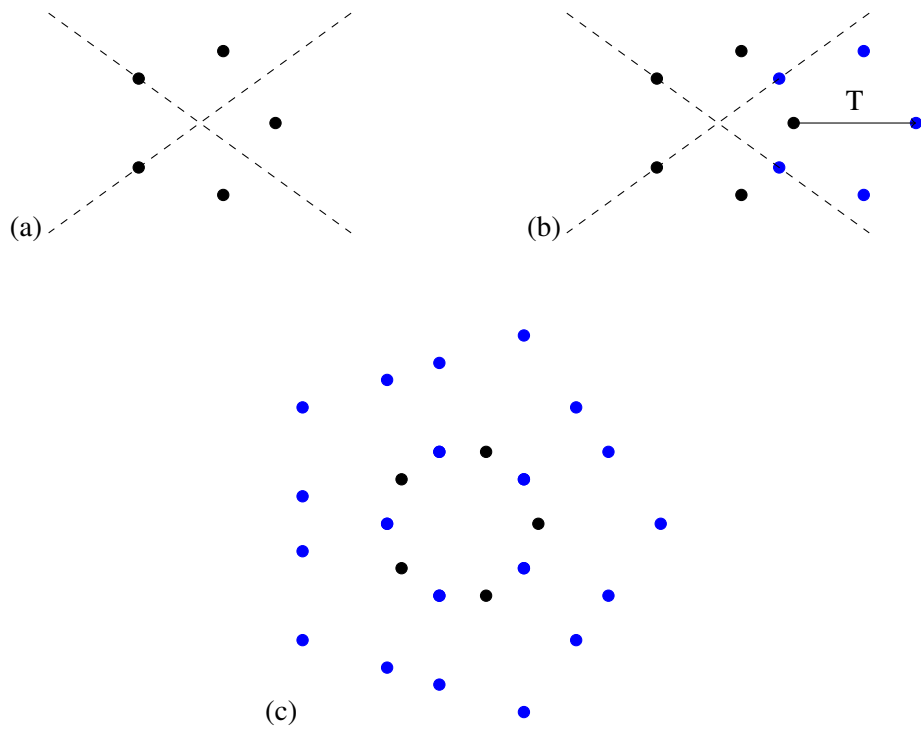


Figure 1.9: Planar example of affine extensions of five-fold symmetry. The orbits of the point $(1,0)$ under cyclic group \mathbb{Z}_5 in (a) is extended via a translation T along the vector $\nu = (\tau, 0)$ in (b). The resulting point set in (c) consists of different radial levels, each possessing five-fold symmetry.

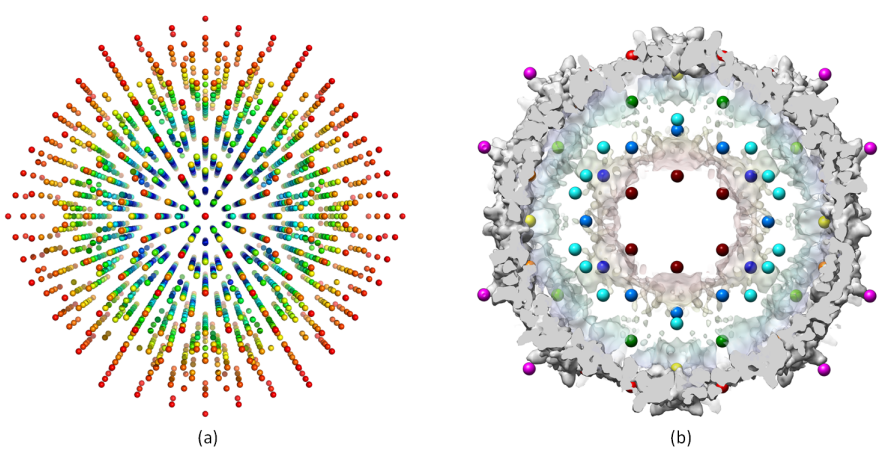


Figure 1.10: Affine extended groups provide structural constraints on virus architecture. (a) Example of a point set obtained via affine extensions of the icosahedral group. (b) Section of the capsid of Pariacoto Virus: the points, derived from icosahedral affine extensions, provide constraints on the overall capsid geometry (adapted from [19]).

Chapter 2

On the subgroup structure of the hyperoctahedral group in six dimensions

Only connect!

E. M. Forster, *Howards End*.

In Chapter 1 it was shown that icosahedral symmetry is fundamental for understanding the structure of quasicrystals and viral capsids. Since the icosahedral group \mathcal{I} is non-crystallographic in the three-dimensional space, the construction of quasilattices with icosahedral symmetry with the projection formalism reviewed in Section 1.2.1 requires a crystallographic embedding of \mathcal{I} . In Section 2.1 we show, following [28], that the minimal crystallographic dimension of \mathcal{I} is six, and construct an explicit crystallographic representation of \mathcal{I} , subgroup of the hyperoctahedral group in six dimensions, which is the point group of the three hypercubic lattices in \mathbb{R}^6 . We then provide a classification of such representations, and in Section 2.2 we analyse their intersections and shared subgroups, thus paving the way for the study of structural transitions of icosahedral quasicrystals with the Schur rotation approach described in Chapter 3. For this purpose, we present a new computational group theoretical method, based on graphs and their spectra.

2.1 Crystallographic embedding of the icosahedral group

Let $\tau := \frac{1}{2}(1 + \sqrt{5})$ denote the golden ratio, and let $\tau' := 1 - \tau$ be its Galois conjugate¹.

The character table of the icosahedral group \mathcal{I} is given by (cf. [1]):

Irrep	E	$C(g_5)$	$C(g_5^2)$	$C(g_2)$	$C(g_3)$
A	1	1	1	1	1
T_1	3	τ	τ'	-1	0
T_2	3	τ'	τ	-1	0
G	4	-1	-1	0	1
H	5	0	0	1	-1

where $g_5 := g_2 g_3$ is a five-fold rotation, and $C(g)$ denotes the conjugacy class of g . The notation A , T_1 , T_2 , G and H for the irreps of \mathcal{I} is standard in the crystallographic literature. The two three-dimensional irreps T_1 and T_2 represent the standard action of \mathcal{I} as a finite subgroup of $SO(3)$, and their characters have irrational values, in accordance with the crystallographic restriction. We note that $\tau + \tau' = 1$ and hence, using (1.11), the representation $T_1 \oplus T_2$ has integer characters and contains a three-dimensional irrep of \mathcal{I} . A straightforward geometrical argument allows for an explicit construction of a six-dimensional crystallographic representation of \mathcal{I} . Indeed, let $\{\hat{e}_i\}_{i=1}^6$ be the unit vectors pointing to the six five-fold axes of an icosahedron (see Figure 2.1 (a)). The generators of \mathcal{I} act on these vectors by permuting them and in some cases also changing their sign. In particular, with reference to Figure 2.1 (b), we obtain the following representation $\tilde{\mathcal{I}}$ of \mathcal{I} :

$$\tilde{\mathcal{I}}(g_2) = \begin{pmatrix} 0 & 0 & 0 & 0 & 0 & 1 \\ 0 & 0 & 0 & 0 & 1 & 0 \\ 0 & 0 & -1 & 0 & 0 & 0 \\ 0 & 0 & 0 & -1 & 0 & 0 \\ 0 & 1 & 0 & 0 & 0 & 0 \\ 1 & 0 & 0 & 0 & 0 & 0 \end{pmatrix}, \quad \tilde{\mathcal{I}}(g_3) = \begin{pmatrix} 0 & 0 & 0 & 0 & 0 & 1 \\ 0 & 0 & 0 & 1 & 0 & 0 \\ 0 & -1 & 0 & 0 & 0 & 0 \\ 0 & 0 & -1 & 0 & 0 & 0 \\ 1 & 0 & 0 & 0 & 0 & 0 \\ 0 & 0 & 0 & 0 & 1 & 0 \end{pmatrix}. \quad (2.1)$$

We have $\tilde{\mathcal{I}} \subseteq GL(6, \mathbb{Z})$, and $\chi_{\tilde{\mathcal{I}}}(g_2) = -2$ and $\chi_{\tilde{\mathcal{I}}}(g_3) = 0$, so that, with reference to the character table of \mathcal{I} , we have $\chi_{\tilde{\mathcal{I}}} = \chi_{T_1} + \chi_{T_2}$, which implies (cf. (1.11)) that $\tilde{\mathcal{I}} \simeq T_1 \oplus T_2$ in $GL(6, \mathbb{R})$. Therefore, $\tilde{\mathcal{I}}$ is a crystallographic representation of \mathcal{I} . Hence, according to Definition 1.2.2, the minimal crystallographic dimension of \mathcal{I} is six².

¹Note that τ and τ' are the two solutions of the equation $x^2 = x + 1$.

²In fact, there exist four dimensional lattices stabilised by \mathcal{I} , classified in [51]. However, the representation induced by this action is isomorphic to the irrep G , hence it is not possible, using these 4D lattices, to construct 3D quasicrystals with the cut-and-project method. Therefore in the following we neglect these lattices.

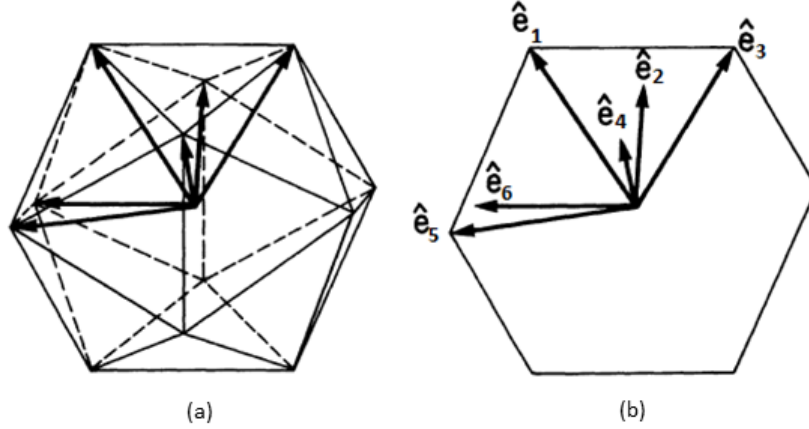


Figure 2.1: An icosahedron, adapted from [28]: (a) the vectors highlighted correspond to the six five-fold axes, which can be “lifted” to form a basis of the simple cubic lattice in six dimensions; (b) projection onto a plane perpendicular to a two-fold axis, showing our labeling convention of the five-fold axes, necessary for the construction of a crystallographic representation of the icosahedral group.

The lattices in \mathbb{R}^6 left invariant by \mathcal{I} have been classified in [28]. There are three inequivalent Bravais lattices of this type, the simple cubic (SC), body-centered cubic (BCC) and face-centered cubic (FCC) lattices (known as the hypercubic lattices) given by, respectively:

$$\begin{aligned}\mathcal{L}_{SC} &= \{\mathbf{x} = (x_1, \dots, x_6) : x_i \in \mathbb{Z}\}, \\ \mathcal{L}_{BCC} &= \left\{ \mathbf{x} = \frac{1}{2}(x_1, \dots, x_6) : x_i \in \mathbb{Z}, x_i = x_j \pmod{2}, \forall i, j = 1, \dots, 6 \right\}, \\ \mathcal{L}_{FCC} &= \left\{ \mathbf{x} = \frac{1}{2}(x_1, \dots, x_6) : x_i \in \mathbb{Z}, \sum_{i=1}^6 x_i = 0 \pmod{2} \right\}.\end{aligned}$$

A basis of the SC lattice is the standard basis of \mathbb{R}^6 . Its point group is given by (cf. (1.2))

$$\mathcal{P}_{SC} = \{Q \in O(6) : Q = M \in GL(6, \mathbb{Z})\} = O(6) \cap GL(6, \mathbb{Z}) \simeq O(6, \mathbb{Z}), \quad (2.2)$$

which is the *hyperoctahedral group* in six dimensions, denoted by B_6 [52]. All three lattices have point group B_6 , whereas their lattice groups are different and, indeed, are not conjugate in $GL(6, \mathbb{Z})$ [28]. Notice that $\tilde{\mathcal{I}}$ in (2.1) is a subgroup of B_6 .

In the remainder of this section we are interested in a classification of the crystallographic representations of \mathcal{I} . For this purpose, we need to investigate the subgroup structure of the hyperoctahedral group. This group is quite large (it has order $2^6 6! = 46,080$),

and we are therefore making use of the software GAP [53], which is designed for problems in computational group theory [54]. Therefore, we need to be able to generate B_6 and obtain a permutation representation of it, i.e. embed B_6 into a suitable permutation group. This is possible since, by Cayley's Theorem [55], every finite group is isomorphic to a subgroup of a permutation group. This choice is convenient for computational purposes, since it is often easier to work with permutation rather than matrix groups. In the following section we briefly revise previous work on the representations of B_6 based on [52].

2.1.1 Representations of the hyperoctahedral group B_6

It follows from (2.2) that B_6 consists of all the orthogonal integral matrices. A matrix $C = (c_{ij})$ of this kind must satisfy $CC^T = I_6$, the 6×6 identity matrix, and have integral entries only. Since

$$(CC^T)_{ij} = \sum_{k=1}^6 c_{ik}(c_{kj})^T = \sum_{k=1}^6 c_{ik}c_{jk},$$

the condition $CC^T = I_6$ is equivalent to

$$\begin{cases} \sum_{k=1}^6 c_{ik}^2 = 1, & i = j \\ \sum_{k=1}^6 c_{ik}c_{jk} = 0 & i \neq j. \end{cases} \quad i, j = 1, \dots, 6. \quad (2.3)$$

Since c_{ij} must be integers, the system (2.3) implies that any matrix $C \in B_6$ admits only six non-zero entries, which we denote by $c_{i(k),k}$, for $k = 1, \dots, 6$, belonging to $\{1, -1\}$, so that each row and column contains 1 or -1 only once, all other entries being zero. These matrices are referred to as *signed permutation matrices*. In fact, let $\mathbf{d} := (c_{i(k),k} : k = 1, \dots, 6)$ be the vector of all the non-zero entries of C , ordered by columns. If D denotes the diagonal matrix with diagonal \mathbf{d} , and Q the 6×6 permutation matrix with entries $Q_{ij} := |C_{ij}|$, then $C = QD$. Writing $c_{i(k),k} = (-1)^{a_k}$, with $a_k \in \{0, 1\}$, we can associate with each matrix in B_6 a pair (\mathbf{a}, π) , where $\mathbf{a} = (a_1, \dots, a_6) \in \mathbb{Z}_2^6$, and $\pi \in S_6$ is the permutation associated with Q , defined by $\pi(k) = i(k)$. The set of all these pairs constitutes a group (called the *wreath product* of \mathbb{Z}_2 and S_6 , and denoted by $\mathbb{Z}_2 \wr S_6$, [55]) with the multiplication rule given by

$$(\mathbf{a}, \pi)(\mathbf{b}, \sigma) := (\mathbf{a}_\sigma +_2 \mathbf{b}, \pi\sigma),$$

where $+_2$ denotes addition modulo 2 and $(\mathbf{a}_\sigma)_k := a_{\sigma(k)} \cdot \mathbb{Z}_2 \wr S_6$ and B_6 are isomorphic, an isomorphism T being the following:

$$[T(\mathbf{a}, \pi)]_{ij} := (-1)^{a_j} \delta_{i, \pi(j)}. \quad (2.4)$$

It immediately follows that $|B_6| = 2^6 6! = 46,080$. A set of generators is given by

$$\alpha := (\mathbf{0}, (1, 2)), \quad \beta := (\mathbf{0}, (1, 2, 3, 4, 5, 6)), \quad \gamma := ((0, 0, 0, 0, 0, 1), \text{id}_{S_6}), \quad (2.5)$$

which satisfy the relations $\alpha^2 = \gamma^2 = \beta^6 = (\mathbf{0}, \text{id}_{S_6})$. Finally, the function $\phi : \mathbb{Z}_2 \wr S_6 \rightarrow S_{12}$, defined by

$$\phi(\mathbf{a}, \pi)(k) := \begin{cases} \pi(k) + 6a_k & \text{if } 1 \leq k \leq 6 \\ \pi(k - 6) + 6(1 - a_{k-6}) & \text{if } 7 \leq k \leq 12, \end{cases} \quad (2.6)$$

is injective and maps any element of $\mathbb{Z}_2 \wr S_6$ into a permutation of S_{12} ; it provides a faithful permutation representation of B_6 as a subgroup of S_{12} . In particular, applying ϕ to the generators of B_6 given in (2.5), we obtain

$$B_6 \simeq \langle (1, 2)(7, 8), (1, 2, 3, 4, 5, 6)(7, 8, 9, 10, 11, 12), (6, 12) \rangle. \quad (2.7)$$

Combining (2.4) with the inverse of (2.6) we get the function

$$\psi := T \circ \phi^{-1} : S_{12} \rightarrow B_6 \quad (2.8)$$

which can be used to map a permutation into a matrix element of B_6 .

2.1.2 Classification of the crystallographic representations of \mathcal{I}

The permutation representation of B_6 given in (2.7) allows the generation of B_6 in GAP and the subsequent analysis of its subgroup structure. Before we continue, we recall the following [55]:

Definition 2.1.1. *Let H be a subgroup of a group G . The conjugacy class of H in G is the set*

$$C_G(H) := \{gHg^{-1} : g \in G\}.$$

We want to find all the subgroups of B_6 isomorphic to \mathcal{I} . For this, we use the following procedure:

1. List all the conjugacy classes of the subgroups of B_6 and find a representative for each class;
2. isolate the classes whose representatives have order 60;
3. check if these representatives are isomorphic to \mathcal{I} .

We implemented these steps in GAP (see Appendix). There are three conjugacy classes of subgroups isomorphic to \mathcal{I} in B_6 . The representatives S_i of the classes returned by GAP are the following:

$$S_1 = \langle (1, 3)(2, 4)(7, 9)(8, 10), (3, 10, 11)(4, 5, 9) \rangle,$$

$$S_2 = \langle (1, 2)(3, 10)(4, 9)(5, 11)(6, 12)(7, 8), (1, 2, 4)(3, 12, 5)(6, 11, 9)(7, 8, 10) \rangle,$$

$$S_3 = \langle (2, 6)(4, 11)(5, 10)(8, 12), (1, 3, 5)(2, 4, 6)(7, 9, 11)(8, 10, 12) \rangle.$$

Using (2.8), we map the generators of S_i , for $i = 1, 2, 3$, into matrix elements of B_6 . The groups $\widetilde{S}_i := \psi(S_i)$ therefore are integral representations of \mathcal{I} ; we compute their characters and, using (1.11), the corresponding decomposition (1.10) into irreps in $GL(6, \mathbb{R})$. The results are:

$$\chi_{\widetilde{S}_1}(g_2) = 2, \chi_{S_1}(g_3) = 3 \Rightarrow \chi_{\widetilde{S}_1} = 2\chi_A + \chi_G \Rightarrow \widetilde{S}_1 \simeq 2A \oplus G,$$

$$\chi_{S_2}(g_2) = -2, \chi_{\widetilde{S}_2}(g_3) = 0 \Rightarrow \chi_{\widetilde{S}_2} = \chi_{T_1} + \chi_{T_2} \Rightarrow \widetilde{S}_2 \simeq T_1 \oplus T_2,$$

$$\chi_{\widetilde{S}_3}(g_2) = 2, \chi_{\widetilde{S}_3}(g_3) = 0 \Rightarrow \chi_{\widetilde{S}_3} = \chi_A + \chi_H \Rightarrow \widetilde{S}_3 \simeq A \oplus H.$$

This is a very interesting result. Indeed, we observe that only the second class S_2 contains representations of \mathcal{I} which contains a three-dimensional irrep, and hence they are crystallographic in the sense of Definition 1.2.2. The other classes contains integral representations of \mathcal{I} which contain a four- or a five-dimensional irrep of \mathcal{I} . For physical and biological applications we will restrict to the study of the second class, which contains all the crystallographic representations of \mathcal{I} . A computation in GAP shows that its order is 192. We thus have the following:

Proposition 2.1.1. *The crystallographic representations of \mathcal{I} in B_6 form a unique conjugacy class in the set of all the classes of subgroups of B_6 , and its order is equal to 192.*

In what follows, we will consider the subgroup $\widetilde{\mathcal{I}}$ in (2.1) as a representative of the class of the crystallographic representations of \mathcal{I} , and denote this class by $C_{B_6}(\widetilde{\mathcal{I}})$. Recalling that two representations $D^{(1)}$ and $D^{(2)}$ of a group G are said to be *equivalent* if they are related via a similarity transformation, i.e. there exists an invertible matrix S such that $D^{(1)} = SD^{(2)}S^{-1}$, then an immediate consequence of Proposition 2.1.1 is the following:

Corollary 2.1.1. *The crystallographic representations of \mathcal{I} are equivalent in B_6 .*

We point out that the other two classes of representations of \mathcal{I} in B_6 have an interesting algebraic interpretation. Indeed, the symmetric group S_6 is a subgroup of B_6 , as a consequence of the wreath product structure of B_6 . Following [56], it is possible to embed the symmetric group S_5 into S_6 in two different ways. The standard embedding is achieved by fixing a point in $\{1, \dots, 6\}$ and permuting the other five, whereas the other embedding is by means of the so-called “exotic map” $\varphi : S_5 \rightarrow S_6$, which acts on the six 5-Sylow subgroups³ of S_5 by conjugation. Since the icosahedral group is isomorphic to the alternating group \mathfrak{A}_5 , which is a normal subgroup of S_5 , these embeddings induce two different ways of embedding \mathcal{I} into S_6 . In the standard embedding, all the permutations representing S_5 have a fixed point, hence the induced permutation matrices in B_6 have non-zero trace. Therefore, this corresponds to the representation $2A \oplus G$ in B_6 ; on the other hand, the representation $A \oplus H$ corresponds to the exotic embedding φ .

2.1.3 Projection into the 3D space

As already discussed in Section 2.1, a crystallographic representation of \mathcal{I} leaves two three-dimensional subspaces invariant, which carry the irreps T_1 and T_2 of \mathcal{I} . These are used to define icosahedral model sets with the cut-and-project method (cf. (1.16)). In order to explicitly construct these model sets, we use the results from the representation theory of finite groups revised in Section 1.2.2. Indeed, let $\widetilde{\mathcal{I}}$ be the representative of the class of crystallographic representations of \mathcal{I} given in (2.1). The decomposition (1.10) implies that there exists a matrix $R \in GL(6, \mathbb{R})$ such that

$$\widehat{\mathcal{I}} := R^{-1}\widetilde{\mathcal{I}}R = \rho_3 \oplus \rho'_3, \quad (2.9)$$

³A p -Sylow subgroup of a finite group G , where p is a prime number, is a maximal subgroup of G whose order is a power of p .

where $\rho_3 \simeq T_1$ and $\rho'_3 \simeq T_2$ in $GL(3, \mathbb{R})$. This induces a decomposition of \mathbb{R}^6 into two three-dimensional \tilde{T} -invariant subspaces, usually denoted by E^\parallel and E^\perp [57]. A basis of each of these subspaces can be found using the projection operators given in (1.12); specifically, we obtain:

$$P^\parallel = \frac{1}{2\sqrt{5}} \begin{pmatrix} \sqrt{5} & 1 & -1 & -1 & 1 & 1 \\ 1 & \sqrt{5} & 1 & -1 & -1 & 1 \\ -1 & 1 & \sqrt{5} & 1 & -1 & 1 \\ -1 & -1 & 1 & \sqrt{5} & 1 & 1 \\ 1 & -1 & -1 & 1 & \sqrt{5} & 1 \\ 1 & 1 & 1 & 1 & 1 & \sqrt{5} \end{pmatrix}, P^\perp = \frac{1}{2\sqrt{5}} \begin{pmatrix} \sqrt{5} & -1 & 1 & 1 & -1 & -1 \\ -1 & \sqrt{5} & -1 & 1 & 1 & -1 \\ 1 & -1 & \sqrt{5} & -1 & 1 & -1 \\ 1 & 1 & -1 & \sqrt{5} & -1 & -1 \\ -1 & 1 & 1 & -1 & \sqrt{5} & -1 \\ -1 & -1 & -1 & -1 & -1 & \sqrt{5} \end{pmatrix}.$$

The rank of these two matrices is three, and we have $\text{Im}(P^\parallel) = E^\parallel$ and $\text{Im}(P^\perp) = E^\perp$. If $\{e_j, j = 1, \dots, 6\}$ is the standard basis of \mathbb{R}^6 , then a basis of E^\parallel (respectively E^\perp) can be found by considering the sets $\{e_j^\parallel := P^\parallel e_j, j = 1, \dots, 6\}$ (respectively P^\perp) and then extracting a basis \mathcal{B}^\parallel (respectively \mathcal{B}^\perp) from it. The matrix R can then be written as

$$R = \begin{pmatrix} \underbrace{e_1^\parallel, e_2^\parallel, e_3^\parallel}_{\text{basis of } E^\parallel}, \underbrace{e_1^\perp, e_2^\perp, e_3^\perp}_{\text{basis of } E^\perp} \end{pmatrix}. \quad (2.10)$$

With a suitable rescaling, we can choose the matrix $R \in O(6)$, i.e. R to be orthogonal. The explicit form is given by

$$R = \frac{1}{\sqrt{2(2+\tau)}} \begin{pmatrix} \tau & 1 & 0 & \tau & 0 & 1 \\ 0 & \tau & 1 & -1 & \tau & 0 \\ -1 & 0 & \tau & 0 & -1 & \tau \\ 0 & -\tau & 1 & 1 & \tau & 0 \\ \tau & -1 & 0 & -\tau & 0 & 1 \\ 1 & 0 & \tau & 0 & -1 & -\tau \end{pmatrix}. \quad (2.11)$$

The explicit forms of the irreps ρ_3 and ρ'_3 are given in Table 2.1.3. Denoting by π^\parallel and π^\perp the 3×6 matrices which represent P^\parallel and P^\perp in the bases \mathcal{B}^\parallel and \mathcal{B}^\perp , respectively, we have, by linear algebra

$$R^{-1} = \begin{pmatrix} \pi^\parallel \\ \pi^\perp \end{pmatrix}. \quad (2.12)$$

In particular, we have

$$\pi^\parallel = \frac{1}{k} \begin{pmatrix} \tau & 0 & -1 & 0 & \tau & 1 \\ 1 & \tau & 0 & -\tau & -1 & 0 \\ 0 & 1 & \tau & 1 & 0 & \tau \end{pmatrix}, \quad \pi^\perp = \frac{1}{k} \begin{pmatrix} \tau & -1 & 0 & 1 & -\tau & 0 \\ 0 & \tau & -1 & \tau & 0 & -1 \\ 1 & 0 & \tau & 0 & 1 & -\tau \end{pmatrix}. \quad (2.13)$$

Generator	Irrep $\rho_3 \simeq T_1$	Irrep $\rho'_3 \simeq T_2$
g_2	$\frac{1}{2} \begin{pmatrix} \tau - 1 & 1 & \tau \\ 1 & -\tau & \tau - 1 \\ \tau & \tau - 1 & -1 \end{pmatrix}$	$\frac{1}{2} \begin{pmatrix} \tau - 1 & -\tau & -1 \\ -\tau & -1 & \tau - 1 \\ -1 & \tau - 1 & -\tau \end{pmatrix}$
g_3	$\frac{1}{2} \begin{pmatrix} \tau & \tau - 1 & 1 \\ 1 - \tau & -1 & \tau \\ 1 & -\tau & 1 - \tau \end{pmatrix}$	$\frac{1}{2} \begin{pmatrix} -1 & 1 - \tau & -\tau \\ \tau - 1 & \tau & -1 \\ \tau & -1 & 1 - \tau \end{pmatrix}$

Table 2.1: Explicit forms of the irreps ρ_3 and ρ'_3 with $\tilde{\mathcal{I}} \simeq \rho_3 \oplus \rho'_3$.

with $k = \sqrt{2(2 + \tau)}$. Since $R^{-1}\tilde{\mathcal{I}} = \hat{\mathcal{I}}R^{-1}$ (cf. (2.9)), we obtain

$$\pi^{\parallel}(\tilde{\mathcal{I}}(g)\mathbf{v}) = \rho_3(g)(\pi^{\parallel}(\mathbf{v})), \quad \pi^{\perp}(\tilde{\mathcal{I}}(g)\mathbf{v}) = \rho'_3(g)(\pi^{\perp}(\mathbf{v})), \quad (2.14)$$

for all $g \in \mathcal{I}$ and $\mathbf{v} \in \mathbb{R}^6$. This proves that icosahedral symmetry is preserved in projection (compare with (1.15)). With these results, we define the icosahedral cut-and-project scheme (cf. (1.16)):

$$\begin{array}{c} E^{\parallel} \xleftarrow{\pi^{\parallel}} E^{\parallel} \oplus E^{\perp} \xrightarrow{\pi^{\perp}} E^{\perp} \\ \cup \\ \mathcal{L} \end{array}$$

where \mathcal{L} is one of the hypercubic lattices in \mathbb{R}^6 . With this setup, it is possible to compute model sets and induced tilings of \mathbb{R}^3 with icosahedral symmetry with the methods described in Section 1.2.3. An example of such a tiling is given in Figure 2.2. In this case, the window is the projection of the Voronoi cell of the origin of the simple cubic lattice \mathcal{L}_{SC} in \mathbb{R}^6 , whose convex hull is the so-called rhombic triacontrahedron [37].

Crystallographic representations of H_3 . In the case of achiral icosahedral symmetry, the crystallographic representations of H_3 are easily computed using the direct product structure $H_3 \simeq \mathcal{I} \times \mathbb{Z}_2$ (cf. Section 1.1.1). In fact, let $\tilde{\mathcal{I}}$ be a representative of the crystallographic representations of \mathcal{I} in B_6 (cf. (2.1)), and let $\Gamma = \{1, -1\}$ be the one-dimensional non-trivial representation of \mathbb{Z}_2 . Then the representation

$$\tilde{H}_3 := \tilde{\mathcal{I}} \otimes \Gamma, \quad (2.15)$$

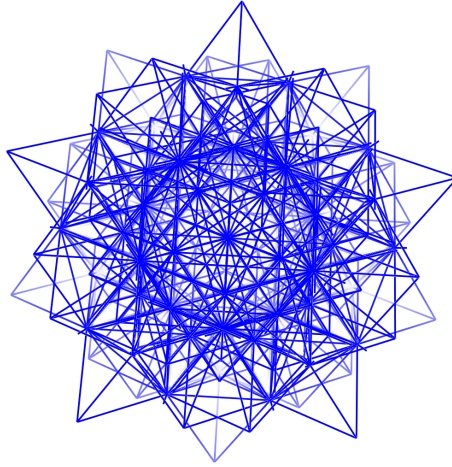


Figure 2.2: Patch of an icosahedral tiling around the origin obtained via projection from the six-dimensional simple cubic lattice.

where \otimes denotes the tensor product of matrices⁴, is a representation of H_3 in B_6 and it is crystallographic in the sense of Definition 1.13. Indeed we have $\tilde{\mathcal{I}} \otimes \Gamma = \tilde{\mathcal{I}} \otimes \{1, -1\} = \tilde{\mathcal{I}} \cup (-\tilde{\mathcal{I}})$ since, for every matrix A , $A \otimes (-1) = -A$. Therefore

$$\begin{aligned} R^{-1}(\tilde{\mathcal{I}} \otimes \Gamma)R &= R^{-1}(\tilde{\mathcal{I}} \cup \{-\tilde{\mathcal{I}}\})R = \{R^{-1}\tilde{\mathcal{I}}R\} \cup \{-R^{-1}\tilde{\mathcal{I}}R\} = \\ &= \{\rho_3 \oplus \rho'_3\} \cup \{-\rho_3 \oplus \rho'_3\} = \{\rho_3 \cup (-\rho_3)\} \oplus \{\rho'_3 \cup (-\rho'_3)\} = (\rho_3 \otimes \Gamma) \oplus (\rho'_3 \otimes \Gamma). \end{aligned} \quad (2.16)$$

The representations $\rho_3 \otimes \Gamma$ and $\rho'_3 \otimes \Gamma$ are two three-dimensional irreducible representations of H_3 . Hence the parallel and orthogonal spaces E^{\parallel} and E^{\perp} , spanned by the columns of R , are both invariant under $\tilde{\mathcal{I}} \otimes \Gamma$.

2.2 Subgroup structure

As pointed out in the Preface, we are interested in the study of structural transitions of icosahedral quasicrystals and viral capsids. These can be analysed in a group theoretical framework as we are going to discuss in Chapter 3. For this purpose, we need to investigate the subgroup structure of the class of crystallographic representations of \mathcal{I} in B_6 . Indeed, we want to characterise their intersections and shared subgroups. In the context of transitions, a shared subgroup of two distinct crystallographic representations encodes the

⁴This corresponds to the Kronecker product for matrices: given a $m \times n$ matrix A and a $p \times q$ matrix B , the matrix $C := A \otimes B$ is the $mp \times nq$ matrix whose entries are given by $C_{ij} = A_{ij}B$.

Subgroup	Generators	Relations	Order
\mathcal{T}	g_2, g_{3d}	$g_2^2 = g_{3d}^3 = (g_2 g_{3d})^3 = e$	12
\mathcal{D}_{10}	g_{2d}, g_{5d}	$g_{2d}^2 = g_{5d}^5 = (g_{5d} g_{2d})^2 = e$	10
\mathcal{D}_6	g_{2d}, g_3	$g_{2d}^2 = g_3^3 = (g_3 g_{2d})^2 = e$	6
\mathbb{Z}_5	g_{5d}	$g_{5d}^5 = e$	5
\mathcal{D}_4	g_{2d}, g_2	$g_{2d}^2 = g_2^2 = (g_2 g_{2d})^2 = e$	4
\mathbb{Z}_3	g_3	$g_3^3 = e$	3
\mathbb{Z}_2	g_2	$g_2^2 = e$	2

Table 2.2: Non-trivial subgroups of the icosahedral group: \mathcal{T} stands for the tetrahedral group, \mathcal{D}_{2n} for the dihedral group of order $2n$, and \mathbb{Z}_n for the cyclic group of order n .

symmetry which is preserved during the transformations, and hence allows for the identification of the order parameters of the transitions.

We start by listing all the non-trivial subgroups of \mathcal{I} in Table 2.2, together with their generators [58]. Note that \mathcal{T} , \mathcal{D}_{10} and \mathcal{D}_6 are maximal subgroups of \mathcal{I} , and that \mathcal{D}_4 , \mathbb{Z}_5 and \mathbb{Z}_3 are normal subgroups of \mathcal{T} , \mathcal{D}_{10} and \mathcal{D}_6 , respectively [1, 55].

The following definition, due to Soicher [59], will be particularly useful for our purposes:

Definition 2.2.1. *A subgroup H of a group G is a friendly subgroup of G if every subgroup K of G isomorphic to H is conjugate to H in G .*

Since \mathcal{I} is a small group, its subgroup structure can easily be obtained in GAP by computing explicitly all its conjugacy classes of subgroups, denoted by $C_{\mathcal{I}}(\mathcal{G})$, for \mathcal{G} subgroup of \mathcal{I} . (cf. Definition 2.1.1). The results are given in Table 2.3. In particular, there are 7 classes of non-trivial subgroups in \mathcal{I} , which is equal to the number of non-trivial subgroups of \mathcal{I} (compare with Table 2.2). In other words, denoting by $n_{\mathcal{G}}$ the number of subgroups of \mathcal{I} isomorphic to \mathcal{G} , i.e.

$$n_{\mathcal{G}} := |\{H < \mathcal{I} : H \simeq \mathcal{G}\}|, \quad (2.17)$$

then $n_{\mathcal{G}} = |C_{\mathcal{I}}(\mathcal{G})|$, and hence every subgroup of \mathcal{I} is friendly in the sense of Definition 2.2.1. Geometrically, different copies of \mathbb{Z}_2 , \mathbb{Z}_3 and \mathbb{Z}_5 correspond to the different two-, three- and five-fold axes of the icosahedron, respectively. In particular, different copies of \mathcal{D}_{10} stabilise one of the 6 five-fold axes of the icosahedron, and each copy of \mathcal{D}_6 stabilises

Subgroup	$ C_{\mathcal{I}}(\mathcal{G}) $	$ C_{B_6}(\tilde{\mathcal{G}}) $
\mathcal{T}	5	480
\mathcal{D}_{10}	6	576
\mathcal{D}_6	10	960
\mathcal{D}_4	5	120
\mathbb{Z}_5	6	576
\mathbb{Z}_3	10	320
\mathbb{Z}_2	15	180

Table 2.3: Order of the classes of subgroups of the icosahedral group in \mathcal{I} and B_6 .

one of the 10 three-fold axes. Moreover, it is possible to inscribe 5 tetrahedra into a dodecahedron, and each different copy of the tetrahedral group in \mathcal{I} stabilises one of these tetrahedra.

2.2.1 Subgroups of the crystallographic representations of \mathcal{I}

Let \mathcal{G} be a subgroup of \mathcal{I} , and let $\tilde{\mathcal{G}}$ be a subgroup of $\tilde{\mathcal{I}}$ in (2.1) isomorphic to \mathcal{G} . Let us denote by $C_{B_6}(\tilde{\mathcal{G}})$ the conjugacy class of $\tilde{\mathcal{G}}$ in B_6 . The next lemma shows that this class contains all the subgroups of the crystallographic representations of \mathcal{I} in B_6 .

Lemma 2.2.1. *Let $\mathcal{H}_i \in C_{B_6}(\tilde{\mathcal{I}})$ be a crystallographic representation of \mathcal{I} in B_6 , and let $\mathcal{K}_i \subseteq \mathcal{H}_i$ be a subgroup of \mathcal{H}_i isomorphic to \mathcal{G} . Then $\mathcal{K}_i \in C_{B_6}(\tilde{\mathcal{G}})$.*

Proof. Since $\mathcal{H}_i \in C_{B_6}(\tilde{\mathcal{I}})$, there exists $g \in B_6$ such that $g\mathcal{H}_i g^{-1} = \tilde{\mathcal{I}}$, and therefore $g\mathcal{K}_i g^{-1} = \mathcal{K}'$ is a subgroup of $\tilde{\mathcal{I}}$ isomorphic to \mathcal{G} . Due to the ‘‘friendliness’’ of the subgroups of \mathcal{I} , these subgroups are conjugate in $\tilde{\mathcal{I}}$, hence there exists $h \in \tilde{\mathcal{I}}$ such that $h\mathcal{K}'h^{-1} = \tilde{\mathcal{G}}$. Thus $(hg)\mathcal{K}_i(hg)^{-1} = \tilde{\mathcal{G}}$, implying that $\mathcal{K}_i \in C_{B_6}(\tilde{\mathcal{G}})$. \square

We next show that every element of $C_{B_6}(\tilde{\mathcal{G}})$ is a subgroup of a crystallographic representation of \mathcal{I} .

Lemma 2.2.2. *Let $\mathcal{K}_i \in C_{B_6}(\tilde{\mathcal{G}})$. There exists $\mathcal{H}_i \in C_{B_6}(\tilde{\mathcal{I}})$ such that \mathcal{K}_i is a subgroup of \mathcal{H}_i .*

Proof. Since $\mathcal{K}_i \in C_{B_6}(\tilde{\mathcal{G}})$, there exists $g \in B_6$ such that $g\mathcal{K}_i g^{-1} = \tilde{\mathcal{G}}$. We define $\mathcal{H}_i := g^{-1}\tilde{\mathcal{I}}g$. It is immediate to see that \mathcal{K}_i is a subgroup of \mathcal{H}_i . \square

As a consequence of these Lemmata, $C_{B_6}(\widetilde{\mathcal{G}})$ contains all the subgroups of B_6 which are isomorphic to \mathcal{G} and are subgroups of a crystallographic representation of \mathcal{I} . Explicit forms of $\widetilde{\mathcal{G}}$ will be given in Chapter 3, where their decomposition into irreps will be analysed. We point out that it is possible to find subgroups of B_6 isomorphic to a subgroup \mathcal{G} of \mathcal{I} which are *not* subgroups of any crystallographic representation of \mathcal{I} . For example, the following subgroup

$$\overline{\mathcal{T}} = \left\langle \left(\begin{array}{cccccc} 1 & 0 & 0 & 0 & 0 & 0 \\ 0 & -1 & 0 & 0 & 0 & 0 \\ 0 & 0 & -1 & 0 & 0 & 0 \\ 0 & 0 & 0 & -1 & 0 & 0 \\ 0 & 0 & 0 & 0 & -1 & 0 \\ 0 & 0 & 0 & 0 & 0 & 1 \end{array} \right), \left(\begin{array}{cccccc} 0 & 0 & -1 & 0 & 0 & 0 \\ 1 & 0 & 0 & 0 & 0 & 0 \\ 0 & -1 & 0 & 0 & 0 & 0 \\ 0 & 0 & 0 & 0 & 0 & 1 \\ 0 & 0 & 0 & 1 & 0 & 0 \\ 0 & 0 & 0 & 0 & 1 & 0 \end{array} \right) \right\rangle$$

is isomorphic to the tetrahedral group \mathcal{T} ; a computation in GAP shows that it is not a subgroup of any elements in $C_{B_6}(\widetilde{\mathcal{I}})$. Indeed, the two classes of subgroups, $C_{B_6}(\widetilde{\mathcal{T}})$ and $C_{B_6}(\overline{\mathcal{T}})$, are disjoint.

Using GAP, we compute the size of each $C_{B_6}(\widetilde{\mathcal{G}})$ (see Table 2.3). We observe that $|C_{B_6}(\widetilde{\mathcal{G}})| < |C_{B_6}(\widetilde{\mathcal{I}})| \cdot n_{\mathcal{G}}$. This implies that crystallographic representations of \mathcal{I} may share subgroups. For the analysis of transitions of icosahedral structures, it is necessary to know, given a subgroup \mathcal{G} of \mathcal{I} , if there exist elements in $C_{B_6}(\widetilde{\mathcal{I}})$ whose intersections is isomorphic to \mathcal{G} . In order to classify the shared subgroups and intersections, due to the complexity of the problem, we present here a new computational method in group theory based on results from graph theory and their spectra. To this purpose, we revise some concepts in the next section.

2.2.2 Some basic results of graph theory and their spectra

In this section we recall, without proofs, some concepts and results from graph theory and spectral graph theory. Proofs and further results can be found, for example, in [60] and [61].

Let G be a graph with vertex set $V = \{v_1, \dots, v_n\}$. The number of edges incident with a vertex v is called the *degree* of v . If all vertices have the same degree d , then the graph is called *regular of degree d* . A *walk of length l* is a sequence of l consecutive edges, and it is called a *path* if they are all distinct. A *circuit* is a path starting and ending at the same vertex, and the *girth* of the graph is the length of the shortest circuit. Two vertices p and

q are *connected* if there exists a path containing p and q . The *connected component* of a vertex v is the set of all vertices connected to v .

The *adjacency matrix* A of G is the $n \times n$ matrix $A = (a_{ij})$ whose entries a_{ij} are equal to 1 if the vertex v_i is adjacent to the vertex v_j , and 0 otherwise. It is immediate to see from its definition that A is symmetric and $a_{ii} = 0$ for all i , so that $\text{Tr}(A) = 0$. It follows that A is diagonalisable and all its eigenvalues are real. The *spectrum of the graph* is the set of all the eigenvalues of its adjacency matrix A , usually denoted by $\sigma(A)$.

Theorem 2.2.1. *Let A be the adjacency matrix of a graph G with vertex set $V = \{v_1, \dots, v_n\}$. Let $N_k(i, j)$ denote the number of walks of length k starting at vertex v_i and finishing at vertex v_j . We have*

$$N_k(i, j) = (A^k)_{ij}.$$

We recall that the *spectral radius* of a matrix A is defined by $\rho(A) := \max\{|\lambda| : \lambda \in \sigma(A)\}$. If A is a non-negative matrix, i.e. if all its entries are non-negative, then $\rho(A) \in \sigma(A)$ [62]. Since the adjacency matrix of a graph is non-negative, $|\lambda| \leq \rho(A) := r$, where $\lambda \in \sigma(A)$ and r is the largest eigenvalue. r is called the *index* of the graph G .

Theorem 2.2.2. *Let $\{\lambda_1, \dots, \lambda_n\}$ be the spectrum of a graph G , and let r denote its index. Then G is regular of degree r if and only if*

$$\frac{1}{n} \sum_{i=1}^n \lambda_i^2 = r.$$

Moreover, if G is regular the multiplicity of its index is equal to the number of its connected components.

2.2.3 Applications to the subgroup structure

Let \mathcal{G} be a subgroup of \mathcal{I} . In the following we represent the subgroup structure of the class of crystallographic representations of \mathcal{I} in $B_6, C_{B_6}(\widetilde{\mathcal{I}})$, as a graph. We say that $\mathcal{H}_1, \mathcal{H}_2 \in C_{B_6}(\widetilde{\mathcal{I}})$ are adjacent to each other (i.e. connected by an edge) in the graph if there exists $P \in C_{B_6}(\widetilde{\mathcal{G}})$ such that $P = \mathcal{H}_1 \cap \mathcal{H}_2$. We can therefore consider the graph $G = (C_{B_6}(\widetilde{\mathcal{I}}), E)$, where an edge $e \in E$ is of the form $(\mathcal{H}_1, \mathcal{H}_2)$. We call this graph \mathcal{G} -*graph*. These graphs are difficult to visualise; however, by analysing their spectra, we can study their topology in some detail, hence describing the intersection and the subgroups shared by different representations.

\mathcal{T} -Graph		\mathcal{D}_{10} -Graph		\mathcal{D}_6 -Graph		\mathbb{Z}_5 -graph	
Eig.	Mult.	Eig.	Mult.	Eig.	Mult.	Eig.	Mult.
5	1	6	6	10	6	0	192
3	45	2	90	2	90		
-3	45	-2	90	-2	90		
1	50	-6	6	-10	6		
-1	50						
-5	1						
\mathcal{D}_4 -graph		\mathbb{Z}_3 -graph		\mathbb{Z}_2 -graph		$\{e\}$ -graph	
Eig.	Mult.	Eig.	Mult.	Eig.	Mult.	Eig.	Mult.
30	1	20	2	60	2	60	1
18	5	4	90	4	90	12	5
12	5	-4	100	-4	90	4	90
6	15			-12	10	-4	90
2	45					-12	5
0	31					-60	1
-2	30						
-4	45						
-8	15						

Table 2.4: Spectra of the \mathcal{G} -graphs, with \mathcal{G} a non-trivial subgroup of \mathcal{I} and $\mathcal{G} = \{e\}$, the trivial subgroup consisting of only the identity element e . The numbers highlighted are the indices of the graphs, and correspond to their degrees $d_{\mathcal{G}}$.

Using GAP, we compute the adjacency matrices of the \mathcal{G} -graphs. The algorithms used are shown in the Appendix. The spectra of the \mathcal{G} -graphs are given in Table 2.4. We first of all notice that the adjacency matrix of the \mathbb{Z}_5 -graph is the null matrix, implying that there are no two representations sharing precisely a subgroup isomorphic to \mathbb{Z}_5 , i.e. not a subgroup containing \mathbb{Z}_5 . We point out that, since the adjacency matrix of the \mathcal{D}_{10} -graph is not the null one, then there exist crystallographic representations, say \mathcal{H}_i and \mathcal{H}_j , sharing a maximal subgroup isomorphic to \mathcal{D}_{10} . Since \mathbb{Z}_5 is a (normal) subgroup of \mathcal{D}_{10} , then \mathcal{H}_i and \mathcal{H}_j do share a \mathbb{Z}_5 subgroup, but also a \mathbb{Z}_2 subgroup. In other words, if two representations share a five-fold axis, then necessarily they also share a two-fold axis.

A straightforward calculation based on Theorem 2.2.2 leads to the following:

Proposition 2.2.1. *Let \mathcal{G} be a subgroup of \mathcal{I} . Then the corresponding \mathcal{G} -graph is regular.*

In particular, the degree $d_{\mathcal{G}}$ of each \mathcal{G} -graph is equal to the largest eigenvalue of the corresponding spectrum. As a consequence we have the following:

Proposition 2.2.2. *Let \mathcal{H} be a crystallographic representation of \mathcal{I} in B_6 . Then there are exactly $d_{\mathcal{G}}$ representations $\mathcal{K}_j \in C_{B_6}(\widetilde{\mathcal{I}})$ such that*

$$\exists P_j \in C(\widetilde{\mathcal{G}}) : \quad \mathcal{H} \cap \mathcal{K}_j = P_j, \quad j = 1, \dots, d_{\mathcal{G}}.$$

In particular, we have $d_{\mathcal{G}} = 5, 6, 10, 0, 30, 20, 60$ and 60 for $\mathcal{G} = \mathcal{T}, \mathcal{D}_{10}, \mathcal{D}_6, \mathbb{Z}_5, \mathcal{D}_4, \mathbb{Z}_3, \mathbb{Z}_2$ and $\{e\}$, respectively.

In particular, this means that for any crystallographic representation of \mathcal{I} there are precisely $d_{\mathcal{G}}$ other such representations which share a subgroup isomorphic to \mathcal{G} . In other words, we can associate to the class $C_{B_6}(\widetilde{\mathcal{I}})$ the “subgroup matrix” S whose entries are defined by

$$S_{ij} = |\mathcal{H}_i \cap \mathcal{H}_j|, \quad i, j = 1, \dots, 192.$$

The matrix S is symmetric and $S_{ii} = 60$, for all i , since the order of \mathcal{I} is 60. It follows from Proposition 2.2.2 that each row of S contains $d_{\mathcal{G}}$ entries equal to $|\mathcal{G}|$. Moreover, a rearrangement of the columns of S shows that the 192 crystallographic representations of \mathcal{I} can be grouped into 12 sets of 16 such that any two of these representations in such a set of 16 share a \mathcal{D}_4 -subgroup. This implies that the corresponding subgraph of the \mathcal{D}_4 -graph is a *complete graph*, i.e. every two distinct vertices are connected by an edge. From a geometric point of view, these 16 representations correspond to “6-dimensional icosahedra”. This ensemble of 16 such icosahedra embedded into a six-dimensional hypercube can be viewed as 6D analogue of the 3D ensemble of five tetrahedra inscribed into a dodecahedron, sharing pairwise a \mathbb{Z}_3 -subgroup.

We now consider in more detail the case when \mathcal{G} is a maximal subgroup of \mathcal{I} . Let $\mathcal{H} \in C_{B_6}(\widetilde{\mathcal{I}})$ and let us consider its vertex star in the corresponding \mathcal{G} -graph, i.e.

$$V(\mathcal{H}) := \{\mathcal{K} \in C_{B_6}(\widetilde{\mathcal{I}}) : \mathcal{K} \text{ is adjacent to } \mathcal{H}\}. \quad (2.18)$$

A comparison of Tables 2.2 and 2.4 shows that $d_{\mathcal{G}} = n_{\mathcal{G}}$ (i.e. the number of subgroups isomorphic to \mathcal{G} in \mathcal{I} , cf. (2.17)) and therefore, since the graph is regular, $|V(\mathcal{H})| = d_{\mathcal{G}} =$

$n_{\mathcal{G}}$. This suggests that there is a 1-1 correspondence between elements of the vertex star of \mathcal{H} and subgroups of \mathcal{H} isomorphic to \mathcal{G} ; in other words, if we fix any subgroup P of \mathcal{H} isomorphic to \mathcal{G} , then P “connects” \mathcal{H} with exactly another representation \mathcal{K} . We thus have the following:

Proposition 2.2.3. *Let \mathcal{G} be a maximal subgroup of \mathcal{I} . Then for every $P \in C_{B_6}(\widetilde{\mathcal{G}})$ there exist exactly two crystallographic representations of \mathcal{I} , $\mathcal{H}_1, \mathcal{H}_2 \in C_{B_6}(\widetilde{\mathcal{I}})$, such that $P = \mathcal{H}_1 \cap \mathcal{H}_2$.*

In order to prove this proposition, we first need the following lemma:

Lemma 2.2.3. *Let \mathcal{G} be a maximal subgroup of \mathcal{I} . Then the corresponding \mathcal{G} -graph is triangle-free, i.e. it has no circuits of length three.*

Proof. Let $A_{\mathcal{G}}$ be the adjacency matrix of the \mathcal{G} -graph. By Theorem 2.2.1, its third power $A_{\mathcal{G}}^3$ determines the number of walks of length 3, and in particular its diagonal entries, $(A_{\mathcal{G}}^3)_{ii}$, for $i = 1, \dots, 192$, correspond to the number of triangular circuits starting and ending in vertex i . A direct computation shows that $(A_{\mathcal{G}}^3)_{ii} = 0$, for all i , thus implying the non-existence of triangular circuits in the graph. \square

Proof of Proposition 2.2.3. If $P \in C_{B_6}(\widetilde{\mathcal{G}})$, then, using Lemma 2.2.2, there exists $\mathcal{H}_1 \in C_{B_6}(\widetilde{\mathcal{I}})$ such that P is a subgroup of \mathcal{H}_1 . Let us consider the vertex star $V(\mathcal{H}_1)$. We have $|V(\mathcal{H}_1)| = d_{\mathcal{G}}$ and we call its elements $\mathcal{H}_2, \dots, \mathcal{H}_{d_{\mathcal{G}}+1}$. Let us suppose that P is not a subgroup of any \mathcal{H}_j , for $j = 2, \dots, d_{\mathcal{G}} + 1$. This implies that P does not connect \mathcal{H}_1 with any of these \mathcal{H}_j . However, since \mathcal{H}_1 has exactly $n_{\mathcal{G}}$ different subgroups isomorphic to \mathcal{G} , then at least two vertices in the vertex star, say \mathcal{H}_2 and \mathcal{H}_3 , are connected by the same subgroup isomorphic to \mathcal{G} , which we denote by Q . Therefore, we have

$$Q = \mathcal{H}_1 \cap \mathcal{H}_2, \quad Q = \mathcal{H}_1 \cap \mathcal{H}_3 \Rightarrow Q = \mathcal{H}_2 \cap \mathcal{H}_3.$$

This implies that $\mathcal{H}_1, \mathcal{H}_2$ and \mathcal{H}_3 form a triangular circuit in the graph, which is a contradiction due to Lemma 2.2.3, hence the result is proved. \square

Chapter 3

A group theoretical approach to structural transitions of icosahedral quasicrystals

In nova fert animus mutatas dicere formas | corpora;

Ovid, *Metamorphoses*.

In this Chapter we show how the group theoretical analysis of the hyperoctahedral group in six dimensions provides the starting point to study continuous phase transitions between icosahedral aperiodic structures. Specifically, we define continuous rotations in $SO(6)$ that “connect” two crystallographic representations of the icosahedral group, and fix their shared maximal subgroup. These rotations, called *Schur rotations*, induce a rotation of the physical and orthogonal spaces invariant under the icosahedral group, and hence, via the cut-and-project method, a continuous transformations of the corresponding model sets.

3.1 Schur rotations between icosahedral quasicrystals

The concept of Schur rotation was first introduced by Kramer *et al.* [29,63], where transitions between cubic and aperiodic order were analysed. These were then studied with the phason strain approach [64], which was later proved to be equivalent to the Schur rotation method [65]. In this section we study Schur rotations between icosahedral aperiodic structures, and discuss comparisons with the Bain strain method given in [66, 67].

Let \mathcal{G} be a maximal subgroup of the icosahedral group \mathcal{I} , namely the tetrahedral group \mathcal{T} or the dihedral groups \mathcal{D}_{10} and \mathcal{D}_6 , and let $\tilde{\mathcal{G}}$ be a crystallographic representation of \mathcal{G} embedded into the hyperoctahedral group B_6 . Without loss of generality, we consider $\tilde{\mathcal{G}}$ as a subgroup of the crystallographic representation $\tilde{\mathcal{I}}$ given in (2.1). From Proposition 2.2.3, there exists a unique crystallographic representation of \mathcal{I} in B_6 , which we denote by $\tilde{\mathcal{I}}_{\mathcal{G}}$, such that $\tilde{\mathcal{G}}$ is a subgroup of $\tilde{\mathcal{I}}$ and $\tilde{\mathcal{I}}_{\mathcal{G}}$, i.e. $\tilde{\mathcal{G}} = \tilde{\mathcal{I}} \cap \tilde{\mathcal{I}}_{\mathcal{G}}$. The matrix R in (2.11), which reduces into irreps $\tilde{\mathcal{I}}$ as in (2.9), decomposes the representation $\tilde{\mathcal{G}}$ as follows:

$$\hat{\mathcal{G}} := R^{-1}\tilde{\mathcal{G}}R = \mathcal{G}_1 \oplus \mathcal{G}_2, \quad (3.1)$$

where \mathcal{G}_1 and \mathcal{G}_2 are matrix subgroups of the irreps ρ_3 and ρ'_3 given in Table 2.1.3, respectively. Notice that \mathcal{G}_1 and \mathcal{G}_2 are not necessarily irreducible representations of $\tilde{\mathcal{G}}$.

The matrix R in general does not reduce the representation $\tilde{\mathcal{I}}_{\mathcal{G}}$, since the subspaces E^{\parallel} and E^{\perp} , which are invariant under $\tilde{\mathcal{I}}$, are not necessarily invariant under $\tilde{\mathcal{I}}_{\mathcal{G}}$. Let us denote by $R_{\mathcal{G}} \in O(6)$ the orthogonal matrix that reduces into irreps $\tilde{\mathcal{I}}_{\mathcal{G}}$, i.e.

$$\hat{\mathcal{I}}_{\mathcal{G}} := R_{\mathcal{G}}^{-1}\tilde{\mathcal{I}}_{\mathcal{G}}R_{\mathcal{G}} \simeq T_1 \oplus T_2,$$

where T_1 and T_2 are the two non-equivalent three-dimensional irreps of \mathcal{I} (cf. Section 2.1). This matrix carries the bases of a physical and a parallel space which are invariant under $\tilde{\mathcal{I}}_{\mathcal{G}}$. We denote these spaces by $E_{\mathcal{G}}^{\parallel}$ and $E_{\mathcal{G}}^{\perp}$, respectively, and we write $\pi_{\mathcal{G}}^{\parallel}$ and $\pi_{\mathcal{G}}^{\perp}$ for the corresponding projections. By (2.12), we have

$$R_{\mathcal{G}}^{-1} = \begin{pmatrix} \pi_{\mathcal{G}}^{\parallel} \\ \pi_{\mathcal{G}}^{\perp} \end{pmatrix}.$$

The matrix $R_{\mathcal{G}}$ is in general not unique. With a suitable choice of the basis vectors constituting the columns of $R_{\mathcal{G}}$ (compare with (2.10)), we assume $\det(R_{\mathcal{G}})$ and $\det(R)$ have the same sign, i.e. R and $R_{\mathcal{G}}$ belong to the same connected component of $O(6)^1$. Furthermore, since $\tilde{\mathcal{G}}$ is a common subgroup of $\tilde{\mathcal{I}}$ and $\tilde{\mathcal{I}}_{\mathcal{G}}$, it is possible to choose $R_{\mathcal{G}} \in O(6)$ such that $\hat{\mathcal{G}} = \hat{\mathcal{I}} \cap \hat{\mathcal{H}}_{\mathcal{G}}$, i.e.

$$R^{-1}GR = R_{\mathcal{G}}^{-1}GR_{\mathcal{G}}, \quad \forall G \in \tilde{\mathcal{G}} \Rightarrow (R_{\mathcal{G}}R^{-1})^{-1}G(R_{\mathcal{G}}R^{-1}) = G, \quad \forall G \in \tilde{\mathcal{G}}. \quad (3.2)$$

¹The orthogonal group $O(n)$ splits into two (path) connected components, $SO(n)$ and $O(n)^- = \{A \in O(n) : \det A = -1\}$.

Therefore $R_{\mathcal{G}}R^{-1}$ belongs to the centraliser of $\tilde{\mathcal{G}}$ in $GL(6, \mathbb{R})$, i.e. the set

$$\mathcal{Z}(\tilde{\mathcal{G}}, \mathbb{R}) := \{A \in GL(6, \mathbb{R}) : AG = GA, \forall G \in \tilde{\mathcal{G}}\},$$

which consists of all the matrices in $GL(6, \mathbb{R})$ commuting with all the matrices of $\tilde{\mathcal{G}}$. Hence there exists a matrix $M_{\mathcal{G}} \in \mathcal{Z}(\tilde{\mathcal{G}}, \mathbb{R}) \cap O(6)$, denoted as the *Schur operator* related to \mathcal{G} , such that $R_{\mathcal{G}} = M_{\mathcal{G}}R$. Since R and $R_{\mathcal{G}}$ have determinants with equal signs by assumption, we have that $\det(M_{\mathcal{G}}) > 0$, hence $M_{\mathcal{G}}$ is a rotation in $SO(6)$. Let us consider a path

$$M_{\mathcal{G}}(t) : [0, 1] \longrightarrow \mathcal{Z}(\tilde{\mathcal{G}}, \mathbb{R}) \cap SO(6) \quad (3.3)$$

that connects $M_{\mathcal{G}}$ to the identity matrix I_6 , i.e. $M_{\mathcal{G}}(0) = I_6$ and $M_{\mathcal{G}}(1) = M_{\mathcal{G}}$. Such a path is referred to as the *Schur rotation* associated with $\tilde{\mathcal{G}}$. The name comes from Schur's Lemma in Representation Theory, that gives constraints on the matrices that commute with a representation of a group [68]. In Section 3.2 we prove the existence and determine the explicit forms of (3.3) for all the maximal subgroups of the icosahedral group.

Let us consider the path $R_{\mathcal{G}}(t) : [0, 1] \rightarrow O(6)$ defined by $R_{\mathcal{G}}(t) := M_{\mathcal{G}}(t)R$. Comparing with (2.10), for every $t \in [0, 1]$ the matrix $R_{\mathcal{G}}(t)$ encodes the basis of a physical space E_t^{\parallel} and an orthogonal space E_t^{\perp} that carry the representations \mathcal{G}_1 and \mathcal{G}_2 of \mathcal{G} as in (3.1) since

$$R_{\mathcal{G}}(t)^{-1}\tilde{\mathcal{G}}R_{\mathcal{G}}(t) = R^{-1}M_{\mathcal{G}}(t)^{-1}\tilde{\mathcal{G}}M_{\mathcal{G}}(t)R = R^{-1}\tilde{\mathcal{G}}R = \mathcal{G}_1 \oplus \mathcal{G}_2. \quad (3.4)$$

In particular, we have $E_t^{\parallel} = M_{\mathcal{G}}(t)E^{\parallel}$ and $E_0^{\parallel} \equiv E^{\parallel}$, $E_1^{\parallel} \equiv E_{\mathcal{G}}^{\parallel}$ (and similarly for the orthogonal spaces). For $t \in [0, 1]$, the projections $\pi_t^{\parallel} : \mathbb{R}^6 \rightarrow E_t^{\parallel}$ and $\pi_t^{\perp} : \mathbb{R}^6 \rightarrow E_t^{\perp}$ are given by (compare with (2.12)):

$$\begin{pmatrix} \pi_t^{\parallel} \\ \pi_t^{\perp} \end{pmatrix} = R_{\mathcal{G}}^{-1}(t) = R^{-1}M_{\mathcal{G}}(t)^{-1} = \begin{pmatrix} \pi^{\parallel} \\ \pi^{\perp} \end{pmatrix} M_{\mathcal{G}}(t)^{-1} = \begin{pmatrix} \pi^{\parallel} M_{\mathcal{G}}(t)^{-1} \\ \pi^{\perp} M_{\mathcal{G}}(t)^{-1} \end{pmatrix}. \quad (3.5)$$

With this setup, we can define structural transitions between icosahedral quasicrystals that keep the symmetry encoded by \mathcal{G} preserved. Specifically, let \mathcal{L} be one of the three hypercubic lattices in \mathbb{R}^6 described in Section 2.1; if $W := \pi^{\perp}(\mathcal{V}(\mathbf{0}))$ denotes the projection of the Voronoi cell $\mathcal{V}(\mathbf{0})$ of the origin (cf. (1.17)), then we can define the model set $\Sigma(W)$ as in (1.18), which displays icosahedral symmetry by construction. Let us then consider, for all $t \in [0, 1]$, the projection $W_t := \pi_t^{\parallel}(\mathcal{V}(\mathbf{0}))$ of $\mathcal{V}(\mathbf{0})$ into the space E_t^{\perp} . We can define the family of model sets

$$\Sigma_t \equiv \Sigma(W_t) := \{\pi_t^{\parallel}(\mathbf{v}) : \mathbf{v} \in \mathcal{L}, \pi_t^{\perp}(\mathbf{v}) \in W_t\}. \quad (3.6)$$

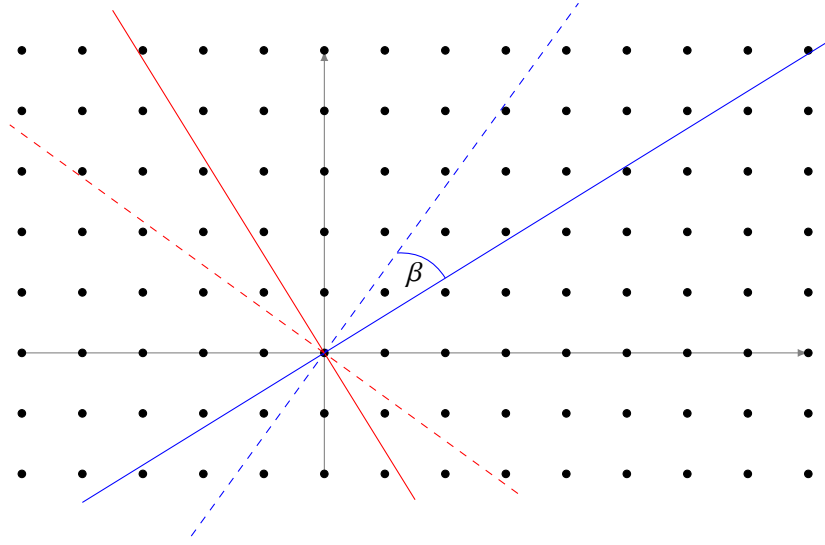


Figure 3.1: Illustration of the Schur rotation for a one-dimensional quasicrystal (compare with Figure 1.2). The physical space (straight line in red) and the orthogonal space (straight line in blue) undergo a rotation of an angle β , resulting in the new physical and orthogonal spaces (dashed lines). The two-dimensional lattice remains fixed throughout the rotation.

By construction, $\Sigma_0 \equiv \Sigma(W)$ and Σ_1 possess icosahedral symmetry, whereas the intermediate states Σ_t , for $t \in (0, 1)$, display \mathcal{G} -symmetry since, by (3.4) (compare with (1.15)):

$$\pi_t^{\parallel}(\tilde{\mathcal{G}}\mathbf{v}) = \mathcal{G}_1 \pi_t^{\parallel}(\mathbf{v}), \quad \forall t \in (0, 1). \quad (3.7)$$

Hence, the Schur rotation $M_{\mathcal{G}}(t)$ as in (3.3) defines a continuous transformation of the model set $\Sigma(W)$ into another icosahedral quasilattice, where \mathcal{G} -symmetry is preserved. We point out that, in the higher dimensional space, the lattice \mathcal{L} is *fixed* and the transformation is induced by the rotation of the physical and orthogonal spaces (see Figure 3.1). The angle(s) of rotation correspond(s) to the degree(s) of freedom of the transformation, and can be chosen as the *order parameter(s)* of the transition in the framework of the Landau theory [13].

Transitions of finite icosahedral point sets. In the context of virology and carbon chemistry, the arrangements of viral proteins and carbon atoms in fullerenes are modeled via finite point sets (arrays) with icosahedral symmetry. The method developed here can also be applied to analyse structural transitions between icosahedral arrays, creating finite point sets via projection, as opposed to the infinite ones generated by the cut-and-project scheme,

at every time t of the transformation. Indeed, let $C = \{\pi^{\parallel}(\mathbf{v}_i) : \mathbf{v}_i \in \mathcal{L}, i = 1, \dots, n\}$ be a finite point set in E^{\parallel} , obtained via the projection of points of a hypercubic lattice \mathcal{L} in \mathbb{R}^6 . Let us assume that C is closed under the action of the irrep ρ_3 of \mathcal{I} (cf. (2.9)), i.e. $\rho_3 C \subseteq C$. The projection operators π_t^{\parallel} given in (3.5) can be used to define a family of arrays C_t , for $t \in [0, 1]$, given by:

$$C_t := \{\pi_t^{\parallel}(\mathbf{v}_i) : \mathbf{v}_i \in C, i = 1, \dots, n\}. \quad (3.8)$$

It follows from (3.7) that the point sets C_t are invariant under the representation \mathcal{G}_1 of \mathcal{G} (cf. (3.1)) for all $t \in (0, 1)$, and moreover possess icosahedral symmetry for $t = 0$ and $t = 1$. In Chapter 4 a new method will be introduced for the construction of finite point sets with non-crystallographic symmetry via projection and studied in detail.

Connection with the Bain strain method. In crystallography and condensed matter physics, the concept of Bain strain relates to deformations of three-dimensional lattices that keep some symmetry preserved, described by a common subgroup of the point groups of the lattices which constitute the initial and final states [33]. Indelicato *et al.* [66, 67] provided a higher-dimensional generalisation of the Bain strain for lattices in \mathbb{R}^n . In this context, given two lattices \mathcal{L}_0 and \mathcal{L}_1 with generator matrices B_0 and B_1 , respectively, and a subgroup \mathcal{H} of $\mathcal{P}(\mathcal{L}_0)$ and $\mathcal{P}(\mathcal{L}_1)$, a transition between \mathcal{L}_0 and \mathcal{L}_1 with symmetry \mathcal{H} is a path $B(t) : [0, 1] \rightarrow GL(n, \mathbb{R})$ such that, if \mathcal{L}_t denotes the intermediate lattice with generator matrix $B(t)$, then $\mathcal{H} \subseteq \mathcal{P}(\mathcal{L}_t)$, for all $t \in [0, 1]$. If \mathcal{L}_0 and \mathcal{L}_1 are 6D hypercubic lattices, and $\mathcal{H} = \tilde{\mathcal{G}}$ a maximal subgroup of $\tilde{\mathcal{I}}$, then $B(t)$ induces a continuous transformation

$$\tilde{\Sigma}_t := \{\pi^{\parallel}(\mathbf{v}_t) : \pi^{\perp}(\mathbf{v}_t) \in \pi^{\perp}(\mathcal{V}_t(\mathbf{0}))\}, \quad (3.9)$$

where $\mathbf{v}_t := B(t)\mathbf{m}$, $\mathbf{m} \in \mathbb{Z}^6$, is a point in the intermediate lattice \mathcal{L}_t , and $\mathcal{V}_t(\mathbf{0})$ denotes the Voronoi cell of \mathcal{L}_t at the origin. The symmetry identified by \mathcal{G} is preserved since, again by (1.15), $\mathcal{G}_1 \pi^{\parallel}(\mathbf{v}_t) = \pi^{\parallel}(\tilde{\mathcal{G}}\mathbf{v}_t)$, and $\tilde{\mathcal{G}}\mathbf{v}_t \in \mathcal{L}_t$ since $\tilde{\mathcal{G}} \subseteq \mathcal{P}(\mathcal{L}_t)$ for all $t \in [0, 1]$. We notice that in this approach the lattice undergoes a transformation, whereas the physical and orthogonal spaces remain fixed.

As already pointed out in [66], the Schur rotation and the generalised Bain strain are related. This can easily be proved with the mathematics developed so far. In particular, if $M_{\mathcal{G}}(t)$ is a Schur rotation associated with \mathcal{G} as in (3.3), let us define the path $\hat{B}(t) : [0, 1] \rightarrow$

$GL(6, \mathbb{R})$ as

$$\hat{B}(t) := M_{\mathcal{G}}(t)^{-1} B_0. \quad (3.10)$$

We have, using (3.5),

$$\pi^{\parallel}(\hat{B}(t)) = \pi^{\parallel}(M_{\mathcal{G}}(t)^{-1} B_0) = \pi_t^{\parallel}(B_0),$$

and similarly for π_t^{\perp} . Therefore

$$\widetilde{\Sigma}_t = \{\pi^{\parallel}(\mathbf{v}_t) : \pi^{\perp}(\mathbf{v}_t) \in \pi^{\perp}(\mathcal{V}_t(\mathbf{0}))\} = \{\pi_t^{\parallel}(B_0 \mathbf{m}) : \pi_t^{\perp}(B_0 \mathbf{m}) \in \pi_t^{\perp}(\mathcal{V}(\mathbf{0}))\} = \Sigma_t,$$

and moreover $\widetilde{\mathcal{G}} \subseteq \mathcal{P}(\mathcal{L}_t)$, since $\mathcal{P}(\hat{B}(t)) = M_{\mathcal{G}}^{-1}(t) \mathcal{P}(B_0) M_{\mathcal{G}}(t)$ (cf. (1.5)) and $M_{\mathcal{G}}(t) \in \mathbb{Z}(\widetilde{\mathcal{G}}, \mathbb{R})$ for all t . Hence the Schur rotation is equivalent to a Bain strain transformation between *congruent* lattices (compare with (1.6)). The advantage of the former is that the use of Schur's Lemma and tools from representation theory can be used in the computation and allow a characterisation of such transitions in a purely group theoretical framework.

3.2 Computations and applications

In this section we compute the Schur rotations for the maximal subgroups of the icosahedral group, and discuss applications and specific examples. First of all, we recall the statement of Schur's Lemma in the matrix form (for the proof see, for example, [68]):

Lemma 3.2.1 (Schur). *Let $D : G \rightarrow GL(n, \mathbb{C})$ be an irreducible representation of a group G . If $B \in GL(n, \mathbb{C})$ is a matrix that commutes with all the matrix representatives of D , i.e.*

$$BD(g) = D(g)B, \quad \forall g \in G,$$

then $B = \lambda I_n$, with $\lambda \in \mathbb{C}$, i.e. B is a multiple of the identity matrix I_n . Let $D' : G \rightarrow GL(n, \mathbb{C})$ be another irreducible representation of G which is inequivalent to D . If $C \in GL(n, \mathbb{C})$ is such that

$$CD(g) = D'(g)C, \quad \forall g \in G,$$

then $C = 0_n$, the null matrix of size n .

In order to compute the possible Schur rotations associated with a maximal subgroup \mathcal{G} of \mathcal{I} , we need to consider the matrix group $\mathcal{Z}(\widetilde{\mathcal{G}}, \mathbb{R}) \cap \text{SO}(6)$, where $\widetilde{\mathcal{G}} \subseteq \widetilde{\mathcal{I}}$ is a representation of \mathcal{G} in B_6 . Let us first focus on the group $\mathcal{Z}(\hat{\mathcal{G}}, \mathbb{R}) \cap \text{SO}(6)$, which consists of all

the rotations in $SO(6)$ that commute with the matrices constituting the *reduced* representation $\hat{\mathcal{G}}$. A matrix in this group can be easily computed using Schur's Lemma; the group $\mathcal{Z}(\tilde{\mathcal{G}}, \mathbb{R}) \cap SO(6)$ then easily follows since [55]

$$\mathcal{Z}(\hat{\mathcal{G}}, \mathbb{R}) = \mathcal{Z}(R^{-1}\tilde{\mathcal{G}}R, \mathbb{R}) = R^{-1}\mathcal{Z}(\tilde{\mathcal{G}}, \mathbb{R})R. \quad (3.11)$$

We now consider in detail the computations and examples for each maximal subgroup of the icosahedral group.

3.2.1 Tetrahedral group \mathcal{T}

The tetrahedral group \mathcal{T} is the rotational group of a tetrahedron, generated by a two-fold rotation g_2 and a three-fold rotation g_{3d} such that $g_2^2 = g_{3d}^3 = (g_2g_{3d})^3 = e$ (cf. Table 2.2). It is isomorphic to the alternating group \mathfrak{A}_4 and its character table is given by (cf. [68]):

Irrep	$C(e)$	$4C_3$	$4C_3^2$	$3C_2$
A	1	1	1	1
E_1	1	ω	ω^2	1
E_2	1	ω^2	ω	1
T	3	0	0	-1

where $\omega = e^{\frac{2\pi i}{3}}$. Note that the representations E_1 and E_2 are complex, while their direct sum $E := E_1 \oplus E_2$ is real and irreducible in $GL(2, \mathbb{R})$. An explicit representation $\tilde{\mathcal{T}}$ of \mathcal{T} , which is a subgroup of $\tilde{\mathcal{I}}$, is given by

$$\tilde{\mathcal{T}} = \left\langle \begin{pmatrix} 0 & 0 & 0 & 0 & 0 & 1 \\ 0 & 0 & 0 & 0 & 1 & 0 \\ 0 & 0 & -1 & 0 & 0 & 0 \\ 0 & 0 & 0 & -1 & 0 & 0 \\ 0 & 1 & 0 & 0 & 0 & 0 \\ 1 & 0 & 0 & 0 & 0 & 0 \end{pmatrix}, \begin{pmatrix} 0 & 1 & 0 & 0 & 0 & 0 \\ 0 & 0 & 0 & -1 & 0 & 0 \\ 0 & 0 & 0 & 0 & 0 & -1 \\ -1 & 0 & 0 & 0 & 0 & 0 \\ 0 & 0 & 1 & 0 & 0 & 0 \\ 0 & 0 & 0 & 0 & -1 & 0 \end{pmatrix} \right\rangle,$$

The matrix R as in (2.11) is such that

$$\hat{\mathcal{T}} := R^{-1}\tilde{\mathcal{T}}R = \Gamma_1 \oplus \Gamma_2, \quad (3.12)$$

where Γ_1 and Γ_2 are matrix subgroups of ρ_3 and ρ'_3 as in (2.9), respectively, and both are equivalent to the irrep T of \mathcal{T} . Due to this equivalence, there exists a matrix $Q \in GL(3, \mathbb{R})$

such that $Q^{-1}\Gamma_2Q = \Gamma_1$. The explicit forms of Γ_1 , Γ_2 and Q are given in the Appendix. Note that Q can be chosen to be orthogonal. Let us define $\hat{Q} := I_3 \oplus Q \in O(6, \mathbb{R})$, where I_3 denotes the 3×3 identity matrix; then we have

$$\bar{\mathcal{T}} := \hat{Q}^{-1}\hat{\mathcal{T}}\hat{Q} = \Gamma_1 \oplus \Gamma_1. \quad (3.13)$$

We consider the set $\mathcal{Z}(\bar{\mathcal{T}}, \mathbb{R}) \cap \text{SO}(6)$. Writing a matrix N in this group as

$$N = \begin{pmatrix} N_1 & N_2 \\ N_3 & N_4 \end{pmatrix},$$

where N_i are 3×3 matrices, for $i = 1, \dots, 4$, we impose $N\bar{\mathcal{T}} = \bar{\mathcal{T}}N$, i.e. $N(\Gamma_1 \oplus \Gamma_1) = (\Gamma_1 \oplus \Gamma_1)N$. Using Schur's Lemma and imposing orthogonality, we obtain

$$N = N(\beta) = \begin{pmatrix} \cos(\beta)I_3 & -\sin(\beta)I_3 \\ \sin(\beta)I_3 & \cos(\beta)I_3 \end{pmatrix},$$

where β belongs to the unit circle S^1 . Notice that $N(\alpha)N(\beta) = N(\alpha + \beta)$. Putting together (3.13) and (3.11) we obtain

$$\mathcal{Z}(\tilde{\mathcal{T}}, \mathbb{R}) \cap \text{SO}(6) = \left\{ (R\hat{Q})N(\beta)(R\hat{Q})^{-1} : N(\beta) = \begin{pmatrix} \cos(\beta)I_3 & -\sin(\beta)I_3 \\ \sin(\beta)I_3 & \cos(\beta)I_3 \end{pmatrix}, \beta \in S^1 \right\}.$$

It follows that the group $\mathcal{Z}(\tilde{\mathcal{T}}, \mathbb{R}) \cap \text{SO}(6)$ is isomorphic to S^1 , hence it is a compact and connected Lie group. Therefore, the angle $\beta \in S^1$ can be chosen as an order parameter for the transitions with tetrahedral symmetry.

In order to compute the Schur rotations between icosahedral quasicrystals with \mathcal{T} -symmetry, we need to fix the boundary conditions, i.e. imposing the end and the start of the transition to have icosahedral symmetry. In particular, we consider the crystallographic representation $\tilde{\mathcal{I}}_{\mathcal{T}}$ of \mathcal{I} with the property that $\tilde{\mathcal{T}} = \tilde{\mathcal{I}} \cap \tilde{\mathcal{I}}_{\mathcal{T}}$:

$$\tilde{\mathcal{I}}_{\mathcal{T}} = \left\langle \begin{pmatrix} 0 & 0 & 0 & -1 & 0 & 0 \\ 0 & 0 & 0 & 0 & 0 & -1 \\ 0 & 0 & -1 & 0 & 0 & 0 \\ -1 & 0 & 0 & 0 & 0 & 0 \\ 0 & 0 & 0 & 0 & -1 & 0 \\ 0 & -1 & 0 & 0 & 0 & 0 \end{pmatrix}, \begin{pmatrix} 0 & 0 & 0 & -1 & 0 & 0 \\ 0 & 0 & 0 & 0 & -1 & 0 \\ 0 & -1 & 0 & 0 & 0 & 0 \\ 0 & 0 & 0 & 0 & 0 & 1 \\ 0 & 0 & 1 & 0 & 0 & 0 \\ -1 & 0 & 0 & 0 & 0 & 0 \end{pmatrix} \right\rangle.$$

Given $M_{\mathcal{T}}(\beta) \in \mathcal{Z}(\tilde{\mathcal{T}}, \mathbb{R}) \cap \text{SO}(6)$, we consider the matrix $R_{\mathcal{T}}(\beta) := M_{\mathcal{T}}(\beta)R \in O(6)$ and impose

$$R_{\mathcal{T}}(\beta)^{-1}\tilde{\mathcal{I}}_{\mathcal{T}}R_{\mathcal{T}}(\beta) \simeq T_1 \oplus T_2, \quad (3.14)$$

We solve the equation 3.14 with respect to β ; in other words, we look for angles $\hat{\beta} \in S^1$ such that the corresponding matrix $R_{\mathcal{T}}(\hat{\beta})$ decomposes into irreps the representation $\widetilde{\mathcal{I}}_{\mathcal{T}}$. Specifically, let M_2 and M_3 denote the generators of $\widetilde{\mathcal{I}}_{\mathcal{T}}$, and let us define the matrices $K_j(\beta) := R_{\mathcal{T}}(\beta)^{-1} M_j R_{\mathcal{T}}(\beta)$, for $j = 2, 3$. Condition (3.14) is then equivalent to the following system of 36 equations:

$$\begin{cases} (K_2(\beta))_{ij} = 0, (K_2(\beta))_{ji} = 0 \\ (K_3(\beta))_{ij} = 0, (K_3(\beta))_{ji} = 0 \end{cases} \quad \text{for } i = 1, 2, 3 \text{ and } j = 4, 5, 6. \quad (3.15)$$

The solutions of (3.15) are given by:

$$\hat{\beta} \in \left\{ -\arctan\left(\frac{1}{2}\right), -\arctan\left(\frac{1}{2}\right) + \pi, \arctan(2), \arctan(2) - \pi \right\} =: S_{\mathcal{T}}.$$

Hence the number of Schur operators associated with \mathcal{T} is finite; the elements in $S_{\mathcal{T}}$ provide all the possible boundary conditions for the analysis of transitions with \mathcal{T} -symmetry between icosahedral order. Specifically, since S^1 is connected, we can consider any path $\beta(t) : [0, 1] \rightarrow S^1$ that connects 0 with $\hat{\beta} \in S_{\mathcal{T}}$, i.e. $\beta(0) = 0$ and $\beta(1) = \hat{\beta}$. Then the corresponding Schur rotation $M_{\mathcal{T}}(t)$ is given by $M_{\mathcal{T}}(\beta) \circ \beta(t) = M_{\mathcal{T}}(\beta(t)) : [0, 1] \rightarrow \mathcal{Z}(\widetilde{\mathcal{T}}, \mathbb{R}) \cap \text{SO}(6)$.

Example: tetrahedral transition with an intermediate cubic lattice. We consider as an explicit example of a tetrahedral transition the path $\beta(t) = \hat{\beta}t$, that connects 0 with $\hat{\beta} = -\arctan\left(\frac{1}{2}\right)$. The lattice \mathcal{L} in \mathbb{R}^6 is taken as the simple cubic lattice with basis the standard basis in \mathbb{R}^6 . The matrix $R_{\mathcal{T}}(t) = M_{\mathcal{T}}(\hat{\beta}t)R$ encodes the projections π_i^{\parallel} and π_i^{\perp} as in (3.5), that define the family of model sets Σ_t as in (3.6). In Figure 3.2 we show a patch of the resulting quasilattices for $t = 0, 0.5$ and 1. These are very interesting results; indeed, the starting and final states display icosahedral aperiodicity, as expected by the boundary conditions, while for $t = 0.5$ the corresponding quasilattice is actually a three-dimensional lattice, i.e. periodic. Hence such a transition has an intermediate periodic order, which is in accordance to the previous result by Kramer [29]. From a group theoretical point of view, this implies that there exists a subgroup of B_6 isomorphic to the octahedral group \mathcal{O} (i.e. the symmetry group of a cube, with order 48), which contains $\widetilde{\mathcal{T}}$ as a subgroup.

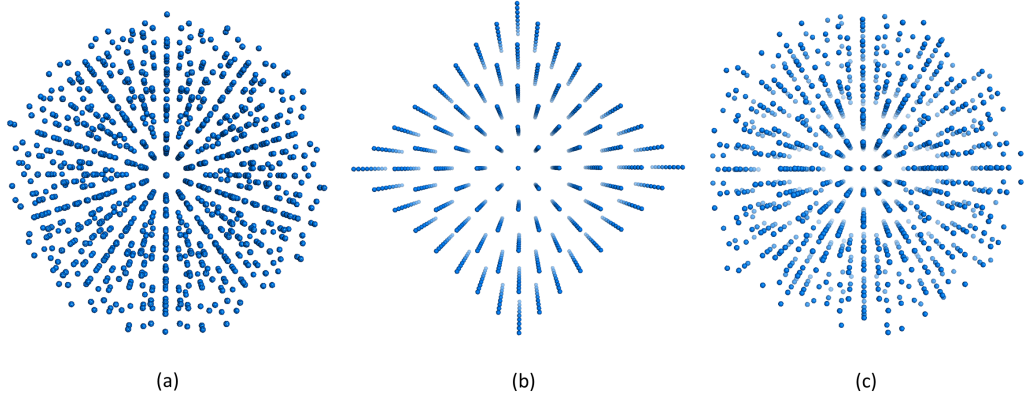


Figure 3.2: Example of a transition with tetrahedral symmetry. The model sets in (a) and (c) correspond to the starting and final states, respectively, and display icosahedral symmetry. The intermediate state in (b) is compatible with octahedral symmetry and defines a three-dimensional cubic lattice.

3.2.2 Dihedral group \mathcal{D}_{10}

The dihedral group \mathcal{D}_{10} is generated by two elements g_{2d} and g_{5d} such that $g_{2d}^2 = g_{5d}^5 = (g_{2d}g_{5d})^2 = e$ (cf. Table 4.1). Its character table is as follows [68]:

Irrep	E	$2C_5$	$2C_5^2$	$5C_2$
A_1	1	1	1	1
A_2	1	1	1	-1
E_1	2	$\tau - 1$	$-\tau$	0
E_2	2	$-\tau$	$\tau - 1$	0

An explicit representation $\widetilde{\mathcal{D}}_{10}$ as a matrix subgroup of $\widetilde{\mathcal{I}}$ is given by

$$\widetilde{\mathcal{D}}_{10} = \left\langle \begin{pmatrix} 0 & 0 & 0 & 0 & 0 & -1 \\ 0 & -1 & 0 & 0 & 0 & 0 \\ 0 & 0 & 0 & 1 & 0 & 0 \\ 0 & 0 & 1 & 0 & 0 & 0 \\ 0 & 0 & 0 & 0 & -1 & 0 \\ -1 & 0 & 0 & 0 & 0 & 0 \end{pmatrix}, \begin{pmatrix} 0 & 0 & 0 & 0 & 0 & 1 \\ 0 & 1 & 0 & 0 & 0 & 0 \\ 0 & 0 & 0 & 0 & -1 & 0 \\ -1 & 0 & 0 & 0 & 0 & 0 \\ 0 & 0 & 0 & 1 & 0 & 0 \\ 0 & 0 & 1 & 0 & 0 & 0 \end{pmatrix} \right\rangle.$$

In order to compute the Schur rotations associated with \mathcal{D}_{10} , we proceed in a similar way as in the tetrahedral case. The projection matrix R in (2.11) decomposes $\widetilde{\mathcal{D}}_{10}$ as

$$\widehat{\mathcal{D}}_{10} := R^{-1}\widetilde{\mathcal{D}}_{10}R = D_1 \oplus D_2, \quad (3.16)$$

where D_1 and D_2 are matrix subgroups of ρ_3 and ρ'_3 , respectively, that are *reducible* representations of \mathcal{D}_{10} . In particular, from its character table we have that $D_1 \simeq A_2 \oplus E_1$ and $D_2 \simeq A_2 \oplus E_2$ in $GL(3, \mathbb{R})$. In order to find the Schur operators for \mathcal{D}_{10} , we first reduce D_1 and D_2 into irreps, using the projection operators given in (1.12). In particular, we determine two orthogonal matrices, P_1 and P_2 , such that

$$\hat{D}_1 := P_1^{-1} D_1 P_1 \simeq A_2 \oplus E_1, \quad \hat{D}_2 := P_2^{-1} D_2 P_2 \simeq A_2 \oplus E_2. \quad (3.17)$$

The explicit forms of D_1 , D_2 , P_1 and P_2 are given in the Appendix. The matrix $Z := P_1 \oplus P_2$ is such that (cf. (3.16)):

$$Z^{-1}(R^{-1} \tilde{\mathcal{D}}_{10} R) Z = Z^{-1} \hat{\mathcal{D}}_{10} Z = \hat{D}_1 \oplus \hat{D}_2 =: \overline{\mathcal{D}}_{10}.$$

By Schur's Lemma, a matrix $M \in \mathcal{Z}(\overline{\mathcal{D}}_{10}, \mathbb{R}) \cap \text{SO}(6)$ must be of the form

$$M = M(\beta) = \begin{pmatrix} \cos(\beta) & 0 & 0 & -\sin(\beta) & 0 & 0 \\ 0 & 1 & 0 & 0 & 0 & 0 \\ 0 & 0 & 1 & 0 & 0 & 0 \\ \sin(\beta) & 0 & 0 & \cos(\beta) & 0 & 0 \\ 0 & 0 & 0 & 0 & 1 & 0 \\ 0 & 0 & 0 & 0 & 0 & 1 \end{pmatrix}.$$

Combining these results, we obtain

$$\mathcal{Z}(\tilde{\mathcal{D}}_{10}, \mathbb{R}) \cap \text{SO}(6) = \{(RZ)M(\beta)(RZ)^{-1} : M(\beta) \in \mathcal{Z}(\overline{\mathcal{D}}_{10}, \mathbb{R}) \cap \text{SO}(6)\}.$$

Hence, as in the tetrahedral case, the group $\mathcal{Z}(\tilde{\mathcal{D}}_{10}, \mathbb{R}) \cap \text{SO}(6)$ is isomorphic to S^1 and therefore the Schur rotations associated with \mathcal{D}_{10} are parameterised by an angle $\beta \in S^1$. As in the \mathcal{T} -case, in order to fix the boundary conditions of the transitions we consider the unique crystallographic representation $\tilde{\mathcal{I}}_{\mathcal{D}_{10}}$ in B_6 such that $\tilde{\mathcal{D}}_{10} = \tilde{\mathcal{I}} \cap \tilde{\mathcal{I}}_{\mathcal{D}_{10}}$, whose explicit form is

$$\tilde{\mathcal{I}}_{\mathcal{D}_{10}} = \left\langle \begin{pmatrix} 0 & 0 & 0 & 0 & -1 & 0 \\ 0 & 0 & 0 & 1 & 0 & 0 \\ 0 & 0 & -1 & 0 & 0 & 0 \\ 0 & 1 & 0 & 0 & 0 & 0 \\ -1 & 0 & 0 & 0 & 0 & 0 \\ 0 & 0 & 0 & 0 & 0 & -1 \end{pmatrix}, \begin{pmatrix} 0 & 0 & 0 & 0 & -1 & 0 \\ 0 & 0 & -1 & 0 & 0 & 0 \\ 0 & 0 & 0 & 0 & 0 & 1 \\ 1 & 0 & 0 & 0 & 0 & 0 \\ 0 & 0 & 0 & -1 & 0 & 0 \\ 0 & -1 & 0 & 0 & 0 & 0 \end{pmatrix} \right\rangle.$$

Let $R_{\mathcal{D}_{10}}(\beta) := M_{\mathcal{D}_{10}}(\beta)R$, where $M_{\mathcal{D}_{10}}(\beta) \in \mathcal{Z}(\tilde{\mathcal{D}}_{10}, \mathbb{R}) \cap \text{SO}(6)$. We impose

$$R_{\mathcal{D}_{10}}(\beta)^{-1} \tilde{\mathcal{I}}_{\mathcal{D}_{10}} R_{\mathcal{D}_{10}}(\beta) \simeq T_1 \oplus T_2. \quad (3.18)$$

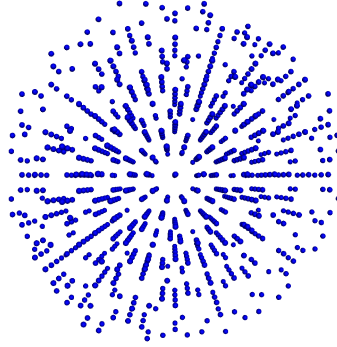


Figure 3.3: Patch of a quasilattice with \mathcal{D}_{10} -symmetry, obtained from the Schur rotation associated with \mathcal{D}_{10} and corresponding to the intermediate state $\beta = \frac{\pi}{4}$.

The corresponding systems of equations (compare with (3.15)) has only one solution, namely $\hat{\beta} = \frac{\pi}{2}$. Hence any path $\beta_{\mathcal{D}_{10}}(t) : [0, 1] \rightarrow S^1$ connecting 0 with $\frac{\pi}{2}$ induces a Schur rotation as in (3.3) given by $M_{\mathcal{D}_{10}}(\beta) \circ \beta_{\mathcal{D}_{10}}(t) = M_{\mathcal{D}_{10}}(\beta_{\mathcal{D}_{10}}(t)) : [0, 1] \rightarrow \mathcal{Z}(\tilde{\mathcal{D}}_{10}, \mathbb{R}) \cap \text{SO}(6)$. In Figure 3.3 we show the quasilattice corresponding to the intermediate state $\beta = \frac{\pi}{4}$.

3.2.3 Dihedral group \mathcal{D}_6

The dihedral group \mathcal{D}_6 is isomorphic to the symmetric group S_3 and is generated by two elements g_{2d} and g_3 such that $g_{2d}^2 = g_3^3 = (g_2 g_3)^2 = e$ (cf. Table 4.1). Its character table is as follows (cf. [68]):

Irrep	E	$3C_2$	$2C_3$
A_1	1	1	1
A_2	1	-1	1
E	2	0	-1

In order to compute the Schur rotations associated with \mathcal{D}_6 , we proceed in complete analogy with \mathcal{D}_{10} . Indeed, let $\tilde{\mathcal{D}}_6$ be the representation of \mathcal{D}_6 as a subgroup of $\tilde{\mathcal{I}}$ given by

$$\tilde{\mathcal{D}}_6 = \left\langle \left(\begin{array}{cccccc} 0 & 0 & 0 & 0 & 0 & -1 \\ 0 & -1 & 0 & 0 & 0 & 0 \\ 0 & 0 & 0 & 1 & 0 & 0 \\ 0 & 0 & 1 & 0 & 0 & 0 \\ 0 & 0 & 0 & 0 & -1 & 0 \\ -1 & 0 & 0 & 0 & 0 & 0 \end{array} \right), \left(\begin{array}{cccccc} 0 & 0 & 0 & 0 & 0 & 1 \\ 0 & 0 & 0 & 1 & 0 & 0 \\ 0 & -1 & 0 & 0 & 0 & 0 \\ 0 & 0 & -1 & 0 & 0 & 0 \\ 1 & 0 & 0 & 0 & 0 & 0 \\ 0 & 0 & 0 & 0 & 1 & 0 \end{array} \right) \right\rangle.$$

The matrix R , given by (2.9), reduces this representation as

$$\hat{\mathcal{D}}_6 := R^{-1}\tilde{\mathcal{D}}_6R = S_1 \oplus S_2, \quad (3.19)$$

where S_1 and S_2 are representations of \mathcal{D}_6 that are reducible. Using formula (1.11), both split into $A_2 \oplus E$ in $GL(3, \mathbb{R})$, and therefore are equivalent in $GL(3, \mathbb{R})$. Using the projection operators in (1.12), we identify two matrices R_1 and R_2 in $GL(3, \mathbb{R})$ that reduce into the same irreps S_1 and S_2 , i.e.

$$R_1^{-1}S_1R_1 = R_2^{-1}S_2R_2 \simeq A_2 \oplus E. \quad (3.20)$$

The explicit forms of such matrices are given in the Appendix. Let V be the matrix in $GL(6, \mathbb{R})$ given by $V := R_1 \oplus R_2$. We have

$$\overline{\mathcal{D}}_6 := V^{-1}\hat{\mathcal{D}}_6V \simeq A_2 \oplus E \oplus A_2 \oplus E.$$

Schur's Lemma forces a matrix $P \in \mathcal{Z}(\overline{\mathcal{D}}_6, \mathbb{R}) \cap \text{SO}(6)$ to have the form

$$P = P(\alpha, \beta) = \begin{pmatrix} \cos(\alpha) & 0 & 0 & -\sin(\alpha) & 0 & 0 \\ 0 & \cos(\beta) & 0 & 0 & -\sin(\beta) & 0 \\ 0 & 0 & \cos(\beta) & 0 & 0 & -\sin(\beta) \\ \sin(\alpha) & 0 & 0 & \cos(\alpha) & 0 & 0 \\ 0 & \sin(\beta) & 0 & 0 & \cos(\beta) & 0 \\ 0 & 0 & \sin(\beta) & 0 & 0 & \cos(\beta) \end{pmatrix},$$

where $(\alpha, \beta) \in S^1 \times S^1$. Hence

$$\mathcal{Z}(\tilde{\mathcal{D}}_6, \mathbb{R}) \cap \text{SO}(6) = \{(RV)P(\alpha, \beta)(RV)^{-1} : P(\alpha, \beta) \in \mathcal{Z}(\overline{\mathcal{D}}_6, \mathbb{R}) \cap \text{SO}(6)\}.$$

Therefore, contrary to the other maximal subgroups of \mathcal{I} , the Schur rotations associated with \mathcal{D}_6 are parameterised by two angles belonging to a two-dimensional torus $\mathbb{T}^2 \simeq S^1 \times S^1$. In other words, the less the symmetry is preserved during the transition, the more the physical and orthogonal space are free to rotate. As before, to fix the boundary conditions, we consider the representation $\tilde{\mathcal{I}}_{\mathcal{D}_6}$ such that $\tilde{\mathcal{D}}_6 = \tilde{\mathcal{I}} \cap \tilde{\mathcal{I}}_{\mathcal{D}_6}$:

$$\tilde{\mathcal{I}}_{\mathcal{D}_6} = \left\langle \begin{pmatrix} 0 & 0 & -1 & 0 & 0 & 0 \\ 0 & 0 & 0 & 0 & 0 & -1 \\ -1 & 0 & 0 & 0 & 0 & 0 \\ 0 & 0 & 0 & -1 & 0 & 0 \\ 0 & 0 & 0 & 0 & -1 & 0 \\ 0 & -1 & 0 & 0 & 0 & 0 \end{pmatrix}, \begin{pmatrix} 0 & 0 & -1 & 0 & 0 & 0 \\ 0 & 0 & 0 & 0 & 1 & 0 \\ 0 & 0 & 0 & 0 & 0 & 1 \\ 0 & -1 & 0 & 0 & 0 & 0 \\ 0 & 0 & 0 & -1 & 0 & 0 \\ -1 & 0 & 0 & 0 & 0 & 0 \end{pmatrix} \right\rangle.$$

Let $R_{\mathcal{D}_6}(\alpha, \beta) := M_{\mathcal{D}_6}(\alpha, \beta)R$, where $M_{\mathcal{D}_6}(\alpha, \beta) \in \mathcal{Z}(\widetilde{\mathcal{D}}_6, \mathbb{R}) \cap \text{SO}(6)$. We impose

$$R_{\mathcal{D}_6}(\alpha, \beta)^{-1} \widetilde{\mathcal{I}}_{\mathcal{D}_6} R_{\mathcal{D}_6}(\alpha, \beta) \simeq T_1 \oplus T_2,$$

and solve for α and β . There are 8 distinct solutions $(\hat{\alpha}, \hat{\beta})$ given by

$$\begin{aligned} (\hat{\alpha}, \hat{\beta}) \in & \left\{ \left(\arctan\left(\frac{1}{2}\right), \arctan(2) \right), \left(\arctan(2), \pi - \arctan\left(\frac{1}{2}\right) \right), \left(\arctan\left(\frac{1}{2}\right), \arctan(2) - \pi \right), \right. \\ & \left(-\arctan(2), -\arctan\left(\frac{1}{2}\right) \right), \left(\arctan\left(\frac{1}{2}\right) - \pi, \arctan(2) - \pi \right), \left(\pi - \arctan(2), -\arctan\left(\frac{1}{2}\right) \right), \right. \\ & \left. \left(\arctan\left(\frac{1}{2}\right) - \pi, \arctan(2) \right), \left(\pi - \arctan(2), \pi - \arctan\left(\frac{1}{2}\right) \right) \right\} =: S_{\mathcal{D}_6}. \end{aligned}$$

Any path $\gamma(t) : [0, 1] \rightarrow \mathbb{T}^2$ connecting $(0, 0)$ with any $(\hat{\alpha}, \hat{\beta}) \in S_{\mathcal{D}_6}$ defines a Schur rotation $M_{\mathcal{D}_6}(t) := M_{\mathcal{D}_6}(\alpha, \beta) \circ \gamma(t) : [0, 1] \rightarrow \mathcal{Z}(\widetilde{\mathcal{D}}_6, \mathbb{R}) \cap \text{SO}(6)$.

Continuous transformation of an icosahedron into a hexagonal prism. Let us consider the path $\gamma : [0, 1] \rightarrow \mathbb{T}^2$ given by $\gamma(t) = (t\hat{\alpha}, t\hat{\beta})$, connecting $(0, 0)$ with the point $(\hat{\alpha}, \hat{\beta}) = \left(\arctan\left(\frac{1}{2}\right), \arctan(2) \right) \in S_{\mathcal{D}_6}$, and let $M_{\mathcal{D}_6}(t)$ be the corresponding Schur rotation. We consider the point set C_0 given by the projection into E^{\parallel} of the orbit under $\widetilde{\mathcal{I}}$ of the lattice point $e_1 = (1, 0, 0, 0, 0, 0)$:

$$C_0 := \pi^{\parallel} \left(\mathcal{O}_{\widetilde{\mathcal{I}}}(e_1) \right) = \left\{ \pi^{\parallel}(Ae_1) : A \in \widetilde{\mathcal{I}} \right\}.$$

The points of C_0 constitute the vertices of an icosahedron (see Figure 3.4 (a)). The Schur rotation $M_{\mathcal{D}_6}(t)$ induces a continuous transformation of C_0 via the corresponding projection operators π_t^{\parallel} ; in particular, we consider the family of finite point set C_t as in (3.8). In Figure 3.4 we plot these point sets for $t = 0, 0.25, 0.5, 0.75$ and 1 : we notice that the icosahedron ($t = 0$) is continuously transformed into a hexagonal prism ($t = 0.5$), and the array for $t = 1$ forms the vertices of an icosahedron, that is distinct from the initial one. The three-fold axis highlighted is fixed during the transition, and the point sets C_t are invariant under the action of the representation S_1 of \mathcal{D}_6 as in the decomposition (3.19). In analogy to the case of the tetrahedral transition, the corresponding model set for $t = 0.5$ defines a lattice in E^{\parallel} (see Figure 3.5).

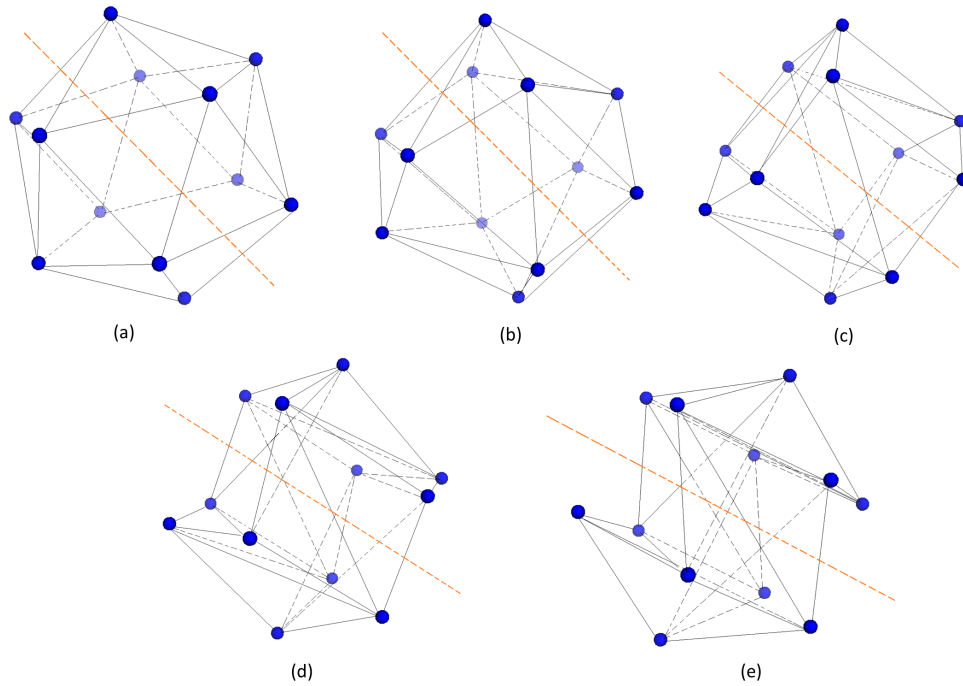


Figure 3.4: Example of a structural transition with \mathcal{D}_6 -symmetry of an icosahedral point array. (a) Initial configuration for $t = 0$, corresponding to the vertices of an icosahedron. (b) Resulting array for $t = 0.25$. (c) The intermediate point set ($t = 0.5$), forming the vertices of a hexagonal prism. (d) Transformed array for $t = 0.75$. (e). Final state of the transition ($t = 1$): the point set forms the vertices of an icosahedron, albeit different from the initial one. The dashed red line corresponds to a three-fold axis of the arrays that is fixed during the entire transition. The lines indicate the relative positions of the icosahedral vertices during the transition.

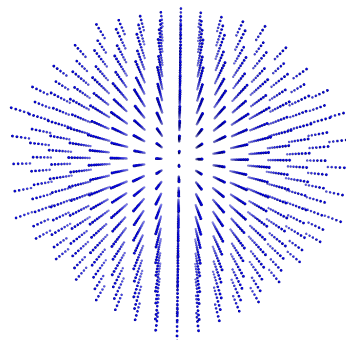


Figure 3.5: The three-dimensional lattice obtained from the transition analysed in Figure 3.4 and corresponding to the intermediate state $t = 0.5$.

Chapter 4

Construction of finite nested point sets with non-crystallographic symmetry

In that blessed region of Four Dimensions, shall we linger on the threshold of the Fifth, and not enter therein? ... Then, yielding to our intellectual onset, the gates of the Sixth Dimension shall fly open; after that a Seventh, and then an Eighth -

E. A. Abbott, *Flatland*.

In this chapter we introduce a new group theoretical method for the construction of finite nested point sets with non-crystallographic symmetry, based on the crystallographic embedding of non-crystallographic groups described in Section 1.2.2. As a first application, we provide in Section 4.2 an analytical construction of such point sets in the case of symmetries described by non-crystallographic irreducible Coxeter groups. The orbits of the latter, due to their geometrical interpretation, can be characterised in terms of their root systems and fundamental weights. The convex hulls of these orbits define compounds of nested polytopes with non-crystallographic symmetry; we characterise such compounds in the case of five-fold symmetry in two, three and four dimensions, described by the Coxeter groups H_2 , H_3 and H_4 , respectively.

4.1 Nested point sets obtained from projection

Let $G \subseteq O(k)$ be a finite non-crystallographic group of isometries acting on \mathbb{R}^k , and let \widetilde{G} be a crystallographic representation of G , subgroup of the point group \mathcal{P} of a lattice \mathcal{L} in \mathbb{R}^d (cf. Definition 1.2.2). \widetilde{G} is not, in general, a maximal subgroup of \mathcal{P} , i.e. there exist proper subgroups of \mathcal{P} which contain \widetilde{G} as a subgroup. Therefore, we introduce the set:

$$\mathcal{A}_{\widetilde{G}} := \{K \leq \mathcal{P} : \widetilde{G} \leq K\}, \quad (4.1)$$

which consists of all the \widetilde{G} -containing subgroups of \mathcal{P} . The elements in $\mathcal{A}_{\widetilde{G}}$ encode the symmetry described by G plus additional generators that extend this symmetry. Let K be an element of $\mathcal{A}_{\widetilde{G}}$, and let $n := [K : \widetilde{G}]$ be the index of \widetilde{G} in K . Let $T = (g_1, \dots, g_n)$ be a transversal of \widetilde{G} in K , i.e. a system of representatives in K of the right cosets of \widetilde{G} in K [54]. Let $\mathbf{v} \in \mathcal{L}$ be a lattice point; \mathbf{v} can be taken as a seed point for the orbit $O_K(\mathbf{v}) = \{k\mathbf{v} : k \in K\}$ under K . Let $V^{(k)}$ be the subspace of \mathbb{R}^d of dimension k carrying the irrep ρ_k of G , and let $\pi^{(k)} : \mathbb{R}^d \rightarrow V^{(k)}$ be the corresponding projection (cf. (1.14)). We assume that the orthogonal complement $V^{(d-k)}$ of $V^{(k)}$ is totally irrational with respect to the lattice \mathcal{L} , so that, by Proposition (1.2.1), $\pi^{(k)}|_{\mathcal{L}}$ is injective. With this setup, we prove the following theorem.

Theorem 4.1.1. *Let $O_i(\mathbf{v}) \equiv O_{\widetilde{G}g_i}(\mathbf{v}) = \{hg_i\mathbf{v} : h \in \widetilde{G}\}$ be the orbit of $\mathbf{v} \in \mathcal{L}$ with respect to the coset $\widetilde{G}g_i$, and let us denote by $P_i(\mathbf{v}) := \pi^{(k)}(O_i(\mathbf{v}))$ the orbit projected into $V^{(k)}$. We have:*

1. $P_i(\mathbf{v})$ is well-defined, i.e. does not depend on the choice of the transversal T ;
2. $P_i(\mathbf{v})$ retains the symmetry described by G ;
3. $P_i(\mathbf{v}) = P_j(\mathbf{v})$ if and only if

$$g_j^{-1}\widetilde{G}g_i \cap \text{Stab}_K(\mathbf{v}) \neq \emptyset, \quad \text{Stab}_K(\mathbf{v}) := \{k \in K : k\mathbf{v} = \mathbf{v}\}. \quad (4.2)$$

4. If \widetilde{G} is normal in K , then all $P_i(\mathbf{v})$ have the same cardinality.

Proof. 1. Let $T' = (g'_1, \dots, g'_n)$ be another transversal for \widetilde{G} in K . This implies that there exist $\hat{h}_i \in \widetilde{G}$, for $i = 1, \dots, n$, such that $g'_i = \hat{h}_i g_i$. We have

$$O'_i(\mathbf{v}) = O_{\widetilde{G}g'_i}(\mathbf{v}) = \{hg'_i\mathbf{v} : h \in \widetilde{G}\} = \{h\hat{h}_i g_i\mathbf{v} : h \in \widetilde{G}\} = O_i(\mathbf{v}), \quad i = 1, \dots, n,$$

and the result follows.

2. It follows from the commutative property in (1.15); in particular, we have

$$\begin{aligned}\pi^{(k)}(\mathcal{O}_i(\mathbf{v})) &= \{\pi^{(k)}(hg_i\mathbf{v}) : h \in \widetilde{G}\} = \{\pi^{(k)}(\widetilde{G}(g)g_i\mathbf{v}) : g \in G\} \\ &= \{\rho_k(g)\pi^{(k)}(g_i\mathbf{v}) : g \in G\} = \{\hat{h}\pi^{(k)}(g_i\mathbf{v}) : \hat{h} \in \rho_k\} = \mathcal{O}_{\rho_k}(\pi^{(k)}(g_i\mathbf{v})),\end{aligned}$$

for $i = 1, \dots, n$. The orbit $\mathcal{O}_{\rho_k}(\pi^{(k)}(g_i\mathbf{v}))$ has G -symmetry by construction.

3. We have

$$\begin{aligned}P_i(\mathbf{v}) = P_j(\mathbf{v}) &\Leftrightarrow \pi^{(k)}(\mathcal{O}_i(\mathbf{v})) = \pi^{(k)}(\mathcal{O}_j(\mathbf{v})) \Leftrightarrow \mathcal{O}_i(\mathbf{v}) \stackrel{\text{(since } \pi^{(k)}|_{\mathcal{L}} \text{ is injective)}}{=} \mathcal{O}_j(\mathbf{v}) \\ &\Leftrightarrow \{hg_i\mathbf{v} : h \in \widetilde{G}\} = \{hg_j\mathbf{v} : h \in \widetilde{G}\} \Leftrightarrow \exists h, k \in \widetilde{G} : hg_i\mathbf{v} = kg_j\mathbf{v} \\ &\Leftrightarrow g_j^{-1}k^{-1}hg_i\mathbf{v} = \mathbf{v} \Leftrightarrow g_j^{-1}k^{-1}hg_i \in \text{Stab}_K(\mathbf{v}),\end{aligned}$$

which proves the statement.

4. Since \widetilde{G} is normal in K , the cosets $\widetilde{G}g_i$ form the quotient group K/\widetilde{G} of size n .

Let $X := \{\mathcal{O}_{\widetilde{G}_i}(\mathbf{v}) : i = 1, \dots, n\}$ be the set of all the orbits with respect to the cosets $\widetilde{G}_i \equiv \widetilde{G}g_i$. We can define an action of K/\widetilde{G} on X as $\widetilde{G}_i \cdot \mathcal{O}_{\widetilde{G}_j}(\mathbf{v}) := \mathcal{O}_{\widetilde{G}_i\widetilde{G}_j}(\mathbf{v})$. This action is well defined since K/\widetilde{G} is a group, and it is transitive since, for every element $\mathcal{O}_{\widetilde{G}_i}(\mathbf{v}) \in X$, we have $\widetilde{G}_j \cdot \mathcal{O}_{\widetilde{G}_j^{-1}\widetilde{G}_i}(\mathbf{v}) = \mathcal{O}_{\widetilde{G}_i}(\mathbf{v})$. Let $S_{\widetilde{G}} := \text{Stab}_{K/\widetilde{G}}(\mathcal{O}_{\widetilde{G}}(\mathbf{v}))$ denote the stabiliser of $\mathcal{O}_{\widetilde{G}}(\mathbf{v})$ under this action. Letting $s := |S_{\widetilde{G}}|$, we have by the orbit-stabiliser theorem

$$r := |X| = \frac{|K/\widetilde{G}|}{|S_{\widetilde{G}}|} = \frac{n}{s},$$

and the elements of X are in bijection with the right cosets of $S_{\widetilde{G}}$ in K/\widetilde{G} . We denote these cosets by A_i , for $i = 1, \dots, r$. These form a partition of the quotient group K/\widetilde{G} , which we write as

$$\underbrace{\widetilde{G}_1^{(1)}, \dots, \widetilde{G}_s^{(1)}}_{A_1}, \dots, \underbrace{\widetilde{G}_1^{(i)}, \dots, \widetilde{G}_s^{(i)}}_{A_i}, \dots, \underbrace{\widetilde{G}_1^{(r)}, \dots, \widetilde{G}_s^{(r)}}_{A_r}.$$

Let $S = (\widetilde{G}_1^{(1)}, \dots, \widetilde{G}_1^{(r)})$ be a transversal for the cosets of $S_{\widetilde{G}}$ in K/\widetilde{G} . The corresponding orbits $\mathcal{O}_{\widetilde{G}_1^{(i)}}$ are distinct by the orbit-stabiliser theorem, and moreover $\mathcal{O}_{\widetilde{G}_j^{(i)}} = \mathcal{O}_{\widetilde{G}_k^{(i)}}$, for $j, k = 1, \dots, s$. Let us define the sets

$$K^{(i)} := \bigcup_{j=1}^s \widetilde{G}_j^{(i)} \subseteq K, \quad i = 1, \dots, r. \quad (4.3)$$

The set $\{K^{(i)} : i = 1, \dots, r\}$ constitutes a partition of K , since it is a union of cosets. Moreover, they all have the same order:

$$|K^{(i)}| = s \cdot |\widetilde{G}| =: N, \quad \forall i = 1, \dots, r. \quad (4.4)$$

It follows from the definition of $K^{(i)}$ given in (4.3) that $\mathcal{O}_{K^{(i)}}(\mathbf{v}) = \{k\mathbf{v} : k \in K^{(i)}\} = \mathcal{O}_{\widetilde{G}_1^{(i)}}(\mathbf{v})$, and that $k \in K^{(i)}$ if and only if $k\mathbf{v} \in \mathcal{O}_{\widetilde{G}_1^{(i)}}(\mathbf{v})$. To conclude, we observe that each $K^{(i)}$ contains complete cosets of $K/\text{Stab}_K(\mathbf{v})$. In fact, let $k\text{Stab}_K(\mathbf{v})$ be a coset in $K/\text{Stab}_K(\mathbf{v})$. If $k \in K^{(i)}$, then an element in $k\text{Stab}_K(\mathbf{v})$ is of the form $k\hat{k}$, with $\hat{k} \in \text{Stab}_K(\mathbf{v})$, and belongs to $K^{(i)}$ since $(k\hat{k})\mathbf{v} = k(\hat{k}\mathbf{v}) = k\mathbf{v} \in \mathcal{O}_{\widetilde{G}_1^{(i)}}(\mathbf{v})$. Therefore, each $K^{(i)}$ is partitioned into $|K^{(i)}|/|\text{Stab}_K(\mathbf{v})|$ sets: each of these sets corresponds to a distinct point in the orbit $\mathcal{O}_{\widetilde{G}_1^{(i)}}(\mathbf{v})$. Since $|K^{(i)}| = N$ for all i due to (4.4), each orbit $\mathcal{O}_{\widetilde{G}_1^{(i)}}(\mathbf{v})$ has the same number of points, and hence also each $P_i(\mathbf{v})$, because the projection is one-to-one. □

As a consequence, the decomposition of $K \in \mathcal{A}_{\widetilde{G}}$ into cosets with respect to \widetilde{G} induces a well-defined decomposition of the projected orbit $\pi^{(k)}(\mathcal{O}_K(\mathbf{v}))$ (cf. (1.14)):

$$\pi^{(k)}(\mathcal{O}_K(\mathbf{v})) = \bigcup_{i=1}^n \pi^{(k)}(\mathcal{O}_i(\mathbf{v})) = \bigcup_{i=1}^n \mathcal{O}_{\rho_k}(\pi^{(k)}(g_i\mathbf{v})). \quad (4.5)$$

It follows that the point set defined by (4.5) consists of k -dimensional orbits situated at different radial levels, since, in general, $|\pi^{(k)}(g_i\mathbf{v})| \neq |\pi^{(k)}(g_j\mathbf{v})|$ for $i \neq j$, where $|\cdot|$ denotes the standard Euclidean norm in \mathbb{R}^k . Hence the projected orbit is an onion-like structure, with each layer being the union of the projected orbits corresponding to different cosets of K . It follows that the number r of distinct radial levels is bounded by the index of \widetilde{G} in K . In Figure 4.1 we show a one dimensional examples of nested set obtained with this construction, where the connection with the cut-and-project method is highlighted (compare with Figure 1.2).

Using these results, we can set up a procedure to extend the non-crystallographic symmetry described by ρ_k in $V^{(k)}$. In particular, let us consider the set $\pi^{(k)}(\mathcal{L}) \subseteq V^{(k)}$, i.e. the projection of the lattice points into $V^{(k)}$, which is a dense set in $V^{(k)}$. Let $\mathbf{x} \in \pi^{(k)}(\mathcal{L})$ be a seed point for the orbit of ρ_k . The pre-image $\mathbf{v} = (\pi^{(k)})^{-1}(\mathbf{x})$ is a point of the lattice \mathcal{L} by construction. Let K be an element of $\mathcal{A}_{\widetilde{G}}$. The projection of $\mathcal{O}_K(\mathbf{v})$ contains the orbit

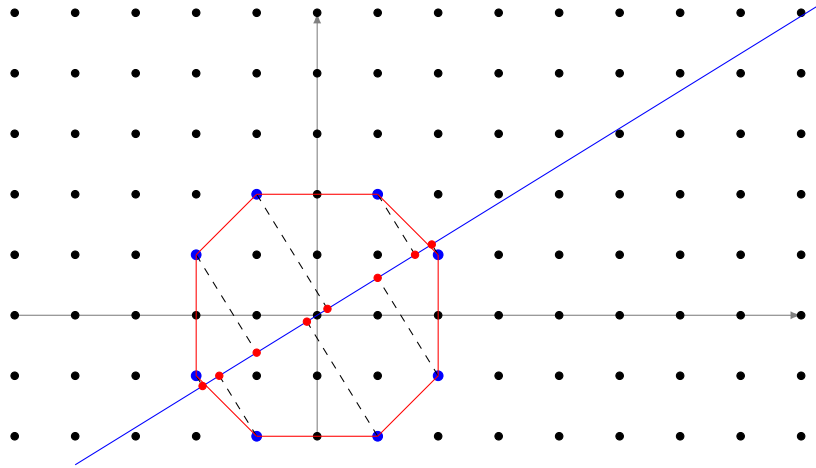


Figure 4.1: Illustration of our method for the construction of nested point sets. Lattice points forming the vertices of a polygon are projected orthogonally into the physical space, resulting in a finite nested point set, in this case one-dimensional.

$O_{\rho_k}(\mathbf{x})$, which corresponds to the coset $\widetilde{G}e$ in K , where e denotes the identity element of G (compare with (4.5)), and possibly more layers with G -symmetry. The situation can be summarised in the following diagramme:

$$\begin{array}{ccc}
 O_{\mathcal{H}}(\mathbf{v}) \subseteq \mathcal{L} & \xrightarrow{\text{extend}} & O_{K_1}(\mathbf{v}) \\
 \uparrow \text{lift} & & \downarrow \text{project} \\
 O_{\rho_k}(\mathbf{x}) & \longrightarrow & \pi^{(k)}(O_{K_1}(\mathbf{v}))
 \end{array} \tag{4.6}$$

This procedure can be iterated; let us consider the chain of subgroups in $\mathcal{A}_{\mathcal{H}}$:

$$\mathcal{H} \subseteq K_1 \subseteq K_2 \subseteq \dots \subseteq K_m \subseteq \Lambda.$$

By ascending the chain we obtain a chain of orbits $O_{K_i}(\mathbf{v}) \subseteq O_{K_{i+1}}(\mathbf{v})$; the projection of such orbits into $V^{(k)}$ induces a chain of nested shells.

We point out that, for computational purposes, it is often convenient to fix the generator matrix B of \mathcal{L} and consider the subgroup structure of the lattice group Λ in that representation. Indeed, if $\Gamma := B^{-1}\widetilde{G}B$ denotes the representation of \widetilde{G} with respect to B , then the set

$$\mathcal{A}_{\Gamma}(B) := \{\mathcal{K} \leq \Lambda : \Gamma \leq \mathcal{K}\} \tag{4.7}$$

consists of the integral representations $\mathcal{K} \subseteq GL(d, \mathbb{Z})$ of the groups K , and is such that $B^{-1}\mathcal{A}_{\widetilde{G}}B = \mathcal{A}_{\Gamma}$ (cf. (1.4)). Note that a different choice of basis results in a set conjugate to \mathcal{A}_{Γ} in $GL(d, \mathbb{Z})$.

4.2 Applications to finite Coxeter groups and polytopes

The nested point sets defined in the previous section display non-crystallographic symmetry G at each radial level. In particular, from (4.5) it follows that the \widetilde{G} -orbits can be characterised according to the coset decomposition of the \widetilde{G} -containing subgroups K of the point group \mathcal{P} . Let $P_i(\mathbf{v}) = \pi^{(k)}(\mathcal{O}_{\widetilde{G}g_i}(\mathbf{v}))$ be the projected orbit in $V^{(k)}$ of $\mathbf{v} \in \mathcal{L}$ under the coset $\widetilde{G}g_i$. The convex hull $\text{Conv}(P_i(\mathbf{v}))$ defines a *polytope*¹ in \mathbb{R}^k . Since $\pi^{(k)}(\mathcal{O}_{\widetilde{G}g_i}(\mathbf{v})) = \mathcal{O}_{\rho_k}(\pi^{(k)}(g_i\mathbf{v}))$, the vertices of $\text{Conv}(P_i(\mathbf{v}))$ form a unique orbit under the representation ρ_k of the symmetry group G . Polytopes with this property are referred to as *isogonal* or *vertex-transitive* [70]. By considering the convex hull of each orbit with respect to the coset decomposition (4.5), we obtain a compound of nested isogonal polytopes with non-crystallographic symmetry G . We show in this section that such compounds can be further characterised when G is a *Coxeter group*.

4.2.1 Finite Coxeter groups

In his celebrated book *Regular polytopes* [69], H.S.M. Coxeter gave a systematic study of multi-dimensional polytopes, and introduced the concept of *reflection groups* to analyse their symmetry properties. On a more abstract level, we have the following definition:

Definition 4.2.1. A Coxeter group W is a group generated by involutions s_i that admits a presentation of the form

$$W = \langle s_i, s_j \mid (s_i s_j)^{m_{ij}} = 1, m_{ii} = 1, m_{ij} = m_{ji} \geq 2, i \neq j \rangle. \quad (4.8)$$

A detailed description of Coxeter groups can be found in [39]. In the finite case, Coxeter groups correspond to groups generated by reflections. Specifically, let V be a finite n -dimensional Euclidean space with inner product $\langle \cdot, \cdot \rangle$, and let $\alpha \in V$ be a vector. The *reflection* r_α associated with α is the linear operator given by

$$r_\alpha(\mathbf{x}) = \mathbf{x} - \frac{2\langle \alpha, \mathbf{x} \rangle}{\langle \alpha, \alpha \rangle} \alpha,$$

where $\mathbf{x} \in V$. r_α is an orthogonal transformation and it is involutive, i.e. $r_\alpha^2 = 1$. A *root system* ϕ is a finite set of vectors in V satisfying the following two conditions:

¹There are many formal definitions of polytope in the literature. In this work, we will consider the ‘‘classic’’ definition of polytope, i.e. a bounded convex region enclosed by a finite number of hyperplanes [69].

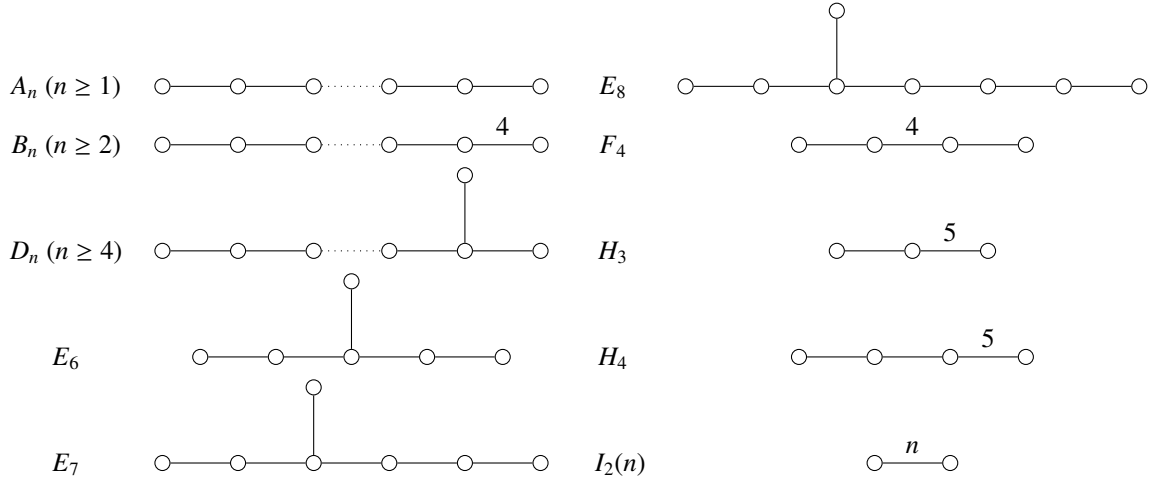


Table 4.1: Coxeter graphs corresponding to the irreducible finite Coxeter groups.

1. $\phi \cap \mathbb{R}\alpha = \{\alpha, -\alpha\}$, for all $\alpha \in \phi$;
2. $r_\alpha\phi = \phi$, for all $\alpha \in \phi$.

The group $W \equiv W(\phi) := \langle r_\alpha : \alpha \in \phi \rangle$ is the finite reflection group associated with ϕ . A subset Δ of ϕ is called a *simple system* (and its elements *simple roots*) if

- $\text{span}_{\mathbb{R}}(\Delta) = \text{span}_{\mathbb{R}}(\phi)$;
- every $\alpha \in \phi$ is a linear combination of elements of Δ with all the coefficients of the same sign.

The reflections associated with a simple system Δ generate the entire group W . The number $k = |\Delta|$ is called the *rank* of W . Denoting by $m(\alpha, \beta)$ the order of the element $r_\alpha r_\beta \in W$, W admits a presentation as in (4.8). Moreover, we can associate with W its *Coxeter graph* Γ , which has k vertices linked by an edge if $m(\alpha, \beta) > 2$, labelled by the number $m(\alpha, \beta)$ (in general omitted if $m(\alpha, \beta) = 3$). A Coxeter group W is *irreducible* if the corresponding graph Γ is connected. These groups correspond to the infinite families A_n, B_n, D_n and $I_2(n)$, together with the exceptional groups F_4, E_6, E_7, E_8, H_3 and H_4 (see Table 4.1).

The *Cartan matrix* of a Coxeter group W with simple system Δ is a $k \times k$ matrix whose entries C_{ij} are given by

$$C_{ij} = \frac{2\langle \alpha_i, \alpha_j \rangle}{\langle \alpha_j, \alpha_j \rangle}, \quad \alpha_i, \alpha_j \in \Delta. \quad (4.9)$$

In analogy with Definition 1.1.1, W is crystallographic if $C_{ij} \in \mathbb{Z}$, for all $i, j = 1, \dots, k$,

otherwise it is non-crystallographic. In fact, if W is crystallographic, then the \mathbb{Z} -module

$$Q = \bigoplus_{i=1}^k \mathbb{Z}\alpha_i \quad (4.10)$$

defines a lattice in \mathbb{R}^k , called the *root lattice* of ϕ , whose point group is equal to W . In this case, W is referred to as the *Weyl group* of the root system ϕ , following terminology from Lie theory [20]. On the other hand, if W is non-crystallographic, the set (4.10) is dense in \mathbb{R}^k , hence not a lattice. All the irreducible Coxeter groups are crystallographic, except for $I_2(n)$, with $n = 5$ and $n > 6$, in accordance with the crystallographic restriction (cf. Theorem 1.1.1), and the exceptional groups H_3 and H_4 . The latter are associated with icosahedral symmetry in three and four dimensions, respectively.

A Coxeter group W of rank k acts on \mathbb{R}^k as an isometry group. Orbits of Coxeter groups have been studied before [21, 71–73]; in the crystallographic case, they provide a powerful tool in the representation theory of Lie groups/algebras [74] and Kac-Moody algebras [75]. A crucial role for their description is played by the set

$$D^+ = \{\mathbf{x} \in \mathbb{R}^k : \langle \mathbf{x}, \alpha_i \rangle \geq 0, \alpha_i \in \Delta, i = 1, \dots, k\}, \quad (4.11)$$

which is referred to as the *dominant chamber* of W and is a fundamental domain of W (cf. Definition 1.1.2). It is convenient to introduce the ω -basis $\omega_1, \dots, \omega_k$ of *fundamental weights* defined by

$$\frac{2\langle \alpha_i, \omega_j \rangle}{\langle \alpha_i, \alpha_i \rangle} = \delta_{ij}, \quad i, j = 1, \dots, k. \quad (4.12)$$

The ω -basis is related to the simple roots via the Cartan matrix:

$$\alpha_i = \sum_{j=1}^k C_{ij}\omega_j, \quad \omega_i = \sum_{j=1}^k C_{ij}^{-1}\alpha_j. \quad (4.13)$$

Let $\mathbf{x} \in \mathbb{R}^k$, and let (m_1, \dots, m_k) be the coordinates of \mathbf{x} in the ω -basis. A straightforward computation shows that

$$\mathbf{x} \in D^+ \iff m_i \geq 0, \quad i = 1, \dots, k. \quad (4.14)$$

The unique point λ of the orbit $O_W(\mathbf{v})$, with $\mathbf{v} \in \mathbb{R}^k$, with non-negative coordinates in the ω -basis is called the *dominant point* of the orbit. Its positive coordinates are referred to as *Wythoff positions* [69] and completely determine the orbit.

With these preliminaries, we are able to apply the new method introduced in Section 4.1 to construct nested point sets with symmetry described by an irreducible non-crystallographic Coxeter group.

4.2.2 Minkowski embedding of $I_2(n)$ and planar nested structures

Let $n > 0$ be a natural number. The group $I_2(n)$ is isomorphic to the dihedral group \mathcal{D}_{2n} , the symmetry group of a regular n -gon, and consists of n rotations and n reflections, with presentation [54]:

$$\mathcal{D}_{2n} = \langle R_n, S : R_n^n = e, S R_n = R_n^{-1} S \rangle, \quad (4.15)$$

where R_n is a rotation by $\frac{2\pi}{n}$ and S is a reflection. It is useful to represent the root system of $I_2(n)$ in the complex plane $\mathbb{C} \simeq \mathbb{R}^2$ as follows:

$$\phi_n = \left\{ \exp\left(\frac{\pi j}{n} i\right) : j = 0, \dots, 2n-1 \right\}. \quad (4.16)$$

The convex hull of ϕ_n is a regular $2n$ -gon. The simple roots can be chosen as

$$\alpha_1 = 1, \quad \alpha_2 = \exp\left(\frac{n-1}{n} i\pi\right), \quad (4.17)$$

and consequently the Cartan matrix C_n is given by

$$C_n = \begin{pmatrix} 2 & -2\cos\left(\frac{\pi}{n}\right) \\ -2\cos\left(\frac{\pi}{n}\right) & 2 \end{pmatrix}. \quad (4.18)$$

Using the relations (4.13), we obtain the ω -basis:

$$\begin{aligned} \omega_1 &= \frac{1}{2\sin^2\left(\frac{\pi}{n}\right)} \left(\alpha_1 + \cos\left(\frac{\pi}{n}\right) \alpha_2 \right), \\ \omega_2 &= \frac{1}{2\sin^2\left(\frac{\pi}{n}\right)} \left(\cos\left(\frac{\pi}{n}\right) \alpha_1 + \alpha_2 \right). \end{aligned}$$

The dominant point can be written as $\lambda = a\omega_1 + b\omega_2 \equiv (a, b)$, where $a, b \geq 0$. The orbits and corresponding polygons are then easily classified:

1. If $\lambda = (a, 0)$, $a \neq 0$, or $\lambda = (0, b)$, $b \neq 0$, then the orbit $\mathcal{O}_W(\lambda)$ consists of n points, and its convex hull is a regular n -gon. Indeed, the reflection r_{α_j} associated with the root α_j perpendicular to the weight ω_i fixes any point of the form $a\omega_i$, hence $\text{Stab}_{I_2(n)}(\lambda) = \{r_{\alpha_j}, e\} \simeq \mathbb{Z}_2$; by the orbit-stabiliser theorem, we have

$$|\mathcal{O}_{I_2(n)}(\lambda)| = \frac{|I_2(n)|}{|\text{Stab}_{I_2(n)}(\lambda)|} = \frac{2n}{2} = n.$$

2. If $\lambda = (a, b)$, $a, b \neq 0$, then no reflections in $I_2(n)$ fixes λ , and therefore $\mathcal{O}_W(\lambda)$ is made up of $2n$ points; its convex hull is a (not necessarily regular) $2n$ -gon.

For the construction of nested point sets with dihedral symmetry, we need a crystallographic embedding of $I_2(n)$ into a higher dimensional lattice. This is achieved with the aid of number theoretical tools, in particular via the *Minkowski embedding* of \mathbb{Z} -modules. We review this construction, following [2]. For the underlying number theoretical concepts, we refer to [41] for a detailed description.

Let $\xi_n = \exp \frac{2\pi i}{n} \in \mathbb{C}$ be a primitive n -th root of unity, i.e. $\xi_n^m = 1$ if and only if n divides m . Let $\mathbb{Q}(\xi_n)$ be the extension of \mathbb{Q} obtained by adjoining ξ_n to \mathbb{Q} . $\mathbb{Q}(\xi_n)$ is a field, known as a *cyclotomic field*, which can be written as

$$\mathbb{Q}(\xi_n) = \left\{ \sum_j a_j \xi_n^j : j \leq n, \text{g.c.d.}(n, j) = 1, a_j \in \mathbb{Q} \right\}.$$

Hence the degree of $\mathbb{Q}(\xi_n)$ over \mathbb{Q} , i.e. the dimension of $\mathbb{Q}(\xi_n)$ as a vector space over \mathbb{Q} , is $\phi(n)$, the Euler function of n [41]. Let $\mathbb{Z}[\xi_n]$ denote the set

$$\mathbb{Z}[\xi_n] = \left\{ \sum_j m_j \xi_n^j : j \leq n, \text{g.c.d.}(n, j) = 1, m_j \in \mathbb{Z} \right\},$$

which is the *ring of integers* of $\mathbb{Q}(\xi_n)$, and is a \mathbb{Z} -module of rank $\phi(n)$. Using the isomorphism $\mathbb{C} \simeq \mathbb{R}^2$, $\mathbb{Z}[\xi_n]$ can be seen as a point set in \mathbb{R}^2 , and is dense for $n = 5$ and $n > 6$, as a consequence of the crystallographic restriction.

Using Galois theory, we can construct a crystallographic representation of $I_2(n)$. Let \mathcal{G} denote the Galois group² of $\mathbb{Q}(\xi_n)$. \mathcal{G} is isomorphic to $\mathbb{Z}_n^\times := \{m \in \mathbb{Z}_n : \text{gcd}(m, n) = 1\}$, the multiplicative group of \mathbb{Z}_n , and therefore consists of $\phi(n)$ elements. Such elements are automorphisms of $\mathbb{Q}(\xi_n)$ given by $\xi_n \mapsto \xi_n^m$, where n and m are coprime, and they are pairwise conjugate. We can then choose $\frac{\phi(n)}{2}$ non-conjugate elements σ_i in \mathcal{G} , where σ_1 is the identity. The Minkowski embedding of $\mathbb{Z}[\xi_n]$ is given by

$$\mathcal{L}_{\phi(n)} := \left\{ (\mathbf{x}, \sigma_2(\mathbf{x}), \dots, \sigma_{\frac{\phi(n)}{2}}(\mathbf{x})) : \mathbf{x} \in \mathbb{Z}[\xi_n] \right\} \subseteq \mathbb{C}^{\frac{\phi(n)}{2}} \simeq \mathbb{R}^{\phi(n)}, \quad (4.19)$$

which is a lattice in $\mathbb{R}^{\phi(n)}$. The projection $\pi^{(2)} : \mathcal{L}_{\phi(n)} \rightarrow \mathbb{C}$ on the first coordinate is, by construction, one-to-one on its image $\pi^{(2)}(\mathcal{L}_{\phi(n)}) = \mathbb{Z}[\xi_n]$.

We can define an action of $I_2(n)$ on $\mathbb{Z}[\xi_n]$ as follows

$$R_n \mathbf{x} := \xi_n \mathbf{x}, \quad S \mathbf{x} := \bar{\mathbf{x}},$$

²In general terms, the Galois group of an extension \mathbb{K} of a field \mathbb{F} is the set of all the automorphisms of \mathbb{K} that fix \mathbb{F} .

where R_n and S are the generators of $I_2(n) \simeq \mathcal{D}_{2n}$ as in (4.15), and $\mathbf{x} \in \mathbb{Z}[\xi_n]$. This action is well-defined as every element of $I_2(n)$ stabilises $\mathbb{Z}[\xi_n]$. If g is an element of $I_2(n)$, g can be lifted to an element \tilde{g} via the action

$$\tilde{g} \left(\pi^{(2)} \right)^{-1} (\mathbf{x}) := \left(\pi^{(2)} \right)^{-1} (g\mathbf{x}), \quad (4.20)$$

which is well-defined since the projection is one-to-one. In particular, we have

$$\tilde{R}_n \left(\pi^{(2)} \right)^{-1} (\mathbf{x}) = \left(\pi^{(2)} \right)^{-1} (R_n \mathbf{x}) = \left(\pi^{(2)} \right)^{-1} (\xi_n \mathbf{x}) = (\xi_n \mathbf{x}, \sigma_2(\xi_n \mathbf{x}), \dots, \sigma_{\frac{\phi(n)}{2}}(\xi_n \mathbf{x})).$$

Similarly we have

$$\tilde{S} \left(\pi^{(2)} \right)^{-1} (\mathbf{x}) = \left(\pi^{(2)} \right)^{-1} (S \mathbf{x}) = \left(\pi^{(2)} \right)^{-1} (\bar{\mathbf{x}}) = \left(\bar{\mathbf{x}}, \overline{\sigma_2(\mathbf{x})}, \dots, \overline{\sigma_{\frac{\phi(n)}{2}}(\mathbf{x})} \right).$$

It follows that the transformations \tilde{R}_n and \tilde{S} are orthogonal and stabilise the lattice $\mathcal{L}_{\phi(n)}$.

Therefore, the set

$$\widetilde{I_2(n)} := \{\tilde{g} : g \in I_2(n)\} \quad (4.21)$$

is an embedding of $I_2(n)$ into the point group of $\mathcal{L}_{\phi(n)}$. Furthermore, the action of $\widetilde{I_2(n)}$ is reducible since

$$\pi^{(2)}(\tilde{g}\mathbf{v}) = \pi^{(2)} \left(\tilde{g} \left(\pi^{(2)} \right)^{-1} (\mathbf{x}) \right) \stackrel{\text{by(4.20)}}{=} \pi^{(2)} \left(\left(\pi^{(2)} \right)^{-1} (g\mathbf{x}) \right) = g\mathbf{x} = g\pi^{(2)}(\mathbf{v}),$$

for $\mathbf{v} \in \mathcal{L}_{\phi(n)}$ and $\mathbf{x} \in \mathbb{Z}[\xi_n]$. Hence the diagramme

$$\begin{array}{ccc} \mathcal{L}_{\phi(n)} & \xrightarrow{\tilde{g}} & \mathcal{L}_{\phi(n)} \\ \downarrow \pi^{(2)} & & \downarrow \pi^{(2)} \\ \mathbb{Z}[\xi_n] & \xrightarrow{g} & \mathbb{Z}[\xi_n] \end{array}$$

is commutative (compare with (1.14)). As a consequence, having fixed a basis of $\mathcal{L}_{\phi(n)}$, the action of $\widetilde{I_2(n)}$ on $\mathcal{L}_{\phi(n)}$ induces a representation of $I_2(n)$ which contains an irrep of $I_2(n)$ of degree two. Therefore, $\widetilde{I_2(n)}$ constitutes a crystallographic representation of $I_2(n)$ in the sense of Definition 1.2.2.

We point out that, although this construction is a priori possible and well-defined for all natural numbers, it is difficult to find the explicit form of the point group of $\mathcal{L}_{\phi(n)}$ in (4.19) for general n . The explicit form is known, in particular, for $n = 5, 8$ and 12 [2].

We now prove analytically the existence of an *extension* \widetilde{K} of $I_2(n)$ embedded into $\mathcal{P}(\mathcal{L}_{\phi(n)})$, i.e. a subgroup \widetilde{K} of $\mathcal{P}(\mathcal{L}_{\phi(n)})$ that contains $\widetilde{I_2(n)}$ as a normal subgroup:

$$\widetilde{I_2(n)} \triangleleft \widetilde{K} < \mathcal{P}(\mathcal{L}_{\phi(n)}). \quad (4.22)$$

We start with some properties from group theory. We have already remarked that the group $I_2(n)$ is isomorphic to \mathcal{D}_{2n} , with presentation given in (4.15). If $\langle R_n \rangle \simeq \mathbb{Z}_n$ is the subgroup of rotations, then

$$\mathcal{D}_{2n} = \langle R_n \rangle \cup \langle R_n \rangle S.$$

\mathcal{D}_{2n} can be seen as a subgroup of the symmetric group S_n , i.e. as acting on the vertices of a regular n -gon. More precisely, let $R'_n = (1, 2, \dots, n)$ be an n -cycle and let S' be the permutation defined by $S'(j) = -j \bmod n$, for $j = 1, \dots, n$; then $\langle R'_n, S' \rangle$ defines a permutation representation of \mathcal{D}_{2n} . Let $T = \langle R'_n \rangle \simeq \mathbb{Z}_n$, and define K as the normaliser of T in S_n :

$$K := N_{S_n}(T) = \{\sigma \in S_n : \sigma^{-1}T\sigma = T\}. \quad (4.23)$$

K thus constructed is referred to as the *holomorph* of the group \mathbb{Z}_n , and denoted by $\text{Hol}(\mathbb{Z}_n)$ [76]. We have the following:

Lemma 4.2.1. \mathcal{D}_{2n} is a proper normal subgroup of $\text{Hol}(\mathbb{Z}_n)$ when $n = 5$ or $n \geq 7$.

Proof. We have

$$\begin{aligned} \sigma \in K &\Leftrightarrow \sigma T \sigma^{-1} = T \Leftrightarrow \sigma R_n \sigma^{-1} \in T \Leftrightarrow \sigma(1, 2, \dots, n) \sigma^{-1} = (1, 2, \dots, n)^m \\ &\text{for some } m \in \mathbb{Z}_n \text{ with } \gcd(m, n) = 1, \text{ otherwise } (1, 2, \dots, n)^m \\ &\text{decomposes into disjoint cycles} \Leftrightarrow (\sigma(1), \sigma(2), \dots, \sigma(n)) = (1, 2, \dots, n)^m \\ &\Leftrightarrow \forall j \in \mathbb{Z}_n, \sigma(j) = mj + l \text{ for some } m, l \in \mathbb{Z}_n \text{ with } \gcd(m, n) = 1. \end{aligned}$$

To sum up:

$$K = \{\sigma \in S_n : \exists m \in \mathbb{Z}_n^\times, l \in \mathbb{Z}_n : \sigma(j) = mj + l, \forall j \in \mathbb{Z}_n\}.$$

K contains R'_n and S' , which correspond to $m = 1, l = 1$ and $m = -1, l = 0$, respectively. It follows that \mathcal{D}_{2n} is a subgroup of K . We notice that $|K| = \phi(n)n$, which is greater than $2n$ for $n = 5$ or $n \geq 7$. Hence \mathcal{D}_{2n} is a proper subgroup of K for these values of n , which correspond to the non-crystallographic cases.

In order to prove normality, we first of all notice that we can write

$$\mathcal{D}_{2n} \simeq \langle R'_n \rangle \cup \langle R'_n \rangle S' = T \cup TS'.$$

Let $\sigma \in K$ defined by $\sigma(j) = mj + l$. We want to prove that $\sigma \mathcal{D}_{2n} = \mathcal{D}_{2n} \sigma$. Clearly $\sigma T = T \sigma$ by definition of K (cf. (4.23)). We are then left to show that $\sigma TS' = TS' \sigma$. For

$s, j \in \mathbb{Z}_n$ we have $((R'_n)^s S')(j) = s - j$; combined with $\sigma^{-1}(j) = m^{-1}j - m^{-1}l$, this implies that $(\sigma((R'_n)^s S'))\sigma^{-1}(j) = ms - j + 2l$. Therefore $\sigma((R'_n)^s S')\sigma^{-1} = (R'_n)^{ms+2l}S'$, hence $\sigma TS' = TS'\sigma$, and the result follows. \square

We are now able to prove (4.22). In particular, we have the following:

Proposition 4.2.1. *The point group $\mathcal{P}(\mathcal{L}_{\phi(n)})$ of the Minkowsky embedding $\mathcal{L}_{\phi(n)}$ contains a subgroup \widetilde{K} , isomorphic to $\text{Hol}(\mathbb{Z}_n)$, extending $\widetilde{I_2(n)}$.*

Proof. Let us define the functions $t_{m,l} \in \text{Aut}(\mathbb{Z}[\xi_n])$ by

$$t_{m,l} \left(\sum_{j=0}^{n-1} a_j \xi_n^j \right) := \sum_{j=0}^{n-1} a_j \xi_n^{mj+l}, \quad m \in \mathbb{Z}_n^\times, l \in \mathbb{Z}_n. \quad (4.24)$$

Notice that the elements $t_{m,0}$, with $m \in \mathbb{Z}_n^\times$, correspond to the Galois automorphisms σ_m , which constitute the Galois group \mathcal{G} of $\mathbb{Q}(\xi_n)$. Let $\widetilde{K} := \{t_{m,l} : m \in \mathbb{Z}_n^\times, l \in \mathbb{Z}_n\}$. \widetilde{K} is a subgroup of $\text{Aut}(\mathbb{Z}[\xi_n])$ which contains \mathcal{G} . In particular, the composition of two elements is given by

$$t_{m,l} \cdot t_{m',l'} = t_{mm', ml'+l}, \quad (4.25)$$

and the inverse of an element $t_{m,l}$ is $t_{m^{-1}, -m^{-1}l}$. Let $\theta : \text{Hol}(\mathbb{Z}_n) \rightarrow \widetilde{K}$ be the function

$$\theta(\sigma) := t_{m,l}, \quad \sigma(j) = mj + l.$$

θ is an isomorphism by construction. Writing the Minkowski embedding of $\mathbb{Z}[\xi_n]$ as $\mathcal{L}_{\phi(n)} = \{t_{y_1,0}(\mathbf{z}), \dots, t_{y_{\phi(n)/2},0}(\mathbf{z}) : \mathbf{z} \in \mathbb{Z}[\xi_n]\} \subseteq \mathbb{C}^{\frac{1}{2}\phi(n)} \cong \mathbb{R}^{\phi(n)}$, where $1 = y_1 < \dots < y_{\phi(n)/2} < \frac{n}{2}$ and $\gcd(y_j, n) = 1$, for all j , we can then lift $t_{m,l}$ with the projection $\pi^{(2)}$ as in (4.20), and obtain:

$$\begin{aligned} \tilde{t}_{m,l}(\pi^{(2)})^{-1}(\mathbf{z}) &= (\pi^{(2)})^{-1}(t_{m,l}(\mathbf{z})) = (t_{m,0}(t_{m,l}(\mathbf{z})), \dots, t_{m y_{\phi(n)/2},0}(t_{m,l}(\mathbf{z}))) \\ &\stackrel{\text{(by (4.25))}}{=} (t_{m y_1, y_1 l}(\mathbf{z}), \dots, t_{m y_{\phi(n)/2}, y_{\phi(n)/2} l}(\mathbf{z})) \stackrel{\text{(by (4.24))}}{=} (\xi_n^{y_1 l} t_{m y_1, 0}(\mathbf{z}), \dots, \xi_n^{y_{\phi(n)/2} l} t_{m y_{\phi(n)/2}, 0}(\mathbf{z})). \end{aligned}$$

Therefore, $\tilde{t}_{m,l}$ just rearranges the coordinates of $(\pi^{(2)})^{-1}(\mathbf{z})$, possibly converting some of them to their complex conjugates and/or multiplying them by a power of ξ_n . Hence \widetilde{K} stabilises the lattice \mathcal{L}_n , and this action is orthogonal, implying that \widetilde{K} is a subgroup of $\mathcal{P}(\mathcal{L}_n)$. To conclude, we observe that $\theta(\mathcal{D}_{2n})$ is actually the embedding $\widetilde{I_2(n)}$, and it is a normal subgroup of \widetilde{K} by Lemma 4.2.1, hence the result is proved. \square

Since the embedding $\widetilde{I_2(n)}$ is normal in $\widetilde{K} \simeq \text{Hol}(\mathbb{Z}_n)$, the orbits of points of the lattice $\mathcal{L}_{\phi(n)}$ can be further characterised using Theorem 4.1.1. In fact, each point set obtained by the decomposition into cosets of \widetilde{K} with respect to $\widetilde{I_2(n)}$ as in (4.5) contains the same number of elements, hence, given $\mathbf{v} \in \mathcal{L}_{\phi(n)}$, the projected orbit $\pi^{(2)}(O_{\widetilde{K}}(\mathbf{v}))$ consists of a compound of r n -gons or $2n$ -gons, where r is at most

$$r \leq [\widetilde{K} : \widetilde{I_2(n)}] = \frac{\phi(n)n}{2n} = \frac{\phi(n)}{2}.$$

Planar five-fold symmetry. To illustrate the theory developed so far, we consider the case $n = 5$. In this context, the Coxeter group $I_2(5) \simeq \mathcal{D}_{10}$ is usually denoted as H_2 , due to the chain of inclusions of non-crystallographic Coxeter groups $H_2 \subseteq H_3 \subseteq H_4$ as pictorially seen by their Coxeter graphs:

$$\begin{array}{c} \textcircled{5} \text{---} \textcircled{\quad} \text{---} \textcircled{\quad} \text{---} \textcircled{\quad} \\ \underbrace{\hspace{1.5cm}}_{H_2} \\ \underbrace{\hspace{2.5cm}}_{H_3} \\ \underbrace{\hspace{3.5cm}}_{H_4} \end{array} \quad (4.26)$$

The Minkowski embedding of H_2 is isomorphic to the root lattice of A_4 [2] (cf. (4.10)), which we denote by Q_4 and whose roots are given by $\alpha_i = \mathbf{e}_i - \mathbf{e}_{i+1}$, for $i = 1, \dots, 4$, with \mathbf{e}_i denoting the standard basis of \mathbb{R}^5 . With respect to the basis of simple roots, we obtain a representation \mathcal{H}_2 of H_2 which is a subgroup of the lattice group $\Lambda(Q_4)$:

$$\mathcal{H}_2 = \left\langle \begin{pmatrix} 1 & 0 & 0 & 0 \\ 1 & 0 & 0 & -1 \\ 1 & 0 & -1 & 0 \\ 1 & -1 & 0 & 0 \end{pmatrix}, \begin{pmatrix} -1 & 1 & 0 & 0 \\ 0 & 1 & 0 & 0 \\ 0 & 1 & 0 & -1 \\ 0 & 1 & -1 & 0 \end{pmatrix} \right\rangle. \quad (4.27)$$

Comparing with the character table of \mathcal{D}_{10} given in Section 3.2.2, and using formula (1.11), we have that $\mathcal{H}_2 \simeq E_1 \oplus E_2$ in $GL(4, \mathbb{R})$, inducing a decomposition $\mathbb{R}^4 \simeq E^{(1)} \oplus E^{(2)}$ (cf. (1.9)), where $E^{(1)}$ and $E^{(2)}$ are both totally irrational with respect to the lattice Q_4 . This decomposition can be explicitly found with the results from representation theory reviewed in Section 1.2.2. In particular, the projection $\pi_2^{(1)} : \mathbb{R}^4 \rightarrow E^{(1)}$ is given by

$$\pi_2^{(1)} = \frac{1}{\sqrt{2(3-\tau)}} \begin{pmatrix} -\tau' \sqrt{3-\tau} & \sqrt{3-\tau} & 0 & -\sqrt{3-\tau} \\ -1 & 2-\tau & -2\tau' & 2-\tau \end{pmatrix}, \quad (4.28)$$

which induces the irrep $\hat{\mathcal{H}}_2$:

$$\hat{\mathcal{H}}_2 = \left\langle \left(\begin{array}{cc} 1 & 0 \\ 0 & -1 \end{array} \right), \frac{1}{2} \left(\begin{array}{cc} -\tau' & \sqrt{\tau+2} \\ \sqrt{\tau+2} & \tau' \end{array} \right) \right\rangle. \quad (4.29)$$

With these results, we are able to construct nested point sets in $E^{(1)} \simeq \mathbb{R}^2$ with five-fold symmetry. In particular, with GAP we study the set $\mathcal{A}_{\mathcal{H}_2}$ of subgroups of $\Lambda(Q_4)$ containing \mathcal{H}_2 (compare with (4.1)). There is a unique chain of subgroups containing a proper extension of \mathcal{H}_2 :

$$\mathcal{H}_2 \triangleleft \mathcal{K}_2 \subseteq \Lambda(Q_4),$$

where \mathcal{K}_2 is, in fact, isomorphic to $\text{Hol}(\mathbb{Z}_5)$. We point out that this group corresponds to the point group 54 given in [27]. The explicit representation of \mathcal{K}_2 is given by

$$\mathcal{K}_2 = \left\langle \left(\begin{array}{cccc} 0 & -1 & 1 & 0 \\ -1 & 0 & 1 & 0 \\ 0 & 0 & 1 & 0 \\ 0 & 0 & 1 & -1 \end{array} \right), \left(\begin{array}{cccc} 0 & 0 & 0 & -1 \\ 1 & 0 & 0 & -1 \\ 0 & 1 & 0 & -1 \\ 0 & 0 & 1 & -1 \end{array} \right), \left(\begin{array}{cccc} 1 & 0 & 0 & 0 \\ 1 & 0 & -1 & 1 \\ 0 & 1 & -1 & 1 \\ 0 & 1 & -1 & 0 \end{array} \right) \right\rangle.$$

In order to make computations easier, it is convenient to use as root system of H_2 the set $\tilde{\phi}_5 := i\phi_5 = \{\pm i\xi_5^j : j = 0, \dots, 4\}$, and as simple roots (see (4.17))

$$\tilde{\alpha}_1 = (0, 1), \quad \tilde{\alpha}_2 = \frac{1}{2}(\sqrt{3-\tau}, -\tau).$$

The Cartan matrix C_5 is the same as in (4.18) for $n = 5$. Using the relations (4.13) we obtain the weights (see Figure 4.2)

$$\tilde{\omega}_1 = \frac{1}{2} \left(\frac{\tau}{\sqrt{3-\tau}}, 1 \right), \quad \tilde{\omega}_2 = \left(\frac{1}{\sqrt{3-\tau}}, 0 \right).$$

We can then choose as a basis for the subspace $E^{(1)}$ the vectors

$$\mathbf{v}_1 = \frac{2}{\sqrt{2(3-\tau)}} \tilde{\omega}_1, \quad \mathbf{v}_2 = \frac{1}{\sqrt{2(3-\tau)}} \tilde{\omega}_2.$$

Let $\mathbb{Z}[\tau] = \{a + b\tau : a, b \in \mathbb{Z}\}$ denote the ring of integers of the field $\mathbb{Q}(\tau)$, and let $\pi_2^{(1)} : \mathbb{R}^4 \rightarrow E^{(1)}$ be the projection as in (4.28). With this setup we have

$$\pi_2^{(1)}(Q_4) = \{c_1 \mathbf{v}_1 + c_2 \mathbf{v}_2 : c_1, c_2 \in \mathbb{Z}[\tau]\} = \bigoplus_{i=1}^2 \mathbb{Z}[\tau] \mathbf{v}_i$$

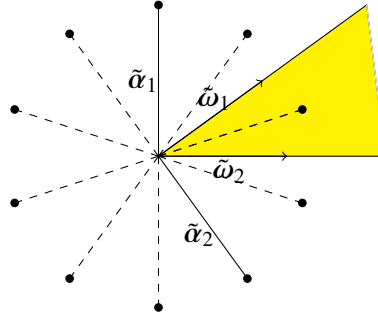


Figure 4.2: The root system, simple roots and fundamental weights for H_2 . The area highlighted corresponds to a patch of the fundamental chamber for the orbits of H_2 .

Hence the image $\pi_2^{(1)}(Q_4)$ of the root lattice Q_4 is a $\mathbb{Z}[\tau]$ -module in \mathbb{R}^2 of rank two³. Since $\pi_2^{(1)}$ is one-to-one on its image due to Proposition 1.2.1, it follows that any $\mathbb{Z}[\tau]$ -linear combination of \mathbf{v}_1 and \mathbf{v}_2 can be lifted to a unique point of the root lattice Q_4 . Notice that, since \mathbf{v}_1 and \mathbf{v}_2 are parallel to the fundamental weights $\tilde{\omega}_1$ and $\tilde{\omega}_2$, respectively, they identify the same dominant chamber D^+ of H_2 (see (4.11)). A dominant point $\mathbf{x} \in \pi_2^{(1)}(Q_4) \cap D^+$ can be written as $\mathbf{x} = a_1\mathbf{v}_1 + a_2\mathbf{v}_2$, with $a_1, a_2 \in \mathbb{Z}[\tau] \cap \mathbb{R}^+$.

With reference to the scheme in (4.6), we consider a dominant point $\mathbf{x} \in \pi_2^{(1)}(Q_4) \cap D^+$ for the orbit $O_{\mathcal{H}_2}(\mathbf{x})$, and lift the point by taking its preimage $\mathbf{w} := (\pi_2^{(1)})^{-1}(\mathbf{x})$. By construction, \mathbf{w} is a point of the lattice Q_4 . We then extend the symmetry and consider the orbit $O_{\mathcal{K}_2}(\mathbf{w})$. Let $g \in \mathcal{K}_2 \setminus \mathcal{H}_2$ be a representative of the coset \mathcal{H}_2g in $\mathcal{K}_2/\mathcal{H}_2$. The projected orbit $\pi_2^{(1)}(O_{\mathcal{K}_2}(\mathbf{w}))$ decomposes as in (4.5):

$$\pi_2^{(1)}(O_{\mathcal{K}_2}(\mathbf{w})) = O_{\mathcal{H}_2}(\pi_2^{(1)}(\mathbf{w})) \cup O_{\mathcal{H}_2}(\pi_2^{(1)}(g\mathbf{w})) = \underbrace{O_{\mathcal{H}_2}(\mathbf{x})}_{P_1(\mathbf{w})} \cup \underbrace{O_{\mathcal{H}_2}(\pi_2^{(1)}(g\mathbf{w}))}_{P_2(\mathbf{w})}.$$

By Theorem 4.1.1, $P_1(\mathbf{w}) = P_2(\mathbf{w})$ if and only if $\mathcal{H}_2g \cap \text{Stab}_{\mathcal{K}_2}(\mathbf{w}) \neq \emptyset$ (cf. (4.2)). Since \mathcal{K}_2 can be written as the disjoint union of \mathcal{H}_2 and \mathcal{H}_2g , this condition is equivalent to

$$\text{Stab}_{\mathcal{K}_2}(\mathbf{w}) \subseteq \mathcal{H}_2 \iff P_1(\mathbf{w}) \neq P_2(\mathbf{w}). \quad (4.30)$$

If (4.30) is true, then $|P_1(\mathbf{w})| = |P_2(\mathbf{w})|$, since \mathcal{H}_2 is normal in \mathcal{K}_2 . Therefore, the projection $\pi_2^{(1)}(O_{\mathcal{K}_2}(\mathbf{w}))$ consists of compounds of (at most) two decagons or two pentagons.

³Here there is an interesting fact to point out. In general terms, given a free module M (i.e. one that admits a basis) over a ring R , the rank of M corresponds to the number of linearly independent vectors that span M , and depends on the base ring $R[1]$. In fact, $\pi_2^{(1)}(Q_4)$ can also be regarded as a \mathbb{Z} -module in \mathbb{R}^2 . In this case, its rank is 4, and it is hence not a lattice in \mathbb{R}^2 (cf. (1.1)).

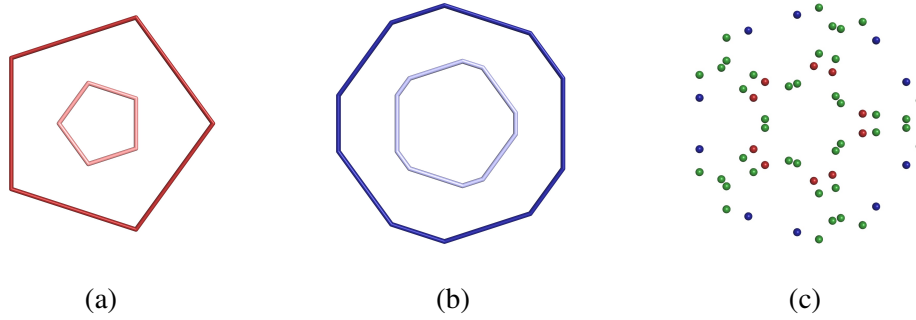


Figure 4.3: Planar nested structures with five-fold symmetry. (a) Two regular pentagons and (b) two irregular (but isogonal) decagons, resulting from the projection of orbits of Q_4 -lattice points under the extension \mathcal{K}_2 of \mathcal{H}_2 (the seed points in terms of the ω -basis are given in the Appendix). (c) Projected orbit of the lattice point $\mathbf{v} = (1, 2, 4, 3)$ under the lattice group $\Lambda(Q_4)$.

Specifically, writing $\mathbf{x} = a_1\mathbf{v}_1 + a_2\mathbf{v}_2$, we have:

1. If $a_1 = 0$ or $a_2 = 0$, then $\pi(\mathcal{O}_K(\mathbf{w}))$ consists of two distinct regular pentagons;
2. if $a_1 \neq 0$ and $a_2 \neq 0$, then $\pi(\mathcal{O}_K(\mathbf{w}))$ consists of two distinct decagons, which are isogonal but not necessarily regular.

We provide examples of double-shell structures with five-fold symmetry in Figure 4.3 (a) and (b). If we consider orbits of points of Q_4 under $\lambda(Q_4) \simeq S_5$, then their projection into $E_2^{(1)}$ consists of at most $|S_5|/|H_2| = 120/10 = 12$ radial levels, each displaying five-fold symmetry. In Figure 4.3 (c) we show an example of a point set thus constructed.

4.2.3 Nested polyhedra with icosahedral symmetry H_3

As already pointed out in Section 2.1, the group H_3 is associated with achiral icosahedral symmetry in \mathbb{R}^3 . It has order 120 and is isomorphic to $\mathcal{I} \times \mathbb{Z}_2$. Its crystallographic embedding has been analysed in Chapter 2; specifically, a crystallographic representation \widetilde{H}_3 of H_3 is given by $\widetilde{\mathcal{I}} \otimes \Gamma$, where $\widetilde{\mathcal{I}}$ is a crystallographic representation of \mathcal{I} in B_6 and $\Gamma = \{1, -1\}$ is the non-trivial irrep of \mathbb{Z}_2 (cf. (2.15)). In Chapter 5 icosahedral point sets obtained from projection of $\widetilde{\mathcal{I}}$ -containing subgroups of B_6 will be analysed in detail, in particular in the context of applications to viral capsid architecture. Here, instead, we provide, based on the results in Section 4.1, an analytical construction of nested polyhedra with H_3 -symmetry in the framework of Coxeter groups.

Polyhedron	Wythoff positions	Number of vertices
Icosahedron	$(0, 0, x_3)$	12
Dodecahedron	$(x_1, 0, 0)$	20
Icosidodecahedron (IDD)	$(0, x_2, 0)$	30
Truncated icosahedron	$(0, x_2, x_3)$	60
Truncated dodecahedron	$(x_1, x_2, 0)$	60
Rhombicosidodecahedron (RIDD)	$(x_1, 0, x_3)$	60
Truncated icosidodecahedron	(x_1, x_2, x_3)	120

Table 4.2: Isogonal polyhedra with H_3 -symmetry.

We recall that $\tau' = 1 - \tau$ denotes the Galois conjugate of the golden ratio τ . The root system ϕ of H_3 can be expressed as [49]

$$\phi = \left\{ \begin{array}{l} (\pm 1, \pm \tau, \pm \tau') \text{ and all even permutations} \\ (\pm 1, 0, 0) \text{ and all permutations} \end{array} \right\}.$$

ϕ consists of 30 roots; its convex hull is an icosidodecahedron, a polyhedron which is made up of 20 regular triangles and 12 regular pentagons [70]. The simple roots can be chosen as

$$\alpha_1 = (0, 0, 1), \quad \alpha_2 = -\frac{1}{2}(\tau', 1, \tau), \quad \alpha_3 = (1, 0, 0).$$

The Cartan matrix (4.9) is then given by

$$C = \begin{pmatrix} 2 & -\tau & 0 \\ -\tau & 2 & -1 \\ 0 & -1 & 2 \end{pmatrix}.$$

The ω -basis consists of the three fundamental weights

$$\omega_1 = \frac{1}{2}(\tau^2, 0, 1), \quad \omega_2 = (\tau, 0, 0), \quad \omega_3 = \frac{1}{2}(\tau, 1, 0). \quad (4.31)$$

We denote by (a, b, c) the coordinates of a vector $v \in \mathbb{R}^3$ in the ω -basis. There are 7 different isogonal polyhedra with H_3 -symmetry [70, 77], which correspond to the 7 possible Wythoff positions given in Table 4.2. We refer to Koca et al. [77] and Cromwell [70] for a visual representation, and their geometric properties.

The set $\mathcal{A}_{\widetilde{H}_3}$ contains all the \widetilde{H}_3 -containing subgroups of B_6 , and will be computed in Chapter 5. Here we focus on the extensions of the embedded H_3 , i.e. the subgroups of

B_6 that contains \widetilde{H}_3 as a normal subgroup. These are easily classified. In particular, with GAP we compute the normaliser $N_{B_6}(\widetilde{H}_3)$ of \widetilde{H}_3 in B_6 ; the explicit representation is given in the Appendix. Its order is 240, which is twice the size of H_3 ; hence $[N_{B_6}(\widetilde{H}_3) : \widetilde{H}_3] = 2$. Therefore, $K_3 := N_{B_6}(\widetilde{H}_3)$ is the *unique* extension of \widetilde{H}_3 in B_6 , since the normaliser of a subgroup H of a group G is the largest subgroup of G in which H is normal [1].

Let E^\parallel be the three-dimensional subspace invariant under \widetilde{H}_3 , carrying the irrep $\rho_3 \otimes \Gamma$ of H_3 (cf. Section 2.1.3 and (2.16)), and let $\pi^\parallel : \mathbb{R}^6 \rightarrow E^\parallel$ be the projection into E^\parallel given in (2.13). Similarly to the case of H_2 , we classify the projected orbits of simple cubic lattice points under the extension K_3 . Since $[K_3 : \widetilde{H}_3] = 2$, the number of nested polyhedra in projection is at most two. We choose as a basis of E^\parallel the vectors

$$\mathbf{v}_1 = c(\tau^2, 0, 1) = 2c\omega_3, \quad \mathbf{v}_2 = c(1, 0, 0) = -\tau'c\omega_2, \quad \mathbf{v}_3 = c(\tau, 1, 0) = 2c\omega_1,$$

where $c = \sqrt{\frac{2}{\tau+2}}$, which are parallel to the weights in (4.31). With this choice, as in the case of H_2 we have that the image $\pi^\parallel(\mathcal{L}_{SC})$ of the simple cubic lattice in \mathbb{R}^6 is a $\mathbb{Z}[\tau]$ -module in \mathbb{R}^3 of rank 3 (and a \mathbb{Z} -module of rank 6):

$$\pi^\parallel(\mathcal{L}_{SC}) = \bigoplus_{i=1}^3 \mathbb{Z}[\tau]\mathbf{v}_i,$$

and moreover, since the projection π^\parallel is one-to-one with its image, any $\mathbb{Z}[\tau]$ -linear combination of \mathbf{v}_1 , \mathbf{v}_2 and \mathbf{v}_3 in E^\parallel can be lifted to a unique point belonging to the SC lattice in \mathbb{R}^6 using the projection π^\parallel .

Let $\mathbf{x} \equiv (x_1, x_2, x_3)$ be the dominant point for the orbit $\mathcal{O}_{\rho_3 \otimes \Gamma}(\mathbf{x})$, written in the basis $\mathbf{v}_1, \mathbf{v}_2, \mathbf{v}_3$, with $x_i \in \mathbb{Z}[\tau]_{\geq 0}$, and let $\mathbf{w} = (\pi^\parallel)^{-1}(\mathbf{x}) \in \mathcal{L}_{SC}$ be the pre-image of \mathbf{x} . Let then $g \in K_3 \setminus \widetilde{H}_3$ be a representative for the coset $\widetilde{H}_3 g \in K_3$. We define the first polyhedron as $\mathcal{Q}_1 := \text{Conv}(\mathcal{O}_{\mathcal{H}_3}(\mathbf{x}))$. The other polyhedron is then given by $\mathcal{Q}_2 := \text{Conv}(\mathcal{O}_{\rho_3 \otimes \Gamma}(\pi^\parallel(g\mathbf{w})))$; as in the case of H_2 , since there are only two cosets in K_3/\mathcal{H}_3 , \mathcal{Q}_1 and \mathcal{Q}_2 are distinct if and only if $\text{Stab}_{K_3}(\mathbf{w}) \subseteq \mathcal{H}_3$. In this latter case, $|\mathcal{Q}_1| = |\mathcal{Q}_2|$ by Theorem 4.1.1. We have the following possibilities (compare with Table 4.2):

1. If \mathcal{Q}_1 is an icosahedron, a dodecahedron, an icosidodecahedron or a truncated icosidodecahedron, then \mathcal{Q}_2 is a polyhedron of the same type;
2. in all the other cases, $|\mathcal{Q}_1| = |\mathcal{Q}_2| = 60$; we have then six possible pairings $\{\mathcal{Q}_1, \mathcal{Q}_2\}$.

In order to test which pairings are possible, we solve

$$\hat{\mathbf{x}} = \pi^\parallel(g\mathbf{w}) \equiv (\hat{x}_1, \hat{x}_2, \hat{x}_3), \quad \text{with} \quad \mathbf{w} = (\pi^\parallel)^{-1}(\mathbf{x}), \quad \mathbf{x} = (x_1, x_2, x_3), \quad (4.32)$$

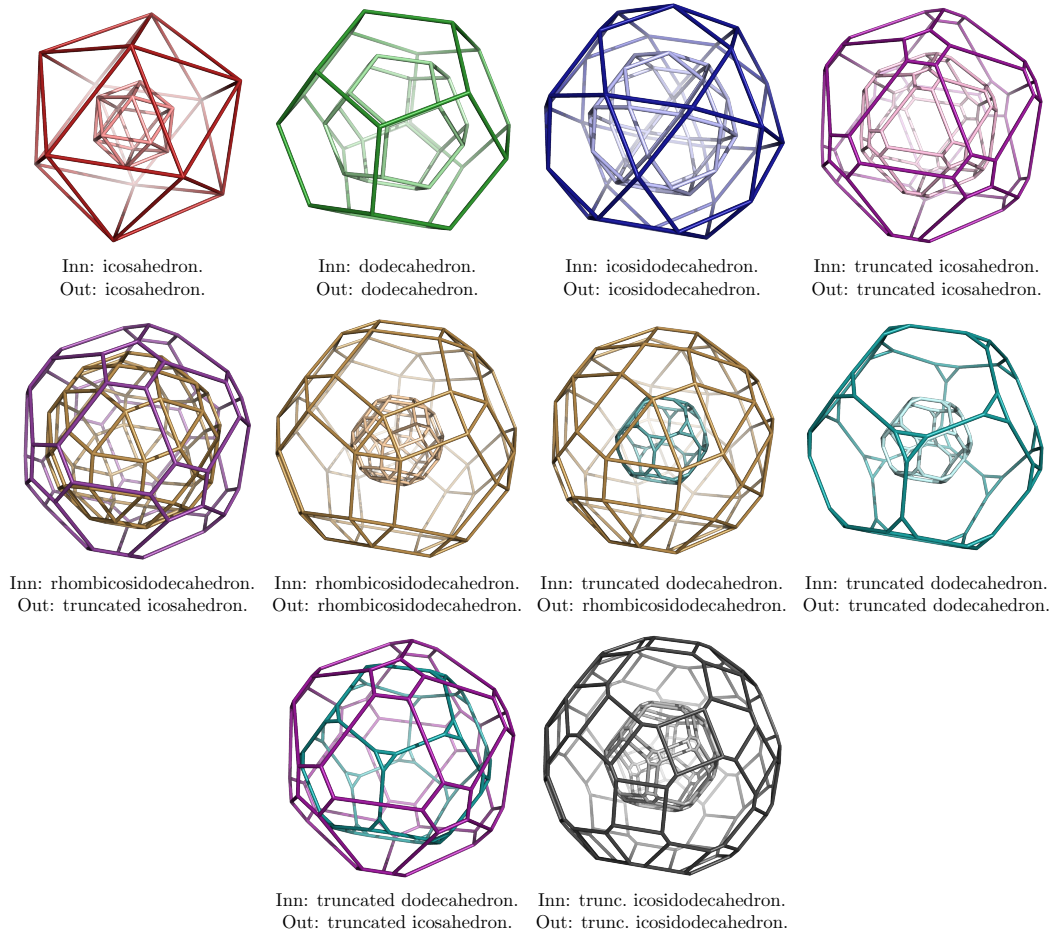


Figure 4.4: A visualisation of all the possible pairings of nested polyhedra with achiral icosahedral symmetry, as projected orbits under the extension K_3 of the embedding \widetilde{H}_3 of H_3 . “Inn” stands for the inner polyhedron and “Out” for the outer one. The explicit forms of the seed points for the orbits are given in the Appendix.

for different combination of \hat{x} and x such that precisely one \hat{x}_i and x_j are zero (compare with Table 4.2).

Representative solutions of (4.32) are shown in the Appendix and displayed in Figure 4.4.

4.2.4 Nested polychora with generalised icosahedral symmetry H_4

The Coxeter group H_4 is the four dimensional analogue of H_3 and therefore represents generalised icosahedral symmetry in \mathbb{R}^4 . Its order is $120^2 = 14,400$ and it contains the groups H_2 and H_3 as subgroups (cf. (4.26)). Due to these inclusions, H_4 is particularly relevant in the construction of quasicrystals with five-fold symmetry in two, three and four

dimensions, by means of the so-called *icosian model sets* [6, 37, 78]. Indeed, let $\mathbb{H} \simeq \mathbb{R}^4$ denote the standard quaternionic algebra over \mathbb{R} with basis $\{1, i, j, k\}$ satisfying the relations $i^2 = j^2 = k^2 = ijk = -1$. Every element $\mathbf{q} \in \mathbb{H}$ is in the form $\mathbf{q} = a+bi+cj+dk \equiv (a, b, c, d)$. The 120 unit quaternions

$$\mathcal{J} = \left\{ \begin{array}{ll} (\pm 1, 0, 0, 0) & \text{and all permutations} \\ \frac{1}{2}(\pm 1, \pm 1, \pm 1, \pm 1) & \\ \frac{1}{2}(0, \pm 1, \pm \tau, \pm \tau') & \text{and all even permutations} \end{array} \right\}$$

form a group under quaternionic multiplication, called the group of *icosians*, which is isomorphic to the binary icosahedral group⁴ $2I$. These can be chosen as a root system for H_4 ; as simple roots we take

$$\alpha_1 = (0, 1, 0, 0), \quad \alpha_2 = \frac{1}{2}(0, -\tau, -\tau', -1), \quad \alpha_3 = (0, 0, 0, 1), \quad \alpha_4 = \frac{1}{2}(-\tau', 0, -\tau, -1), \quad (4.33)$$

and the Cartan matrix is then given by

$$C = \begin{pmatrix} 2 & -\tau & 0 & 0 \\ -\tau & 2 & -1 & 0 \\ 0 & -1 & 2 & -1 \\ 0 & 0 & -1 & 2 \end{pmatrix}.$$

The ω -basis is as follows:

$$\omega_1 = \frac{1}{2}(2 + 3\tau, 1, \tau^2, 0), \quad \omega_2 = (2\tau + 1, 0, \tau, 0), \quad \omega_3 = \frac{1}{2}(3\tau + 1, 0, \tau, 1), \quad \omega_4 = (\tau, 0, 0, 0).$$

The standard crystallographic embedding of H_4 is by means of the Weyl group E_8 [2, 79, 80]. In view of this formalism, we construct, following [79, 80], a simple system Δ_8 for the group E_8 based on the simple roots of H_4 given in (4.33). Specifically, we take

$$\Delta_8 := \{\alpha_i, -\tau' \alpha_i : i = 1, \dots, 4\}. \quad (4.34)$$

It can be proved that Δ_8 form a basis of the root lattice Q_8 of E_8 [79]. By construction, H_4 stabilises Q_8 ; therefore in the basis Δ_8 we obtain a representation \mathcal{H}_4 of H_4 of degree 8 (subgroup of the lattice group $\Lambda(Q_8)$ of Q_8):

$$\mathcal{H}_4 = \langle R_1, R_2, R_3, R_4 \rangle. \quad (4.35)$$

⁴We recall that the group $SU(2)$ of special 2×2 hermitian complex matrices is the double cover of the rotation group $SO(3)$, i.e. there exists a homomorphism $\alpha : SU(2) \rightarrow SO(3)$ whose kernel is isomorphic to \mathbb{Z}_2 , and therefore $SO(3) \simeq SU(2)/\mathbb{Z}_2$. The binary icosahedral group $2I$ is then defined as the preimage $\alpha^{-1}(I)$.

The explicit form of this representation is given in the Appendix. \mathcal{H}_4 is reducible and induces a decomposition of \mathbb{R}^8 into two \mathcal{H}_4 -invariant subspaces of dimension four, denoted by $E_4^{(1)}$ and $E_4^{(2)}$, both totally irrational with respect to the lattice Q_8 . In particular, the irrep $\hat{\mathcal{H}}_4$ carried by the subspace $E_4^{(1)}$ is given by

$$\hat{\mathcal{H}}_4 = \left\langle \begin{pmatrix} 1 & 0 & 0 & 0 \\ 0 & -1 & 0 & 0 \\ 0 & 0 & 1 & 0 \\ 0 & 0 & 0 & 1 \end{pmatrix}, \frac{1}{2} \begin{pmatrix} 2 & 0 & 0 & 0 \\ 0 & \tau & -\tau' & 1 \\ 0 & -\tau' & 1 & -\tau \\ 0 & 1 & -\tau & \tau' \end{pmatrix}, \begin{pmatrix} 1 & 0 & 0 & 0 \\ 0 & 1 & 0 & 0 \\ 0 & 0 & -1 & 0 \\ 0 & 0 & 0 & 1 \end{pmatrix}, \frac{1}{2} \begin{pmatrix} \tau' & 0 & -\tau & 1 \\ 0 & 2 & 0 & 0 \\ -\tau & 0 & 1 & -\tau' \\ 1 & 0 & -\tau' & \tau \end{pmatrix} \right\rangle,$$

and moreover the projection $\pi_4^{(1)} : \mathbb{R}^8 \rightarrow E_4^{(1)}$ is as follows

$$\pi_4^{(1)} = \frac{1}{2} \sqrt{\frac{2+\tau'}{5}} \begin{pmatrix} 0 & 0 & 0 & \tau & 0 & 0 & 0 & -\tau^2 \\ -2 & \tau' & 0 & 0 & 2\tau & 1 & 0 & 0 \\ 0 & 1 & -2 & 1 & 0 & -\tau & 2\tau & -\tau \\ 0 & \tau & 0 & \tau' & 0 & -\tau^2 & 0 & 1 \end{pmatrix}.$$

With these results, we are able to construct, via projection, nested four dimensional point sets and related polytopes with generalised icosahedral symmetry. The standard name for a four-dimensional polytope is *polychoron* [81]. There are 15 isogonal polychora with H_4 -symmetry [82]; we list them in Table 4.3. We refer to Coxeter [69] and Möller [82] for a detailed description of their geometrical properties.

The subgroup structure of $\Lambda(Q_8) \simeq E_8$ is extremely complex, and the classification of all chains of its \mathcal{H}_4 -containing subgroups is a difficult computational task. However, if we restrict to the subgroups containing \mathcal{H}_4 as a normal subgroup, then the classification is straightforward. Indeed, with GAP we find the normaliser of \mathcal{H}_4 in $\Lambda(Q_8)$. Its explicit form is given in the Appendix. As for H_3 , $[N_{\Lambda(Q_8)}(\mathcal{H}_4) : \mathcal{H}_4] = 2$, so that $\mathcal{K}_4 := N_{\Lambda(Q_8)}(\mathcal{H}_4)$ is the unique extension of \mathcal{H}_4 in $\Lambda(Q_8)$. The projection of the orbits under \mathcal{K}_4 consists of at most two nested polychora Q_1 and Q_2 , since the index of K_4 in $\Lambda(Q_8)$ is 2, with $|Q_1| = |Q_2|$, by Theorem 4.1.1. The classification method is the same as for H_3 . The basis of $E_4^{(1)}$ was chosen as

$$\mathbf{v}_1 = x(\tau^2, 2 - \tau, 1, 0) = 2(2 - \tau)x\boldsymbol{\omega}_1, \quad \mathbf{v}_2 = x(\tau, 0, -\tau', 0) = x(2 - \tau)\boldsymbol{\omega}_2,$$

$$\mathbf{v}_3 = x(2 + \tau, 0, 1, -\tau') = -2x\tau'\boldsymbol{\omega}_3, \quad \mathbf{v}_4 = x(1, 0, 0, 0) = -x\tau'\boldsymbol{\omega}_4, \quad \text{with } x = \sqrt{\frac{3 - \tau}{5}}.$$

As before, with this choice we have $\pi_4^{(1)}(Q_8) = \bigoplus_{i=1}^4 \mathbb{Z}[\tau]\mathbf{v}_i$. There are 25 possible different pairings of distinct polychora. Numerical examples are given in the Appendix.

Polychoron	Wythoff positions	Number of vertices
600-cell	$(0, 0, 0, x_4)$	120
120-cell	$(x_1, 0, 0, 0)$	600
Rectified 600-cell	$(0, 0, x_3, 0)$	720
Rectified 120-cell	$(0, x_2, 0, 0)$	1,200
Truncated 600-cell	$(0, 0, x_3, x_4)$	1,440
Truncated 120-cell	$(x_1, x_2, 0, 0)$	2,400
Runcinated 120-cell	$(x_1, 0, 0, x_4)$	2,400
Cantellated 120-cell	$(x_1, 0, x_3, 0)$	3,600
Bitruncated 120-cell	$(0, x_2, x_3, 0)$	3,600
Cantellated 600-cell	$(0, x_2, 0, x_4)$	3,600
Cantitruncated 120-cell	$(x_1, x_2, x_3, 0)$	7,200
Runcitruncated 120-cell	$(x_1, x_2, 0, x_4)$	7,200
Runcitruncated 600-cell	$(x_1, 0, x_3, x_4)$	7,200
Cantitruncated 600-cell	$(0, x_2, x_3, x_4)$	7,200
Omnitruncated 600-cell	(x_1, x_2, x_3, x_4)	14,400

Table 4.3: Isogonal polychora with H_4 -symmetry.

Sections. The polychora obtained from projection are four-dimensional objects. In order to visualise them, we create *3D sections* of them [69]. In general, for an n -polytope Q with symmetry described by a Coxeter group H , let $\alpha_1, \dots, \alpha_n$ be the simple roots of H with $\omega_1, \dots, \omega_n$ denoting the corresponding fundamental weights. Consider the hyperplane L_i through the origin and perpendicular to ω_i , and define $Q' := Q \cap L_i$. Q' is by construction an $(n - 1)$ -dimensional section of Q . Then Q' is invariant under all the reflections r_{α_j} with $j \neq i$. To see this, note that a point \mathbf{v} belongs to L_i if and only if $\langle \mathbf{v}, \omega_i \rangle = c$, with $c \in \mathbb{R}$. Since $\alpha_j \perp \omega_i$ by definition of fundamental weights (cf. (4.12)), we have

$$\langle r_{\alpha_j}(\mathbf{v}), \omega_i \rangle = \langle \mathbf{v} - 2 \frac{\langle \alpha_j, \mathbf{v} \rangle}{\langle \alpha_j, \alpha_j \rangle} \alpha_j, \omega_i \rangle = \langle \mathbf{v}, \omega_i \rangle - 2 \frac{\langle \alpha_j, \mathbf{v} \rangle}{\langle \alpha_j, \alpha_j \rangle} \underbrace{\langle \alpha_j, \omega_i \rangle}_{=0} = \langle \mathbf{v}, \omega_i \rangle = c.$$

Therefore, L_i is invariant under the reflections r_{α_j} , for $j \neq i$, and as a consequence the section Q' is invariant under the Coxeter group H' , whose Coxeter graph is obtained by removing the node corresponding to the root α_i to the graph of H .

In the case of polychora with H_4 symmetry $(\bullet \text{---} \frac{5}{\bullet} \text{---} \bullet \text{---} \bullet)$, we have:

1. Sections through L_1 have A_3 symmetry $(\bullet \text{---} \bullet \text{---} \bullet)$, which corresponds to the sym-

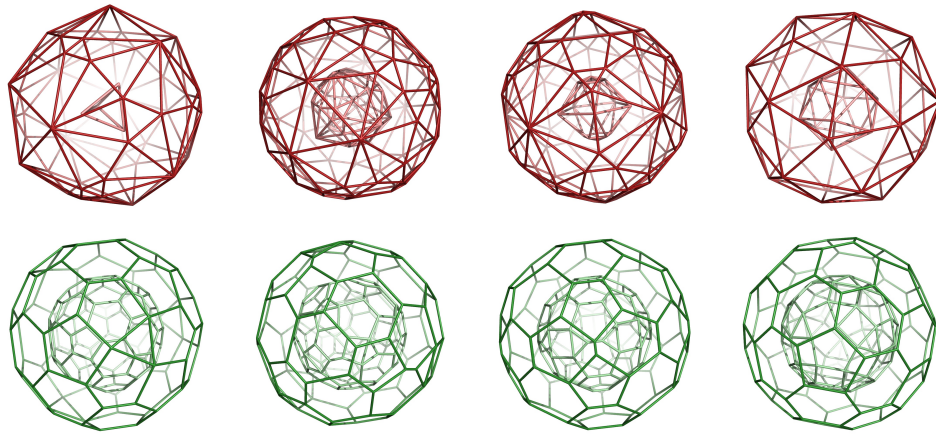


Figure 4.5: Sections of two nested polychora with H_4 symmetry: 600-cell – 600-cell (top row) and 120-cell – 120-cell (bottom row). The cross sections are taken through a hyperplane perpendicular to (from left to right): ω_1 (tetrahedral symmetry), ω_2 (symmetry of a triangular prism), ω_3 (symmetry of a pentagonal prism) and ω_4 (icosahedral symmetry).

metry of a tetrahedron;

2. sections through L_2 have $A_1 \times A_2$ symmetry ($\bullet \quad \bullet \text{---} \bullet$), which is the symmetry of a triangular prism;
3. sections through L_3 have $H_2 \times A_1$ symmetry ($\bullet \text{---} \frac{\bullet}{5} \quad \bullet$), which is the symmetry of a pentagonal prism;
4. sections through L_4 have icosahedral symmetry H_3 ($\bullet \text{---} \frac{\bullet}{5} \text{---} \bullet$).

In Figure 4.5 we display two examples of such sections in the case of two nested 120-cells and two nested 600-cells.

Chapter 5

Applications to viral capsid architecture

*The treacherous instrument is in thy hand,
Unbated and envenomed.*

W. Shakespeare, *Hamlet*.

In this chapter we show that the group theoretical setup introduced in Section 4.1 can be used to rationalise viral capsid architecture. Specifically, we classify all the chains of subgroups containing the icosahedral group embedded into the hyperoctahedral group, based on the analysis carried out in Chapter 2. We then consider the capsids of Paria-coto Virus and Bacteriophage MS2, whose structures have been intensively studied experimentally [15, 16], and show that the projected orbits of the groups provide constraints on their three-dimensional organisation, encoding information on the structural organisation of capsid proteins and the genomic material collectively. Contrary to the affine extensions previously introduced, these orbits endow virus architecture with an underlying higher dimensional finite group structure via projection, which lends itself better for the modeling of its dynamic properties than their infinite dimensional counterpart.

5.1 Nested point sets with icosahedral symmetry

In Section 4.2.3 we classified double-shell structures with achiral icosahedral symmetry H_3 resulting from the projection of orbits of lattice points under the extension of

H_3 embedded into the hyperoctahedral group B_6 . For applications in virology, we need to construct nested point sets with icosahedral symmetry which exhibit wider multi-shell structures, possibly not invariant under reflections since viral capsids in general possess chirality. Therefore, we consider the crystallographic embedding of the icosahedral group \mathcal{I} into the point group B_6 , analysed in Chapter 2, and classify all the chains of subgroups of B_6 containing the representative $\tilde{\mathcal{I}}$ of the class of crystallographic representations of \mathcal{I} (cf. (2.1)). Indeed, we consider the set (cf. (4.1)):

$$\mathcal{A}_{\tilde{\mathcal{I}}} := \{G < B_6 : \tilde{\mathcal{I}} < G\}. \quad (5.1)$$

We compute this set with with GAP. To this purpose, we need to scan through all the conjugacy classes of subgroups of B_6 , in a similar way as was done in Section 2.1.2. In order to make computations faster and more efficient, we use a ‘‘sieve’’ procedure to determine *a priori* which classes of subgroups do not contain any subgroup isomorphic to the icosahedral group. For this, some results from group theory are required. In particular, we use the fact that if G is a soluble group¹, then every subgroup H of G is soluble [55]. Since the icosahedral group is isomorphic to the alternating group \mathfrak{A}_5 , it is not soluble [1]. Therefore, any subgroup G of B_6 containing $\tilde{\mathcal{I}}$ as a subgroup must not be soluble. Moreover, it cannot be Abelian (since \mathcal{I} is not) and the order of G must be divisible by $|\mathcal{I}| = 60$, as a consequence of Lagrange’s Theorem. With these considerations, we provide the following algorithm.

Algorithm 5.1.1. *In order to determine $\mathcal{A}_{\tilde{\mathcal{I}}}$, perform the following steps:*

1. *Compute the conjugacy classes C_i of the subgroups of B_6 .*
2. *List a representative K_i for each class C_i .*
3. *Rule out those representatives which have one of the following properties:*
 - *K_i is soluble;*
 - *K_i is Abelian;*

¹We recall that a group G is *soluble* (or *solvable*) if there exists a chain of subgroups

$$G = M_0 \supset M_1 \supset M_2 \supset \dots \supset M_r = e,$$

such that M_i is normal in M_{i-1} and M_{i-1}/M_i is Abelian, for $i = 1, \dots, r$.

Subgroup	Order	Index
$G_1 \simeq \mathcal{I}$	60	1
$G_2 \simeq H_3$	120	2
$G_3 \simeq N_{B_6}(G_2)$	240	4
G_4	1,920	32
G_5	3,840	64
G_6	3,840	64
G_7	3,840	64
G_8	7,680	128
G_9	11,520	192
G_{10}	23,040	384
G_{11}	23,040	384
G_{12}	23,040	384
$G_{13} \simeq B_6$	46,080	768

Table 5.1: Classification of the subgroups of B_6 containing the crystallographic representation $\widetilde{\mathcal{I}}$ of the icosahedral group \mathcal{I} as a subgroup.

- $60 \nmid |K_i|$.

4. For each K_i not ruled out, compute all the element $G_i \in C_i$. If $\widetilde{\mathcal{I}} < G_i$, then add G_i to $\mathcal{A}_{\widetilde{\mathcal{I}}}$.

The algorithm was implemented in GAP (see Appendix), and the results are given in Table 5.1. For the computations, we used the embedding of B_6 into the symmetric group S_{12} described in Section 2.1.1. There are 13 elements in $\mathcal{A}_{\widetilde{\mathcal{I}}}$, which we denote by G_i , for $i = 1, \dots, 13$. The generators of the groups G_i are given in the Appendix in terms of permutations in S_{12} ; the function $\psi : S_{12} \rightarrow B_6$, given in (2.8), can then be used to map a permutation into a matrix in B_6 . Clearly, G_1 is the crystallographic representation $\widetilde{\mathcal{I}}$ of \mathcal{I} , whereas G_{13} corresponds to the whole hyperoctahedral group. Moreover, the group G_2 is $\widetilde{\mathcal{I}} \otimes \Gamma$, the crystallographic representation \widetilde{H}_3 of H_3 (cf. (2.15)), and G_3 corresponds to the normaliser $N_{B_6}(\widetilde{H}_3)$ of \widetilde{H}_3 (see Section 4.2.3). In Figure 5.1 we show the graph of inclusions of the groups G_i , that indicates the independence of different subgroup chains.

As explained in Section 2.1.3, the representation $\widetilde{\mathcal{I}}$ leaves two three-dimensional subspaces invariant, denoted by E^{\parallel} and E^{\perp} , which carry the two irreps of \mathcal{I} of degree 3, denoted by ρ_3 and ρ'_3 , respectively (see Table 2.1.3). The projection π^{\parallel} into the physical

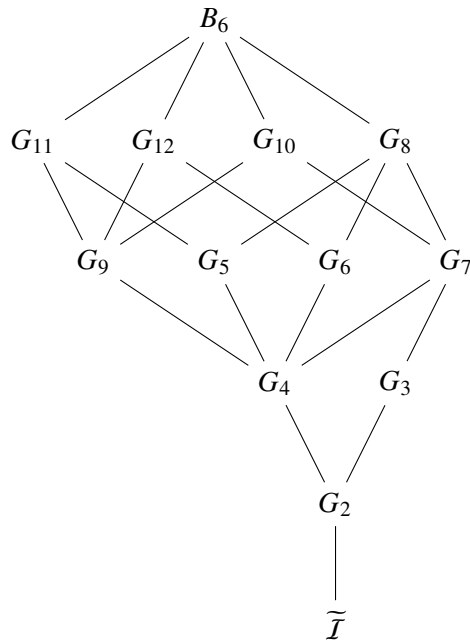


Figure 5.1: Graph of inclusions of the subgroups of the hyperoctahedral group containing the crystallographic representation $\tilde{\mathcal{I}}$ of the icosahedral group.

space E^{\parallel} is given in (2.13). In what follows, we will consider orbits of points of the simple cubic lattice \mathcal{L}_{SC} in \mathbb{R}^6 (cf. Section 2.1). The projection into E^{\parallel} of orbits of such points under the groups G_i produces nested point sets with icosahedral symmetry at each radial level. An example is given in Figure 5.2. Every radial level is the union of cosets of G_i with respect to $\tilde{\mathcal{I}}$.

It is worth pointing out that every group G_i , for $i > 3$, contains H_3 as well as \mathcal{I} as subgroups. From a geometrical point of view, this implies that the resulting orbits in projection are all invariant under reflections, i.e. each radial level possesses full icosahedral symmetry H_3 . This observation provides a sharper bound on the number of distinct radial levels in projection: in fact, this is given by $n/2$, the index of H_3 in G_i , where n is the index of \mathcal{I} in G_i . On the other hand, this does not imply that the point sets thus obtained do not provide constraints on viral capsids with chirality, since they do not fully determine its structure, but rather provide structural constraints for the capsid organisation. Indeed, viruses may realise these blueprints in an asymmetric way; an example, which we are going to discuss later in this chapter, is Bacteriophage MS2, whose genome organisation has been shown to be asymmetric via graph theoretical analysis [83].

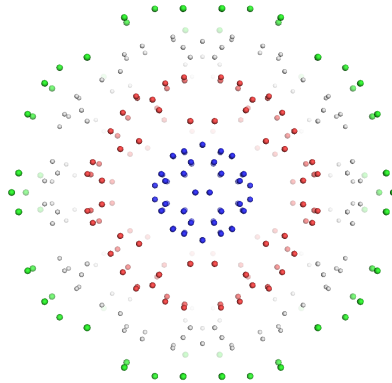


Figure 5.2: The projected orbit of the lattice point $\mathbf{v} = (0, 0, 1, 1, 2, 1)$ under the group G_4 . Each layer in the resulting nested point set possesses achiral icosahedral symmetry.

5.2 Projected orbits as blueprints for viral capsids

The classification of the subgroup chains of B_6 extending icosahedral symmetry, derived in Section 5.1, provides a suitable mathematical framework to understand structural constraints on viral capsids. As a first step towards this goal, we identify a finite library of point arrays, corresponding to the projected orbits of $6D$ lattice points under the groups G_i previously classified. Elements in this library depend on two quantities: the group $G_i \in \mathcal{A}_{\bar{I}}$ and the lattice point $\mathbf{v} \in \mathcal{L}_{SC}$. The G_i are provided by our classification. As can be seen from Figure 5.1 and Table 5.1, the smallest group containing \bar{I} as a proper subgroup and thus giving icosahedral nested shells in projection is G_3 . The index of G_3 with respect to H_3 is 2, therefore the number of radial levels is at most 2: the double-shell structures obtained as projected G_3 -orbits have been classified in Section 4.2.3. In order to obtain deeper information about capsid geometry, more radial levels are necessary. Therefore, we consider in the following the subgroups G_i , for $i = 4, \dots, 13$. Moreover, \mathbf{v} is chosen as follows: since the $6D$ lattice is infinite, we introduce a cut-off parameter $N > 0$ and consider all lattice points within a six-dimensional cube:

$$I_N^6 := [-N, N] \times \dots \times [-N, N] = [-N, N]^6 \subseteq \mathcal{L}_{SC},$$

containing $(2N + 1)^6$ lattice points. In particular, we consider all orbits of the groups G_i within a bounded area around the origin defined by N .

Based on this set-up, the library of point arrays is obtained via the action of the group G_i on the set I_N^6 , for $i = 4, \dots, 13$. This action is well-defined since G_i is a subgroup of the point group of the lattice, and therefore lattice points are mapped into lattice points under elements of G_i . Let $D_N^{(i)} = \{\mathbf{v}_1^{(i)}, \dots, \mathbf{v}_{k_i}^{(i)}\}$ be a set of distinct representatives for the orbits of G_i in I_N^6 . Since $G_4 \subseteq G_i$ for all $i = 5, \dots, 13$, and thus their fundamental domains are contained in that of G_4 , the set $D_N^{(4)}$ contains the sets of representatives $D_N^{(i)}$ for the groups G_i , $i = 5, \dots, 13$, which are not necessarily distinct. Since we do not have information on the group G_4 apart from its generators, the set $D_N^{(4)}$ is computed numerically according to the following procedure:

1. For $\mathbf{v} \in I_N^6$, compute $O_{G_4}(\mathbf{v})$;
2. among all $\mathbf{v}_i \in O_{G_4}(\mathbf{v})$ identify $\hat{\mathbf{v}}$ with the largest number of positive components, choosing at random if two or more points fulfil this property;
3. add $\hat{\mathbf{v}}$ to $D_N^{(4)}$ and repeat from the start until all $\mathbf{v} \in I_N^6$ have been considered.

In particular, $D_N^{(4)}$ thus obtained contains 47, 183 and 529 points for $N = 2, 3$ and 4, respectively. With this setup, the library of constraints is given by

$$\mathcal{S}(N) := \{\pi^{\parallel}(O_{G_j}(\mathbf{v})) : \mathbf{v} \in D_N^{(4)}, j = 4, \dots, 13\}, \quad (5.2)$$

which by construction consists of distinct point arrays.

Once the set $\mathcal{S}(N)$ is computed for a chosen value of N , we retrieve the information of the viral capsid in consideration from the VIPER data bank [84]. These PDB files contain structural data of viral capsids, such as the coordinates of the atomic positions of the capsid proteins and in many cases also of the packaged genome. Following [85], we represent the atomic positions of the proteins by spheres of radius 1.9 Å in the visualisation tool PyMol². In order to compare the point arrays with biological data, and hence find those point sets which best represent the capsid features, we use the following procedure:

1. For any group $G_i \in \mathcal{A}_{\tilde{\mathcal{I}}}$, we compute with GAP a transversal $T^{(i)} = (g_1^{(i)}, \dots, g_{n_i}^{(i)})$ for the right cosets of $\tilde{\mathcal{I}}$ in G_i , where n_i denotes the index of $\tilde{\mathcal{I}}$ in G_i .
2. Given a point array $\pi^{\parallel}(O_{G_i}(\mathbf{v})) \in \mathcal{S}(N)$, we compute the set

$$L^{(i)}(\mathbf{v}) = \{|\pi^{\parallel}(g_j^{(i)}\mathbf{v})| : j = 1, \dots, n_i\}.$$

²This is an approximation for the Van der Waals radii of the atoms.

The cardinality of $L^{(i)}(\mathbf{v})$ corresponds to the number of distinct radial levels in the point set $\pi^{\parallel}(O_{G_i}(\mathbf{v}))$. We denote by $R_{max}^{(i)}(\mathbf{v}) := \max L^{(i)}(\mathbf{v})$ the largest radial level which corresponds to the outermost layer in the nesting. This is used to scale the point set so that the capsid is contained in the convex hull of the projected orbit.

3. The rescaled orbit is then compared with the data in the PDB file. We start by selecting those point arrays whose outermost layer best represents the outermost features of the capsid. Specifically, we consider a coarse-grained representation of the capsid surface by locating the most radially distal clusters of C_{α} atoms using the procedure described by [85]. Denoting these clusters by $C_k, k = 1, \dots, M$, the C_k can be approximated by M spheres $B_k(\tilde{r})$ of radius \tilde{r} (for the numerical implementation, we chose the cutoff $\tilde{r} = 10\text{\AA}$). For any orbit $\pi^{\parallel}(O_{G_i}(\mathbf{v}))$, we isolate its external point layer $L^{(\text{out})}$ by computing the points situated at distance R_{max} (introduced above) from the origin. The orbit is then selected if, for every point $\mathbf{x} \in L^{(\text{out})}$, there exists $k \in \{1, \dots, M\}$ such that $\mathbf{x} \in B_k(\tilde{r})$.
4. Among the point sets thus selected, we determine those that best match the other capsid features. For this, we isolate the inner radial levels using the decomposition of orbits into cosets and compare them with the location of the genomic material and the inner capsid surface. The cardinalities of the point arrays are not large enough to match with atomic positions, but they rather map around material as in [19]; this comparison can be achieved via visual inspection using the surface representation of the capsid in PyMol.

We consider here two case studies: Pariacoto Virus and Bacteriophage MS2, both $T = 3$ capsids in the Caspar-Klug classification. These were chosen in order to facilitate comparison with [19], where point arrays derived from affine extensions of the icosahedral group were used to generate blueprints for viral architecture.

Pariacoto Virus. Pariacoto Virus (PaV) is a single-stranded RNA insect virus, whose X-ray crystal structure reveals approximately 35% of the RNA organised as a dodecahedral cage of duplex RNA in proximity to the inner capsid surface [15]. A characteristic feature of this capsid are the 60 protrusions of approximately 15\AA around the quasi three-fold axes, each formed by three interdigitated subunits. These are the outermost capsid features that

we will match to the largest radial levels in the point arrays of our constraint library in order to identify the best fit point array. For this we performed the procedure described above, and found that the best fit for this capsid is given by the projected orbit of the lattice point $\hat{\mathbf{v}} = (2, 1, -1, -1, 0, 0)$ under the group G_6 (see Figure 5.3). This point set consists of 960 points, arranged into 8 radial levels. The outermost level is formed by 60 points which map onto the spikes at the 60 local three-fold axes, see Figure 5.3 (b). The third radial level from the origin describes the organisation of the RNA inside the capsid. This set is made up of 120 points forming a truncated icosidodecahedron, which maps around the dodecahedral RNA cage, see Figure 5.3 (d). The fifth radial level from the origin, located between the RNA and the spikes, consists of 120 points, organised into 10 and 12 clusters of 6 and 5 points each, which are located around the 3 and 5 fold axes, respectively. In particular, we show in Figure 5.3 (c) a close-up view of the clusters with five-fold symmetry. Note that these points provide constraints on the lengths of the protein helices and the positions of the protein subunits of type C.

We point out that G_6 is the group of smallest order in the set $\mathcal{A}_{\bar{T}}$ providing a blueprint for PaV that captures the locations of both capsid proteins *and* the RNA collectively. The orbit of $\hat{\mathbf{v}}$ under G_4 in projection, which by construction is contained in $\pi^{\parallel}(O_{G_6}(\hat{\mathbf{v}}))$, maps around the spikes, but totally lacks information on the organisation of the genomic material inside. Moreover, all the orbits of $\hat{\mathbf{v}}$ under the G_6 -containing $G_k \in \mathcal{A}_{\bar{T}}$, i.e. G_8 and G_{12} , as well as B_6 (cf. Figure 5.1) coincide in projection, implying that they contain no additional information on capsid architecture. Hence G_6 can be chosen as the six-dimensional symmetry group that induces the three-dimensional structure of the PaV capsid in projection.

Bacteriophage MS2. Like PaV, MS2 is a single-stranded RNA virus, with a $T = 3$ capsid. Cryo-electron microscopy reveals a double-shell structure in the organisation of the genomic RNA; the outermost shell lies closely underneath the capsid proteins, while the innermost one is located at much lower radii [16]. With our procedure as above, we found that the projected orbit of $\tilde{\mathbf{v}} = (2, 1, 1, -1, 0, 1)$ under the group G_4 is the point set that provides the best blueprint for the capsid (see Figure 5.4). Specifically, this orbit contains 960 points, that are arranged, in projection, into 9 radial levels. The two outermost layers, $L^{(9)}$ and $L^{(8)}$, map to the exterior of the capsid: $L^{(9)}$ consists of 60 points, arranged into 12 clusters of 5 points each, positioned around the five-fold symmetry axes of the capsid,

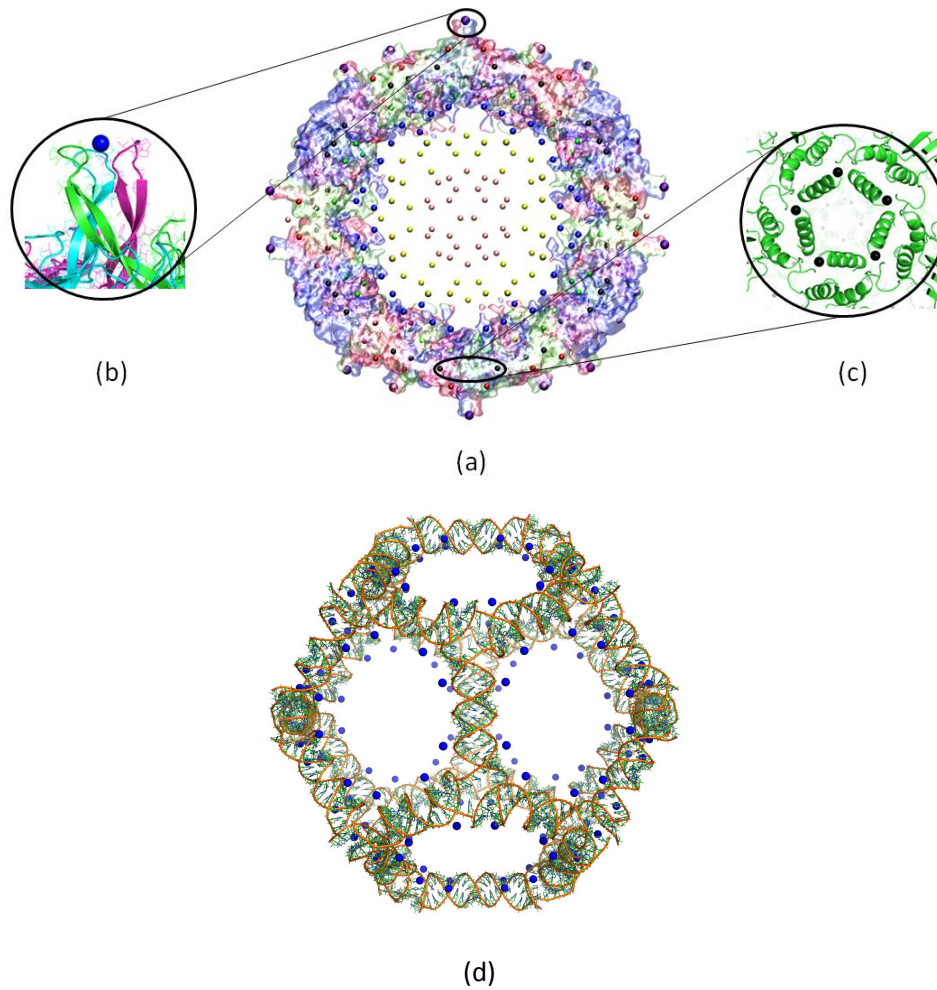


Figure 5.3: Blueprints for the capsid of Pariacoto Virus (based on pdb file 1f8v). (a) A cross-section of the capsid superimposed on the projected orbit of $\hat{v} = (2, 1, -1, -1, 0, 0)$ under the group G_6 . The point set consists of 960 points, situated at 8 distinct radial levels, which provide constraints on the capsid architecture. (b) A close-up view of the outermost layer of the projected orbit, which encodes the locations of the spikes around the quasi three-fold axes. (c) The layers between the spikes and the genomic material map around the inner capsid surface. (d) The third farthest layer from the origin gives information on RNA organisation: the 120 points, forming a truncated icosidodecahedron, map around the dodecahedral RNA cage.

whereas $L^{(8)}$ has size 120 and is made up of 20 clusters of 6 points, located around the three-fold axes. This is consistent with the quasi-equivalent structure of the $T = 3$ capsid.

We point out that $L^{(8)}$ and $L^{(9)}$ are in fact almost situated at the same radial level (the ratio of their radii is ≈ 1.064814), and collectively map around the capsid exterior as shown in the close-up in Figure 5.4 (b).

All other points of the array are from a mathematical point of view related to these outermost layers, and indeed map around material boundaries, capturing the double-shell structure of the genomic material. To prove this, we compare the point array with the icosahedrally averaged cryo-EM structure of MS2 at 8\AA resolution in [16]. As shown in Figure 5.4 (a), the innermost radial levels of the point array define the organisation of the inner RNA shell. Moreover, there are points mapping around the outer and inner surfaces of the outermost shell. There is a layer of points, positioned around the RNA, connecting the outer and inner RNA shells (see the close-up in Figure 5.4 (c)). This icosahedrally averaged data set has been obtained via a superposition of a large number of viral particles, aligned according to their symmetry axes, in order to enhance the resolution. However, in any individual particle, the RNA is organised in an asymmetric way, that is consistent with the icosahedrally averaged density [83]. Therefore, we compare our model with the asymmetric RNA density of a cryo-EM tomogram at about 39\AA resolution [83, 86] (see Figure 5.4 (d)). Since the density is shown in a cross sectional view, the density in the two shells cannot be seen in full. However, the density agrees with the radial levels defined by the point arrays, showing that, although in an asymmetrical way, the points map around genomic material, consistent with our hypothesis that the mathematical model indeed provides blueprints for this virus. Taken together, these results imply that the group G_4 is the group of smallest order in our classification that provides structural constraints on the capsid proteins and the genome organisation of MS2, and is therefore the symmetry group in 6D that describes the structure of this virus in projection.

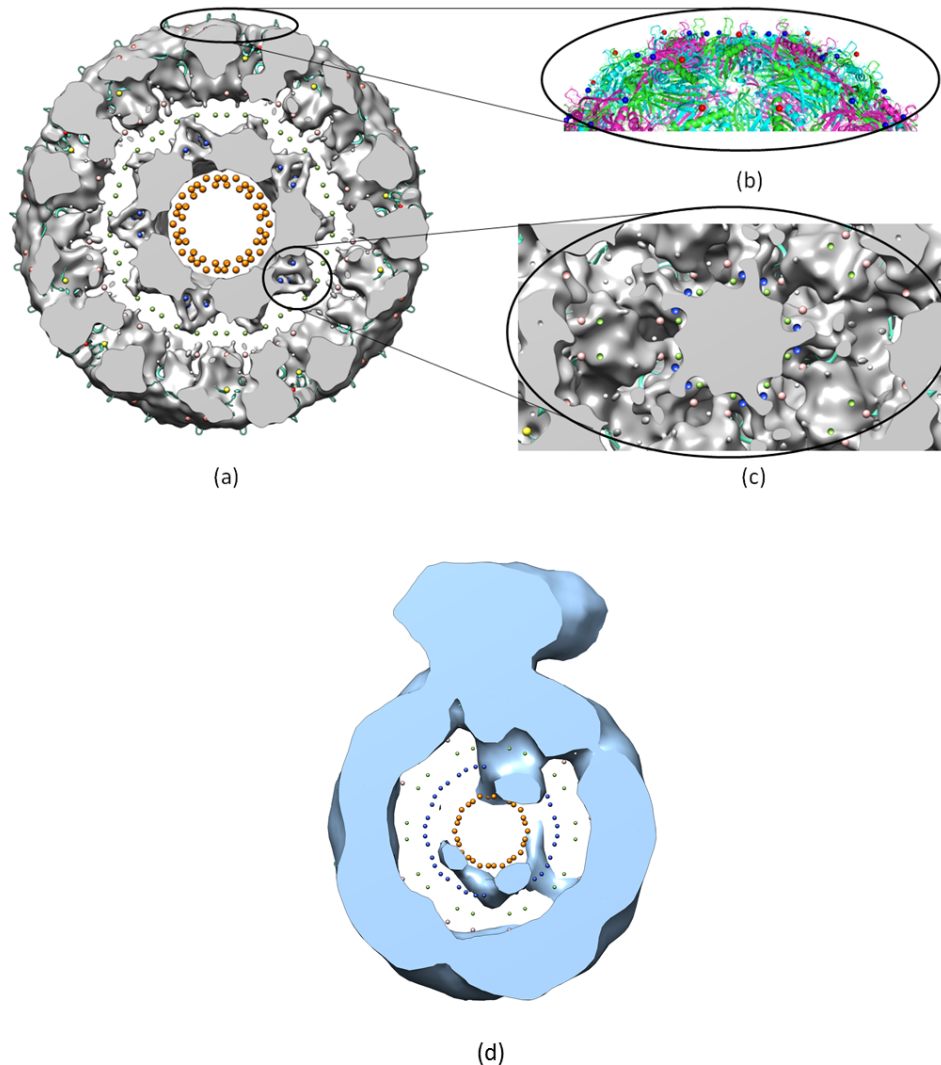


Figure 5.4: The projected orbit of $\tilde{\nu} = (2, 1, 1, -1, 0, 1)$ under the group G_4 provides blueprints for the capsid of Bacteriophage MS2 (based on pdb file 1aq3). (a) Cross section of the virus: the point set consists of 9 different radial levels which encode information on the position of capsid proteins and the genomic material of the virus. (b) Close-up view of the outermost layers of the projected orbit which map around the outer capsid surface. (c) Close-up view of the RNA density. The second and third innermost layers (in blue and green, respectively) map around the five-fold symmetry axes and connect the two RNA shells. (d) A cryo-tomogram of bacteriophage MS2, adapted from [86], superimposed on the point array. The inner and outer RNA shells follow the blueprints of the array points, but realise it in an asymmetric way.

Conclusions

This thesis introduced new group theoretical approaches to characterise the three-dimensional organisation of viral capsids and to model structural changes in structures with non-crystallographic symmetry, such as the capsid transitions that are important in the infection process of many viruses and transitions between different atomic organisations of icosahedral quasicrystals. Both structure prediction and the models for structural transitions rely crucially on a crystallographic embedding of non-crystallographic groups into higher dimensional lattices. In particular, since the icosahedral group \mathcal{I} is non-crystallographic in 3D, we considered its embedding into the hyperoctahedral group in six dimensions, and we developed a new group theoretical approach to classify its crystallographic representations and their intersections and shared subgroups. While of independent mathematical interest, this analysis paved the way for the study of structural transitions, here demonstrated for icosahedral quasicrystals. This was achieved via the computation of the Schur rotations in $SO(6)$ that induce, using the cut-and-project method, continuous transformations of the corresponding model sets, while maintaining the symmetry described by a common subgroup of two distinct representations of \mathcal{I} . On the other hand, we used this embedding to provide a novel way of characterising viral capsid architecture. For this, we classified the chain of \mathcal{I} -containing subgroups of the hyperoctahedral group, and studied the orbits of 6D lattice points of such subgroups. The latter, projected into a three-dimensional \mathcal{I} -invariant subspace, resulted in finite nested point sets with icosahedral symmetry at each radial level, that allow the formulation of simultaneous structural constraints on multiple layers of viral material, thus giving insight into the three-dimensional geometry of viral capsids. As case studies, we considered the capsids of Pariacoto Virus and Bacteriophage MS2, whose structures have been extensively analysed experimentally and which are therefore excellent examples to validate model predictions.

The biological and physical applications inspired the development of new mathematical techniques. In particular, for the analysis of the subgroup structure of the hyperoctahedral group, we introduced a new computational method, based on graphs and their spectra. Moreover, we provided a rigorous mathematical construction of finite nested arrays for general non-crystallographic symmetries, and treated in detail the case of finite irreducible Coxeter groups. In addition, we combined mathematical proofs with computational methods, developing algorithms with specific software, in particular using GAP for solving problems in computational group theory.

The group theoretical analysis carried out in Chapter 4 allows for the first time a characterisation of finite multi-shell structures with non-crystallographic symmetry that is entirely based on the theory of finite groups. Contrary to the affine extensions of non-crystallographic groups previously analysed, these point sets correspond to orbits of lattice points in a higher dimensional space under finite groups extending non-crystallographic symmetry. In the context of virology, this implies that the overall virus architecture is associated with an underlying finite group structure, albeit in a higher dimensional space, that constrains the three-dimensional geometry of multiple layers of viral material simultaneously in projection.

The crystallographic embedding of non-crystallographic groups has already been used in mathematical physics in the theory of integrable systems [87, 88]. In this context, the crystallographic embedding of the non-crystallographic Coxeter groups H_2 , H_3 and H_4 allows the formulation of Hamiltonians that model the motion of the system in terms of a Lie algebraic framework. In fact, as pointed out in Section 4.2.1, the Cartan matrix of a non-crystallographic Coxeter group has irrational entries, and therefore the corresponding root system cannot be associated with a Lie algebra [20], as would be required for the study of many integrable systems. By analogy, we considered here the equivalent for biological applications, in which the six-dimensional crystallographic embedding of the icosahedral group allows the identification of symmetry groups whose orbits of lattice points describe, in projection, the structure of a viral capsid.

This work opens up new directions for the study of thermodynamical properties of viruses and quasicrystals. Indeed, as already mentioned in the Preface, structural transitions of quasicrystals and viruses can be analysed in the framework of the Landau theory for continuous phase transitions [13]. In particular, the transitions are modeled through

Hamiltonians invariant under the symmetry group G of the system, depending on the order parameter(s) of the transition that account(s) for the symmetry breaking, e.g. the Schur rotation angle(s) computed in Chapter 3. Under certain assumptions of regularity, such Hamiltonians can be expanded in terms of G -invariant polynomials [33], and the energy landscape can then be analysed; the (local) minima correspond to (meta)stable phases of the system, and possibly possess different symmetry than the initial state. In virology, initial work in this direction can be found in [89], where structural transitions of Equine Rhinitis A Virus (ERAV) are modeled via a polynomial energy function invariant under the icosahedral group, and in [90], where the Landau theory is applied to predict the positions of the capsid proteins, both for viruses following the Caspar-Klug classification and for those violating it. With the analysis carried out in Chapter 5, the Landau theory can be applied to provide information on the three-dimensional structure and transitions of viral capsids by formulating Hamiltonians invariant under the symmetry group in six dimensions that describes the capsid in projection, in line with arguments given in [87, 88] for integrable systems. In the context of quasicrystals, the group theoretical approach to structural transitions developed in Chapter 3 can be combined with the introduction of Hamiltonians that depend on the Schur rotation angle(s) invariant under the icosahedral group in order to analyse the possible transition paths between icosahedral model sets.

Besides applications in virology and quasicrystals, the mathematical tools developed here can be used in carbon chemistry to analyse the structures of fullerenes, in particular the atomic positions in nested carbon cages with icosahedral symmetry called carbon onions [38, 91]. Indeed, affine extensions of the icosahedral group were applied in this context [50, 92], thus creating a link between viruses and fullerenes that highlights the role of group theory in these topics. The point sets derived in Chapter 4 and the classification of the subgroups of the hyperoctahedral group extending icosahedral symmetry in Section 5.1 provide a suitable framework to model these structures, endowing them, as for viral capsids, with a finite group structure induced by projection. The new mathematical structures developed here, originally inspired by applications in virology, are therefore likely to have a much wider scope of applications in Science.

Appendix

GAP codes

Algorithm 1. Classification of the crystallographic representations of \mathcal{I} (see Section 2.1.2). The algorithm carries out steps 1-4 used to prove Proposition 2.1.1.

```
gap > B6:= Group([(1,2)(7,8), (1,2,3,4,5,6)(7,8,9,10,11,12), (6,12)]);
gap > C:= ConjugacyClassesSubgroups(B6);
gap > C60:= Filtered(C, x->Size(Representative(x))=60);
gap > Size(C60);
3
gap > s60:= List(C60, Representative);
gap > I:= AlternatingGroup(5);
gap> IsomorphismGroups(I, s60[1]);
[(2,4)(3,5), (1,2,3)]- > [(1,3)(2,4)(7,9)(8,10), (3,10,11)(4,5,9)]
gap> IsomorphismGroups(I, s60[2]);
[(2,4)(3,5), (1,2,3)]- > [(1,2)(3,10)(4,9)(5,11)(6,12)(7,8), (1,2,4)(3,12,5)(6,11,9)(7,8,10)]
gap > IsomorphismGroups(I, s60[3]);
[(2,4)(3,5), (1,2,3)]- > [(2,6)(4,11)(5,10)(8,12), (1,3,5)(2,4,6)(7,9,11)(8,10,12)]
gap> CB6s60:= ConjugacyClassSubgroups(B6, s60[2]);
gap> Size(CB6s60);
192
```

In the following, H stands for the class $C_{B_6}(\tilde{\mathcal{I}})$ of the crystallographic representations of \mathcal{I} , $i \in \{1, \dots, 192\}$ denotes a vertex in the \mathcal{G} -graph (cf. Section 2.2.3) corresponding to the representation $H[i]$ and n stands for the size of \mathcal{G} : we can use the size instead of

the explicit form of the subgroup since, in the case of the icosahedral group, all the non isomorphic subgroups have different sizes (cf. Table 2.2).

Algorithm 2. Computation of the vertex star of a given vertex i in the \mathcal{G} -graphs.

```
gap> VertexStar:=function(H,i,n)
> local j,R,S;
> R:=[];
> for j in [1..Size(H)] do
> S:=Intersection(H[i],H[j]);
> if Size(S) = n then
> R:=Concatenation(R,[j]);
> fi;
> od;
> return R;
> end;
```

Algorithm 3. Computation of the adjacency matrix of the \mathcal{G} -graph.

```
gap> AdjacencyMatrix:=function(H,n)
> local i,j,C,A;
> A:=NullMat(Size(H),Size(H));
> for i in [1..Size(H)] do
> C:=VertexStar(H,i,n);
> for j in [1..Size(C)] do
> A[i][C[j]]:=1;
> od;
> od;
> return A;
> end;
```

Algorithm 4. Computation of the set $\mathcal{A}_{\overline{T}}$ (implementation of Algorithm 5.1.1 in Section 5.1).

```

gap> B6:=Group([(1,2)(7,8),(1,2,3,4,5,6)(7,8,9,10,11,12),(6,12)]);;
gap> c:=ConjugacyClassesSubgroups(B6);;
gap> s:=List(c,Representative);;
gap> Size(s);
7440
gap> I:=Group([(1,6)(2,5)(3,9)(4,10)(7,12)(8,11),
(1,5,6)(2,9,4)(7,11,12)(3,10,8)]);;
gap> sieve:=function(L)
> local M,i;
> M:=[];
> for i in [1..Size(L)] do
> if IsAbelian(L[i]) = true then
> continue;
> else if IsSolvable(L[i]) = true then
> continue;
> else
> M:=Concatenation([L[i]],M);
> fi;
> fi;
> od;
> return M;
> end;
function( L ) ... end
gap> M:=sieve(s);;
gap> Size(M);
55
gap> for i in [1..Size(M)] do
> S:=Concatenation([ConjugacyClassSubgroups(B6,M[i])],S);
> od;

```

```

gap> Size(S);
55
gap> sgp:=function(G,S)
> local i,j,L,M;
> L:=[];
> for i in [1..Size(S)] do
> M:=[];
> for j in [1..Size(S[i])] do
> if IsSubgroup(S[i][j],I)=true then
> M:=Concatenation([S[i][j]],M);
> fi;
> od;
> if M = [] then
> continue;
> else
> L:=Concatenation([M],L);
> fi;
> od;
> return L;
> end;
function( G, S ) ... end
gap> L:=sgp(I,S);;
gap> Size(L);
13

```

Numerical results

Computation of the Schur rotations

1. Explicit forms of the irreps Γ_1 and Γ_2 of the tetrahedral group and the matrix $Q \in O(3)$ such that $Q^{-1}\Gamma_2Q = \Gamma_1$ (cf. (3.12)):

Generator	Irrep Γ_1	Irrep Γ_2
g_2	$\frac{1}{2} \begin{pmatrix} \tau-1 & 1 & \tau \\ 1 & -\tau & \tau-1 \\ \tau & \tau-1 & -1 \end{pmatrix}$	$\frac{1}{2} \begin{pmatrix} \tau-1 & -\tau & -1 \\ -\tau & -1 & \tau-1 \\ -1 & \tau-1 & -\tau \end{pmatrix}$
g_{3d}	$\frac{1}{2} \begin{pmatrix} 1-\tau & 1 & \tau \\ 1 & \tau & 1-\tau \\ -\tau & \tau-1 & -1 \end{pmatrix}$	$\frac{1}{2} \begin{pmatrix} 1-\tau & \tau & -1 \\ -\tau & -1 & 1-\tau \\ -1 & \tau-1 & \tau \end{pmatrix}$
$Q = \frac{1}{3} \begin{pmatrix} 3-\tau & 1 & \tau+2 \\ -\tau-2 & 3-\tau & 1 \\ -1 & -\tau-2 & 3-\tau \end{pmatrix}$		

2. Explicit forms of the representations D_1 and D_2 and the corresponding reducing matrices $P_1, P_2 \in GL(3, \mathbb{R})$ (cf. (3.17)):

Generator	Rep. D_1	Rep. D_2
g_{2d}	$\frac{1}{2} \begin{pmatrix} -\tau & \tau-1 & -1 \\ \tau-1 & -1 & -\tau \\ -1 & -\tau & \tau-1 \end{pmatrix}$	$\frac{1}{2} \begin{pmatrix} -1 & \tau-1 & \tau \\ \tau-1 & -\tau & 1 \\ \tau & 1 & \tau-1 \end{pmatrix}$
g_{5d}	$\frac{1}{2} \begin{pmatrix} \tau-1 & -1 & \tau \\ 1 & \tau & \tau-1 \\ -\tau & \tau-1 & 1 \end{pmatrix}$	$\frac{1}{2} \begin{pmatrix} 1-\tau & -\tau & -1 \\ -\tau & 1 & 1-\tau \\ 1 & \tau-1 & -\tau \end{pmatrix}$
$P_1 = \begin{pmatrix} 0 & 1 & 0 \\ \sqrt{\frac{\tau+2}{5}} & 0 & \sqrt{\frac{3-\tau}{5}} \\ \frac{2\tau-1}{\sqrt{5(\tau+2)}} & 0 & \frac{1-2\tau}{\sqrt{5(3-\tau)}} \end{pmatrix} \quad P_2 = \begin{pmatrix} \sqrt{\frac{3-\tau}{5}} & \frac{2\tau-1}{\sqrt{5(3-\tau)}} & 0 \\ \frac{1-2\tau}{\sqrt{5(3-\tau)}} & \sqrt{\frac{3-\tau}{5}} & 0 \\ 0 & 0 & 1 \end{pmatrix}$		

3. Explicit forms of the representations S_1 and S_2 and the corresponding reducing matrices R_1 and $R_2 \in GL(3, \mathbb{R})$ (cf. (3.20)):

Generator	Rep. S_1	Rep. S_2
g_2	$\frac{1}{2} \begin{pmatrix} -\tau & \tau-1 & -1 \\ \tau-1 & -1 & -\tau \\ -1 & -\tau & \tau-1 \end{pmatrix}$	$\frac{1}{2} \begin{pmatrix} -1 & \tau-1 & \tau \\ \tau-1 & -\tau & 1 \\ \tau & 1 & \tau-1 \end{pmatrix}$
g_3	$\frac{1}{2} \begin{pmatrix} \tau & \tau-1 & 1 \\ 1-\tau & -1 & \tau \\ 1 & -\tau & 1-\tau \end{pmatrix}$	$\frac{1}{2} \begin{pmatrix} -1 & 1-\tau & -\tau \\ \tau-1 & \tau & -1 \\ \tau & -1 & 1-\tau \end{pmatrix}$
$R_1 = \frac{1}{\sqrt{3}} \begin{pmatrix} \tau & 0 & 1-\tau \\ 0 & \sqrt{3} & 0 \\ \tau-1 & 0 & \tau \end{pmatrix} \quad R_2 = \frac{1}{\sqrt{3}} \begin{pmatrix} 0 & \sqrt{3} & 0 \\ \tau & 0 & 1-\tau \\ 1-\tau & 0 & -\tau \end{pmatrix}$		

Extensions of embedded non-crystallographic groups and related polytopes

1. Explicit form of the normaliser $\mathcal{N}_{B_6}(\widetilde{H}_3) = \langle a, b, c, \rangle$ of \widetilde{H}_3 of H_3 (cf. Section 4.2.3):

$$a = \begin{pmatrix} 1 & 0 & 0 & 0 & 0 & 0 \\ 0 & 1 & 0 & 0 & 0 & 0 \\ 0 & 0 & 0 & 0 & -1 & 0 \\ 0 & 0 & 0 & 0 & 0 & -1 \\ 0 & 0 & -1 & 0 & 0 & 0 \\ 0 & 0 & 0 & -1 & 0 & 0 \end{pmatrix}, \quad b = \begin{pmatrix} 1 & 0 & 0 & 0 & 0 & 0 \\ 0 & 0 & 0 & 1 & 0 & 0 \\ 0 & 1 & 0 & 0 & 0 & 0 \\ 0 & 0 & 0 & 0 & 1 & 0 \\ 0 & 0 & 1 & 0 & 0 & 0 \\ 0 & 0 & 0 & 0 & 0 & -1 \end{pmatrix}, \quad c = \begin{pmatrix} 0 & 1 & 0 & 0 & 0 & 0 \\ 1 & 0 & 0 & 0 & 0 & 0 \\ 0 & 0 & 0 & 0 & 1 & 0 \\ 0 & 0 & 0 & 1 & 0 & 0 \\ 0 & 0 & 1 & 0 & 0 & 0 \\ 0 & 0 & 0 & 0 & 0 & 1 \end{pmatrix}.$$

2. Explicit forms of the representation \mathcal{H}_4 of H_4 embedded in E_8 (see (4.35)):

$$R_1 = \begin{pmatrix} -1 & 1 & 0 & 0 & 0 & 1 & 0 & 0 \\ 0 & 1 & 0 & 0 & 0 & 0 & 0 & 0 \\ 0 & 0 & 1 & 0 & 0 & 0 & 0 & 0 \\ 0 & 0 & 0 & 1 & 0 & 0 & 0 & 0 \\ 0 & 1 & 0 & 0 & -1 & 0 & 0 & 0 \\ 0 & 0 & 0 & 0 & 0 & 1 & 0 & 0 \\ 0 & 0 & 0 & 0 & 0 & 0 & 1 & 0 \\ 0 & 0 & 0 & 0 & 0 & 0 & 0 & 1 \end{pmatrix}, \quad R_2 = \begin{pmatrix} 1 & 0 & 0 & 0 & 0 & 0 & 0 & 0 \\ 1 & -1 & 1 & 0 & 1 & 0 & 0 & 0 \\ 0 & 0 & 1 & 0 & 0 & 0 & 0 & 0 \\ 0 & 0 & 0 & 1 & 0 & 0 & 0 & 0 \\ 0 & 0 & 0 & 0 & 1 & 0 & 0 & 0 \\ 1 & 0 & 0 & 0 & 0 & -1 & 1 & 0 \\ 0 & 0 & 0 & 0 & 0 & 0 & 1 & 0 \\ 0 & 0 & 0 & 0 & 0 & 0 & 0 & 1 \end{pmatrix}$$

$$R_3 = \begin{pmatrix} 1 & 0 & 0 & 0 & 0 & 0 & 0 & 0 \\ 0 & 1 & 0 & 0 & 0 & 0 & 0 & 0 \\ 0 & 1 & -1 & 1 & 0 & 0 & 0 & 0 \\ 0 & 0 & 0 & 1 & 0 & 0 & 0 & 0 \\ 0 & 0 & 0 & 0 & 1 & 0 & 0 & 0 \\ 0 & 0 & 0 & 0 & 0 & 1 & 0 & 0 \\ 0 & 0 & 0 & 0 & 0 & 1 & -1 & 1 \\ 0 & 0 & 0 & 0 & 0 & 0 & 0 & 1 \end{pmatrix}, \quad R_4 = \begin{pmatrix} 1 & 0 & 0 & 0 & 0 & 0 & 0 & 0 \\ 0 & 1 & 0 & 0 & 0 & 0 & 0 & 0 \\ 0 & 0 & 1 & 0 & 0 & 0 & 0 & 0 \\ 0 & 0 & 1 & -1 & 0 & 0 & 0 & 0 \\ 0 & 0 & 0 & 0 & 1 & 0 & 0 & 0 \\ 0 & 0 & 0 & 0 & 0 & 1 & 0 & 0 \\ 0 & 0 & 0 & 0 & 0 & 0 & 1 & 0 \\ 0 & 0 & 0 & 0 & 0 & 0 & 1 & -1 \end{pmatrix}.$$

3. Explicit form of the normaliser $N_{\Lambda(Q_8)}(\mathcal{H}_4) = \langle M_1, M_2, M_3, M_4, M_5 \rangle$ of the representation \mathcal{H}_4 in the lattice group $\Lambda(Q_8)$ (cf. Section 4.2.4):

$$M_1 = \begin{pmatrix} -1 & 1 & 0 & 0 & 0 & 1 & 0 & 0 \\ 0 & 1 & 0 & 0 & 0 & 0 & 0 & 0 \\ 0 & 0 & 1 & 0 & 0 & 0 & 0 & 0 \\ 0 & 0 & 0 & 1 & 0 & 0 & 0 & 0 \\ 0 & 1 & 0 & 0 & -1 & 0 & 0 & 0 \\ 0 & 0 & 0 & 0 & 0 & 1 & 0 & 0 \\ 0 & 0 & 0 & 0 & 0 & 0 & 1 & 0 \\ 0 & 0 & 0 & 0 & 0 & 0 & 0 & 1 \end{pmatrix}, \quad M_2 = \begin{pmatrix} 1 & 0 & 0 & 0 & 0 & 0 & 0 & 0 \\ 1 & -1 & 1 & 0 & 1 & 0 & 0 & 0 \\ 0 & 0 & 1 & 0 & 0 & 0 & 0 & 0 \\ 0 & 0 & 0 & 1 & 0 & 0 & 0 & 0 \\ 0 & 0 & 0 & 0 & 1 & 0 & 0 & 0 \\ 1 & 0 & 0 & 0 & 0 & -1 & 1 & 0 \\ 0 & 0 & 0 & 0 & 0 & 0 & 1 & 0 \\ 0 & 0 & 0 & 0 & 0 & 0 & 0 & 1 \end{pmatrix}$$

$$M_3 = \begin{pmatrix} 1 & 0 & 0 & 0 & 0 & 0 & 0 & 0 \\ 0 & 1 & 0 & 0 & 0 & 0 & 0 & 0 \\ 0 & 1 & -1 & 1 & 0 & 0 & 0 & 0 \\ 0 & 0 & 0 & 1 & 0 & 0 & 0 & 0 \\ 0 & 0 & 0 & 0 & 1 & 0 & 0 & 0 \\ 0 & 0 & 0 & 0 & 0 & 1 & 0 & 0 \\ 0 & 0 & 0 & 0 & 0 & 1 & -1 & 1 \\ 0 & 0 & 0 & 0 & 0 & 0 & 0 & 1 \end{pmatrix}, \quad M_4 = \begin{pmatrix} 1 & 0 & 0 & 0 & 0 & 0 & 0 & 0 \\ 0 & 1 & 0 & 0 & 0 & 0 & 0 & 0 \\ 0 & 0 & 1 & 0 & 0 & 0 & 0 & 0 \\ 0 & 0 & 1 & -1 & 0 & 0 & 0 & 0 \\ 0 & 0 & 0 & 0 & 1 & 0 & 0 & 0 \\ 0 & 0 & 0 & 0 & 0 & 1 & 0 & 0 \\ 0 & 0 & 0 & 0 & 0 & 0 & 1 & 0 \\ 0 & 0 & 0 & 0 & 0 & 0 & 1 & -1 \end{pmatrix}$$

$$M_5 = \begin{pmatrix} 1 & 0 & 2 & 0 & -1 & 0 & -4 & 0 \\ 0 & 0 & 3 & 0 & -1 & 1 & -5 & 0 \\ 0 & 0 & 2 & 0 & -1 & 1 & -3 & -1 \\ 0 & 0 & 1 & 0 & -1 & 1 & -2 & 0 \\ 0 & 0 & 2 & 0 & -1 & 0 & -2 & 0 \\ 1 & -1 & 2 & 0 & 0 & 0 & -3 & 0 \\ 1 & -1 & 1 & 1 & 0 & 0 & -2 & 0 \\ 1 & -1 & 1 & 0 & 0 & 0 & -1 & 0 \end{pmatrix}.$$

4. Numerical examples of the two possible polygonal nestings with five-fold symmetry arising from the projection of orbits of the extension \mathcal{K}_2 (cf. Section 4.2.2):

Pairing		# vertices	Seed point in terms of ...	
Q_1	Q_2		... weights (2D)	... roots (4D)
Pentagon	pentagon	5	(0, 10)	(2, 4, 1, -2)
Decagon	decagon	10	(1 + 3 τ , -10)	(1, 2, 4, 3)

5. Numerical examples of the possible compounds of nested polyhedra with icosahedral symmetry arising from orbits under the extension K_3 (cf. Section 4.2.3):

Pairing		# vertices	Seed point in terms of ...	
Q_1	Q_2		... weights (3D)	... roots (6D)
Icosahedron	Icosahedron	12	(0, 0, τ)	(1, 1, -1, -1, 1, 1)
Dodecahedron	Dodecahedron	20	(1, 0, 0)	(1, 1, -1, 1, 1, 1)
IDD	IDD	30	(0, 1, 0)	(0, 0, -1, 0, 0, 1)
Trunc. ico	Trunc. ico	60	(0, 1, 1)	(2, 0, -1, 0, 0, 1)
Trunc. ico	Trunc. dodec	60	(0, 2, τ)	(1, 1, -3, -1, 1, 3)
Trunc. ico	RIDD	60	(0, τ , 1)	(3, 0, 0, 0, 1, 0)
Trunc. dodec	Trunc. dodec	60	(1, τ , 0)	(2, 1, -1, 1, 2, 1)
Trunc. dodec	RIDD	60	(1, 0, τ)	(2, 2, -2, 0, 2, 2)
RIDD	RIDD	60	(τ , 0, 1)	(4, 0, 0, 0, 2, 2)
Trunc. IDD	Trunc. IDD	120	(1, 1, 1)	(3, 1, -2, 1, 1, 2)

6. Numerical examples of all the possible nestings of polychora with H_4 symmetry arising from the projection of orbits of \mathcal{K}_4 (cf. Section 4.2.4):

Pairing		# vertices	Seed point in terms of ...	
Q_1	Q_2		... weights (4D)	... roots (8D)
600-cell	600-cell	120	(0, 0, 0, 1)	-(5, 6, 4, 2, 3, 4, 3, 2)
120-cell	120-cell	600	(1, 0, 0, 0)	-(4, 2, 2, 0, 2, 2, 2, 2)
Rect. 600-cell	Rect. 600-cell	720	(0, 0, τ , 0)	(2, 4, 4, 4, 2, 0, 0, -2)
Rect. 120-cell	Rect. 120-cell	1,200	(0, 1, 0, 0)	(3, 4, 4, 2, 2, 2, 2, 0)
Tr. 600-cell	Tr. 600-cell	1,440	(0, 0, 1, 1)	-(9, 10, 8, 4, 5, 8, 7, 6)
Tr. 120-cell	Tr. 120-cell	2,400	(2, τ , 0, 0)	-(10, 6, 6, 0, 5, 6, 6, 6)
Runc. 120-cell	Runc. 120-cell	2,400	(1, 1, 0, 0)	(-1, 2, 2, 2, 0, 0, 0, -2)
Runc. 120-cell	Runc. 120-cell	2,400	(1, 0, 0, 1)	-(9, 8, 6, 2, 5, 6, 5, 4)
Bitr. 120-cell	Bitr. 120-cell	3,600	(0, 2, 1, 0)	(2, 4, 4, 2, 2, 0, 0, -4)
Bitr. 120-cell	Cant. 600-cell	3,600	(0, 1, 1, 0)	-(1, 0, 0, 0, 0, 2, 2, 4)
Bitr. 120-cell	Cant. 120-cell	3,600	(0, 1, 2, 0)	-(5, 4, 4, 2, 2, 6, 6, 8)
Cant. 600-cell	Cant. 600-cell	3,600	(0, τ , 0, τ)	(1, 2, 1, 2, 1, 0, -1, -2)
Cant. 600-cell	Cant. 120-cell	3,600	(0, τ , 0, 1)	-(7, 8, 6, 2, 4, 6, 5, 4)
Cant. 120-cell	Cant. 120-cell	3,600	(τ , 0, 0, 2)	-(6, 6, 6, 2, 2, 8, 8, 10)
Cantitr. 600-cell	Cantitr. 600-cell	7,200	(0, 1, 1, τ)	(2, 4, 3, 2, 2, 0, -1, -4)
Cantitr. 600-cell	Cantitr. 120-cell	7,200	(1, τ , τ , 0)	-(4, 0, 0, -4, 1, 4, 4, 6)
Cantitr. 600-cell	Runcitr. 600-cell	7,200	(1, 0, 1, τ)	-(5, 2, 3, 0, 2, 4, 5, 6)
Cantitr. 600-cell	Runcitr. 120-cell	7,200	(1, τ , 0, 1)	-(11, 10, 8, 2, 6, 8, 7, 6)
Cantitr. 120-cell	Cantitr. 120-cell	7,200	(1, 1, τ , 0)	(1, 6, 6, 6, 2, 0, 0, -4)
Cantitr. 120-cell	Runcitr. 600-cell	7,200	(2, 0, τ , τ)	(-3, 4, 3, 6, 0, -2, -3, -6)
Cantitr. 120-cell	Runcitr. 120-cell	7,200	(1, τ , 0, τ)	-(3, 0, 1, -2, 1, 2, 3, 4)
Runcitr. 600-cell	Runcitr. 600-cell	7,200	(1, 0, 1, 1)	-(13, 12, 10, 4, 7, 10, 9, 8)
Runcitr. 600-cell	Runcitr. 120-cell	7,200	(1, 1, 0, 1)	-(6, 4, 2, 0, 3, 4, 3, 4)
Runcitr. 120-cell	Runcitr. 120-cell	7,200	(2, τ , 0, 1)	-(15, 12, 10, 2, 8, 10, 9, 8)
Omnitr. 120-cell	Omnitr. 120-cell	14,400	(1, 1, 1, 1)	-(10, 8, 6, 2, 5, 8, 7, 8)

Subgroups of B_6 extending icosahedral symmetry

Explicit forms of the groups $G_i \in \mathcal{A}_{\bar{I}}$ (cf. (5.1)), output of Algorithm 4, embedded into the symmetric group S_{12} :

$$G_1 = \langle (1, 6)(2, 5)(3, 9)(4, 10)(7, 12)(8, 11), (1, 5, 6)(2, 9, 4)(7, 11, 12)(3, 10, 8) \rangle$$

$$G_2 = \langle (1, 6)(2, 5)(3, 9)(4, 10)(7, 12)(8, 11), (1, 5, 6)(2, 9, 4)(7, 11, 12)(3, 10, 8), \\ (1, 7)(2, 8)(3, 9)(4, 10)(5, 11)(6, 12) \rangle$$

$$G_3 = \langle (3, 11)(4, 12)(5, 9)(6, 10), (2, 3, 5, 4)(6, 12)(8, 9, 11, 10), (1, 2)(3, 5)(7, 8)(9, 11) \rangle$$

$$G_4 = \langle (1, 3)(2, 8)(4, 5, 10, 11)(7, 9), (1, 3, 4, 7, 9, 10)(2, 5, 12, 8, 11, 6) \rangle$$

$$G_5 = \langle (1, 8, 9, 7, 2, 3)(4, 6, 5)(10, 12, 11), (1, 2)(3, 5)(7, 8)(9, 11), (4, 10) \rangle$$

$$G_6 = \langle (3, 9)(6, 12), (3, 4, 5, 6)(9, 10, 11, 12), (1, 7)(6, 12), (1, 2, 9, 10, 11, 7, 8, 3, 4, 5)(6, 12) \rangle$$

$$G_7 = \langle (1, 7)(6, 12), (2, 8)(6, 12), (1, 2, 9, 10, 11, 7, 8, 3, 4, 5)(6, 12), (3, 4, 5, 12, 9, 10, 11, 6) \rangle$$

$$G_8 = \langle (1, 8, 9, 7, 2, 3)(4, 6, 5)(10, 12, 11), (1, 2)(3, 5)(7, 8)(9, 11), (3, 4, 5, 6)(9, 10, 11, 12), (4, 10) \rangle$$

$$G_9 = \langle (2, 8)(6, 12), (1, 7)(2, 5, 3)(6, 12)(8, 11, 9), (1, 3, 7, 9)(2, 12, 8, 6),$$

$$(1, 3, 2, 7, 9, 8)(4, 5, 12, 10, 11, 6) \rangle$$

$$G_{10} = \langle (1, 2, 6, 4, 3)(7, 8, 12, 10, 9), (5, 11)(6, 12), (1, 2, 6, 5, 3)(7, 8, 12, 11, 9), (5, 12, 11, 6) \rangle$$

$$G_{11} = \langle (1, 8, 9, 7, 2, 3), (1, 7)(2, 3, 4)(8, 9, 10), (1, 7)(2, 3, 5)(8, 9, 11),$$

$$(2, 6, 3, 5, 4)(8, 12, 9, 11, 10), (5, 11) \rangle$$

$$G_{12} = \langle (2, 8)(6, 12), (1, 2, 6, 5, 3)(7, 8, 12, 11, 9), (5, 6)(11, 12), (1, 2, 6, 4, 3)(7, 8, 12, 10, 9) \rangle$$

$$G_{13} = \langle (1, 2)(7, 8), (1, 2, 3, 4, 5, 6)(7, 8, 9, 10, 11, 12), (6, 12) \rangle$$

Bibliography

- [1] M. Artin. *Algebra*. Prentice-Hall, 1991.
- [2] M. Baake and U. Grimm. *Aperiodic Order*, volume 1. Cambridge University Press, 2013.
- [3] D. Shechtman, I. Blech, D. Gratias, and J.W Cahn. Metallic phase with long-range orientational order and no translational symmetry. *Phys. Rev. Lett.*, 53(20):1951, 1984.
- [4] D. Levine and P.S. Steinhardt. Quasicrystals. I. Definition and structure. *Phys. Rev. B*, 34(2):596–616, 1986.
- [5] J.E.S. Socolar and P.S. Steinhardt. Quasicrystals. II. Unit-cells configurations. *Phys. Rev. B*, 34(2):617–647, 1986.
- [6] R.V. Moody. Model sets: a survey. In F. Axel, F. Dénoyer, and J.P. Gazeau, editors, *From Quasicrystals to More Complex Systems*. Springer-Verlag, 2000.
- [7] S. Casjens. *Virus structure and assembly*. Boston, MA: Jones and Bartlett, 1985.
- [8] D.L.D. Caspar and A. Klug. Physical principles in the construction of regular viruses. *Cold Spring Harbor Symp. Quant. Biol.*, 27:1–14, 1962.
- [9] R. Twarock. A tiling approach to virus capsid assembly explaining a structural puzzle in virology. *J. Theor. Biol.*, 226:477–482, 2004.
- [10] R. Penrose. Pentaplexity. *Bulletin of the Institute for Mathematics and Applications*, 10:266–271, 1974.

- [11] D.G. Salthouse, G. Indelicato, P. Cermelli, T. Keef, and R. Twarock. Approximation of virus structure by icosahedral tilings. *Acta Cryst. A*, A71:410–422, 2015.
- [12] W. Steurer. Structural phase transitions from and to the quasicrystalline state. *Acta Cryst.*, A61:28–38, 2005.
- [13] J. P. Sethna. *Statistical Mechanics: Entropy, Order Parameters and Complexity*. Oxford University Press, 2006.
- [14] S.E. Bakker, E. Gropelli, A.R. Pearson, P.G. Stockley, D.J. Rowlands, and N.A. Ranson. Limits of structural plasticity in a Picornavirus capsid revealed by a massively expanded Equine Rhinitis A Virus particle. *Journal of Virology*, 88(11):6093–6096, 2014.
- [15] L. Tang, K.N. Johnson, L.A. Ball, T. Lin, M. Yeager, and J.E. Johnson. The structure of Pariacoto Virus reveals a dodecahedral cage of duplex RNA. *Nat. Struct. Biol.*, 8(1):77–83, 2001.
- [16] K. Toropova, G. Basnak, R. Twarock, P.G. Stockley, and N.A. Ranson. The three-dimensional structure of genomic RNA in Bacteriophage MS2: Implications for assembly. *J. Mol. Biol.*, 375:824–836, 2008.
- [17] T. Keef and R. Twarock. Affine extensions of the icosahedral group with applications to the three-dimensional organisation of simple viruses. *J. Math. Biol.*, 59:287–313, 2009.
- [18] T. Keef, R. Twarock, and K. ElSawy. A new series of polyhedra as blueprints for viral capsids in the family of Papovaviridae. *J. Theor. Biol.*, 253:808–816, 2008.
- [19] T. Keef, J. Wardman, N.A. Ranson, P.G. Stockley, and R. Twarock. Structural constraints on the three-dimensional geometry of simple viruses: case studies of a new predictive tool. *Acta Cryst.*, A69:140–150, 2012.
- [20] R. Carter. *Lie algebras of finite and affine type*. Cambridge University Press, 2005.
- [21] J. Patera and R. Twarock. Affine extensions of noncrystallographic Coxeter groups and quasicrystals. *J. Phys. A: Math. Gen.*, 35:1551–1574, 2002.

- [22] P-P. Dechant, C. Bøehm, and R. Twarock. Novel Kac-Moody-type affine extensions of non-crystallographic Coxeter groups. *J. Phys. A: Math. Theor.*, 45:285202, 2012.
- [23] P-P. Dechant, C. Bøehm, and R. Twarock. Affine extensions of non-crystallographic Coxeter groups induced by projection. *J. Math. Phys.*, 54:093508, 2013.
- [24] A. Janner. Towards a classification of icosahedral viruses in terms of indexed polyhedra. *Acta Cryst.*, A62:319–330, 2006.
- [25] A. Janner. Exploring the interplay between virology and molecular crystallography. *Computational and mathematical methods in medicine*, 9:167–173, 2008.
- [26] A. Janner. Crystallographic structural organization of human rhinovirus serotype 16, 14, 3, 2 and 1a. *Acta Cryst.*, A62:270–286, 2006.
- [27] A. Janner. Higher-dimensional point groups in superspace crystallography. *Acta Cryst.*, A64:280–283, 2008.
- [28] L.S Levitov and J. Rhyner. Crystallography of quasicrystals; application to icosahedral symmetry. *Journal of Physics France*, 49:1835–1849, 1988.
- [29] P. Kramer. Continuous rotation from cubic to icosahedral order. *Acta Cryst.*, A43:486–489, 1987.
- [30] E. Zappa, E.C. Dykeman, and R. Twarock. On the subgroup structure of the hyperoctahedral group in six dimensions. *Acta Cryst.*, A70:417–428, 2014.
- [31] B. Thomas, R. Twarock, M. Valiunas, and E. Zappa. Nested polytopes with non-crystallographic symmetry induced by projection. In *Proceedings of Bridges 2015: Mathematics, Music, Art, Architecture, Culture*, pages 167–174. Tessellations Publishing, 2015.
- [32] R. Twarock, M. Valiunas, and E. Zappa. Orbits of crystallographic embedding of non-crystallographic groups and applications to virology. Accepted for publication by *Acta Cryst. A*, 2015.
- [33] M. Pitteri and G. Zanzotto. *Continuum models for phase transitions and twinning in crystals*. CRC/Chapman and Hall, London, 2002.

- [34] A. Szczepański. *Geometry of crystallographic groups*. World Scientific Publishing, 2012.
- [35] J.H. Conway and N.J.A. Sloane. *Sphere packings, lattices and groups*. Springer-Verlag, 1988.
- [36] H. Hiller. The crystallographic restriction in higher dimensions. *Acta Cryst. A*, A41:541–544, 1985.
- [37] M. Senechal. *Quasicrystals and geometry*. Cambridge University Press, 1995.
- [38] H.W. Kroto, J.R. Heath, S.C. O’Brien, R.F. Curl, and R.E. Smalley. C60: Buckminsterfullerene. *Nature*, 318, 1985.
- [39] J.E. Humphreys. *Reflection groups and Coxeter groups*. Cambridge University Press, 1990.
- [40] W. Steurer. Twenty years of structure research on quasicrystals. part I. Pentagonal, octagonal, decagonal and dodecagonal quasicrystals. *Zeitschrift Fur Kristallographie*, 219:391–446, 2004.
- [41] R.A. Mollin. *Algebraic number theory*. Chapman and Hall/CRC Press, 1999.
- [42] W. Fulton and J. Harris. *Representation Theory: A first Course*. Springer-Verlag, 1991.
- [43] B. Grünbaum and G.C. Shepard. Tilings by regular polygons. *Mathematics Magazine*, 50(1977):227–247.
- [44] R. Twarock. Mathematical virology: a novel approach to the structure and assembly of viruses. *Phil. Trans. R. Soc. A*, 364:3357–3373, 2006.
- [45] R.C. Liddington, Y. Yan, J. Moulai, R. Sahli, T.L. Benjamin, and S.C. Harrison. Structure of simian virus 40 at 3.8-Å resolution. *Nature*, 354:278–284, 1991.
- [46] T. Keef, A. Taormina, and R. Twarock. Classification of capped tubular viral particles in the family of Papovaviridae. *Journal of Physics: Condensed Matter*, 18:S375–S387, 2006.

- [47] T. Keef, A. Taormina, and R. Twarock. Assembly models for Papovaviridae based on tiling theory. *Physical Biology*, 2:175–188, 2005.
- [48] K. ElSawy, A. Taormina, R. Twarock, and L. Vaughan. Dynamical implications of viral tiling theory. *Journal of Theoretical Biology*, 252:357–369, 2008.
- [49] L. Chen, R.V. Moody, and J. Patera. Non-crystallographic root systems. In J. Patera, editor, *Quasicrystals and Discrete Geometry*. Fields Institute Monographs, 1998.
- [50] P-P. Dechant, J. Wardman, T. Keef, and R. Twarock. Viruses and fullerenes- symmetry as a common thread? *Acta Cryst.*, A70:162–167, 2014.
- [51] F. Gálher. *Quasicrystal Structures from the Crystallographic Viewpoint*. PhD thesis, ETH, 1988.
- [52] M. Baake. Structure and representations of the hyperoctahedral group. *Journal of Mathematical Physics*, 25(11):3171–3182, 1984.
- [53] The GAP Group. *GAP – Groups, Algorithms, and Programming, Version 4.7.2*, 2013.
- [54] D.F. Holt, B. Eick, and E.A. O’Brien. *Handbook of computational group theory*. Chapman and Hall/CRC Press, 2005.
- [55] J.F. Humphreys. *A course in group theory*. Oxford University Press, 1996.
- [56] G. Janusz and J. Rotman. Outer automorphisms of S_6 . *The American Mathematical Monthly*, 89:407–410, 1982.
- [57] A. Katz. Some local properties of the three-dimensional Penrose tilings. In M.V Jarić, editor, *Introduction to the Mathematics of Quasicrystals*. Academic Press, 1989.
- [58] R. Hoyle. Shapes and cycles arising at the steady bifurcation with icosahedral symmetry. *Physica D*, 191:261–281, 2004.
- [59] L.H. Soicher. Computational group theory problems arising from computational design theory. *Oberwolfach Rep. 3, Report 30/2006: Computational group theory*, 3:1809–1811, 2006.
- [60] L.R. Foulds. *Graph Theory Applications*. Springer-Verlag, 1992.

- [61] D.M. Cvetkovic, M. Doob, and H. Sachs. *Spectra of Graphs*. Johann Ambrosius Barth, 1995.
- [62] R.A. Horn and C.R. Johnson. *Matrix Analysis*. Cambridge University Press, 1985.
- [63] P. Kramer, M. Baake, and D. Joseph. Schur rotations, transitions between quasiperiodic and periodic phases, and rational approximants. *Journal of Non-Crystalline Solids*, 153-154:650–653, 1993.
- [64] F.H Li and Y. F. Cheng. A simple approach to quasicrystal structure and phason defect formulation. *Acta Cryst.*, A46:142–149, 1990.
- [65] M. Torres, G. Pastor, and I. Jimenez. About hyperplane single rotation and phason strain equivalence in icosahedral and octagonal phases. *J. Phys.: Condensed Matter*, 1:6877–6880, 1989.
- [66] G. Indelicato, T. Keef, P. Cermelli, D.G Salthouse, R. Twarock, and G. Zanzotto. Structural transformations in quasicrystals induced by higher-dimensional lattice transitions. *Proc. Royal Society A*, 568:1452–1471, 2012.
- [67] G. Indelicato, P. Cermelli, D.G. Salthouse, S. Racca, G. Zanzotto, and R. Twarock. A crystallographic approach to structural transitions in icosahedral viruses. *J.Mathematical Biology*, 64:745–773, 2011.
- [68] H.F. Jones. *Groups, Representations and Physics*. Institute of Physics Publishing, 1990.
- [69] H.S.M. Coxeter. *Regular polytopes*. Dover Publications, Inc. New York, 1973.
- [70] P. R. Cromwell. *Polyhedra*. Cambridge University Press, 1997.
- [71] L. Háková, M. Larouche, and J. Patera. The rings of n -dimensional polytopes. *J. Phys. A: Math. Gen.*, 41:495202, 2008.
- [72] A. Klimyk and J. Patera. Orbit functions. *(SIGMA) Symmetry, Integrability and Geometry: Methods and applications*, 2:60pp, 2006.
- [73] A. Tereszkieicz. Complete decompositions of coxeter groups orbit products of A_2 , C_2 , G_2 and H_2 and some limits for them. *arXiv*, 2014. 1304.4998v2 [math-ph].

- [74] J. Patera and R.T. Sharp. Branching rules for representations of simple Lie algebras through Weyl group orbit reduction. *J. Phys. A: Math. Theor.*, 22:2329–2340, 1989.
- [75] F. Bégin and R.T. Sharp. Weyl orbits and their expansions in irreducible representations for affine Kac–Moody algebras. *J. Math. Phys.*, 33:2343, 1992.
- [76] M. Hall. *The theory of groups*. The Macmillan company, 1959.
- [77] M. Koca, M. Al-Ajmi, and R. Ko. Polyhedra obtained from Coxeter groups and quaternions. *J. Math. Phys.*, 48:113514, 2007.
- [78] V. Elser and N.J.A. Sloane. A highly symmetric four-dimensional quasicrystal. *J. Phys. A: Math. Theor.*, 20:6181–6168, 1987.
- [79] R. Moody and J. Patera. Quasicrystals and icosians. *J. Phys. A: Math. Theor.*, 26:2829–2853, 1993.
- [80] M. Koca, R. Koç, and M. Al-Barwani. Noncrystallographic Coxeter group H_4 in E_8 . *J. Phys. A: Math. Gen.*, 34:11201–11213, 2001.
- [81] Jonathan Bowers. Uniform polychora. In Reza Sarhangi, editor, *Bridges: Mathematical Connections in Art, Music, and Science*, pages 239–246. Bridges Conference, 2000.
- [82] M. Möller. *Vierdimensionale Archimedische Polytope*. PhD thesis, Universität Hamburg, 2004.
- [83] J.A. Geraets, E.C. Dykeman, P.G. Stockley, N.A. Ranson, and R. Twarock. Asymmetric genome organization in an RNA virus revealed via graph-theoretical analysis of tomographic data. *PLOS Computational Biology*, 11:e1004146, 2015.
- [84] M. Carrillo-Tripp, C. M. Shepherd, I. A. Borelli, S. Venkataraman, G. Lander, P. Natarajan, J. E. Johnson, C.L. Brooks III, and V. S. Reddy. Viperdb2: an enhanced and web api enabled relational database for structural virology. *Nucleic Acids Research*, 37:D436–D442, 2009.
- [85] J. Wardman. *A symmetry approach to virus architecture*. PhD thesis, University of York, 2012.

- [86] K.C. Dent, R. Thompson, A.M. Barker, J.A. Hiscox, J.N. Barr, P.G. Stockley, and N.A. Ranson. The asymmetric structure of an icosahedral virus bound to its receptor suggests a mechanism for genome release. *Structure*, 21(7), 2013.
- [87] A. Fring and C. Korff. Affine Toda field theories related to Coxeter groups of non-crystallographic type. *Nuclear Physics B*, 729:361–386, 2005.
- [88] A. Fring and C. Korff. Non-crystallographic reduction of generalized Calogero–Moser models. *J. Phys. A: Math. Theor.*, 39:1115–1131, 2006.
- [89] E. Zappa, G. Indelicato, A. Albano, and P. Cermelli. A Ginzburg-Landau model for the expansion of a dodecahedral viral capsid. *International Journal of Non linear Mechanics*, 56:71–78, 2013.
- [90] V.L. Lorman and S.B. Rochal. Landau theory of crystallization and the capsid structures of small icosahedral viruses. *Phys. Rev. B*, 77:224109, 2008.
- [91] H.W. Kroto. Carbon onions introduce new flavour to fullerene studies. *Nature*, 359, 1992.
- [92] R. Twarock. New group structures for Carbon onions and Carbon nanotubes via affine extensions of non-crystallographic Coxeter groups. *Physics Letters A*, 300:437–444, 2002.